Aalto-yliopisto
Insinööritieteiden
korkeakoulu

Matti Hautala

Stresses Induced in Pressurizer Surge Line Due to Thermal Stratification

Author Matti Hautala

Title of thesis Stresses Induced in Pressurizer Surge Line Due to Thermal Stratification

Master programme Mechanical Engineering   **Code** ENG25

Thesis supervisor Prof. Luc St-Pierre

Thesis advisor(s) M.Sc. Yrjö Hytönen

Date 05.04.2019   **Number of pages** 59 + 10   **Language** English

Abstract

Thermal stratification poses significant loads into surge line of pressurized water reactor as thermal stresses are induced due to uneven thermal expansion. Therefore, this phenomenon has reached notable research interest around the world and multiple studies have been conducted on the topic. In this thesis, knowledge relevant for structural assessment of thermal stratification was presented. In addition, foundation for both numerical and analytical assessment of main stress components was given.

First, numerical simulation procedure for both thermal-hydraulic and structural responses were proven to be in relatively good agreement with experimental results from German HDR program. Then these validated models were further utilized in parametric study to examine changes in thermal-hydraulic and mechanical responses. According to this study, pipe diameter based Richardson's number is feasible measure of dynamical similarity in thermally stratified flows. When Richardson's number increases, the height of the mixing layer decreases and vertical position rises. Furthermore, similar correlation was also realized for maximum stresses as larger stresses where associated with larger Richardson's numbers. However, as the correlation was only true for isothermal simulations, Richardson's number can not be used single-handedly to estimate stresses. Finally, based on the parametric study, increase of flow velocity can not be considered as a solution for thermal stratification. In the worst case it might magnify loads induced by thermal striping and promote high cycle fatigue.

In addition to the knowledge obtained from numerical simulations, the main results of the thesis were analytical models which can be applied for estimation of stresses induced by thermal stratification in typical PWR surge lines. These methods are especially important in situations where use of time and resource consuming numerical models is not possible. When support conditions were explicitly known, both temperature profile decomposition and thermal bowing methods were found to give accurate estimates for stresses induced into straight pipe under stratified temperature load. When these formulas were applied into realistic geometry of HDR setup and thermal loading conditions were altered, distinct limitations were realized. Use of thermal bowing method is limited to cases where simple support conditions are realized. Decomposition method on the other hand will produce sufficiently accurate results for wider range on support conditions. However, reliable estimates are only obtained if scale factors for membrane and bending stresses are optimized. Further studies are still needed to validate performance of decomposition method on actual surge line geometries.

Keywords Thermal Stratification, Thermal Stresses, Pressurized Water Reactor, Surge line

Tekijä Matti Hautala

Työn nimi Lämpötilakerrostuman aiheuttamat jännitykset paineistimen yhdyslinjassa

Maisteriohjelma Konetekniikka   **Koodi** ENG25

Työn valvoja Prof. Luc St-Pierre

Työn ohjaaja(t) DI Yrjö Hytönen

Päivämäärä 05.04.2019   **Sivumäärä** 59 +10   **Kieli** Englanti

Tiivistelmä

Lämpötilakerrostuma on virtausilmiö, joka epätasaisen lämpölaajenemisen seurauksena aiheuttaa painevesireaktorin yhdyslinjaan huomattavia jännityksiä. Ilmiö on ollut maailmanlaajuisesti merkittävä tutkimuskohde ja aiheesta on julkaistu useita tutkimuksia. Tässä tutkielmassa esiteltiin rakenteellisen arvioinnin suorittamisen kannalta merkittävät taustatiedot ilmiöstä. Tämän lisäksi tarkasteltiin sekä numeerisia että analyyttisiä laskentamenetelmiä tärkeimmille jännityskomponenteille.

Tutkielmassa hyödynnettiin numeerisia laskentamenetelmiä sekä lämmönsiirtoa että mekaanista vastetta simuloivissa malleissa. Mallien todettiin aluksi Saksalaisen HDR-testiohjelman tulosten perusteella noudattavan todellisuutta riittävällä tarkkuudella, minkä jälkeen malleja sovellettiin parametrisessä tutkimuksessa. Parametrinen tutkimus osoitti, että putken halkaisijaan perustuvaa Richardsonin lukua voidaan käyttää lämpötilakerrostuneen putkivirtauksen dynamiikan kuvaamisessa. Richardsonin luvun kasvaessa sekoittumiskerroksen paksuuden huomattiin pienevän ja keskikohdan sijainnin nousevan. Vastaava korrelaatio ilmeni myös putken maksimijännityksille, joiden havaittiin olevan riippuvaisia Richardsonin luvusta. Richardsonin luku ei kuitenkaan yksin riitä kuvastamaan syntyviä jännityksiä, sillä korrelaatio toteutui ainoastaan simulaatioille joissa lämpötilaerot olivat samoja. Lopuksi numeeristen simulaatioiden perusteella todettiin, että virtausnopeuksien kasvattaminen ei ole sopiva ratkaisu lämpötilakerrostumaongelman ratkaisuksi. Huonoimmassa tapauksessa tämä saattaa lisätä kerrostuman rajapinnan heilahtelua ja näin ollen edesauttaa korkeasyklistä väsymistä.

Numeeristen simulaatioiden perusteella tehtyjen havaintojen lisäksi tämän tutkielman tärkein tulos oli analyyttiset menetelmät, joita voidaan hyödyntää lämpötilakerrostuman painevesireaktorin yhdyslinjaan aiheuttamien jännitysten arvioinnissa. Nämä kaavoihin perustuvat menetelmät ovat erityisen tärkeitä tilanteissa, joissa numeeristen mallien käyttö ei ole ajan tai resurssien puutteen vuoksi mahdollista. Alustavissa suoralla putkella tehdyissä tarkasteluissa molemmat tutkielmassa esitellyt menetelmät antoivat tarkkoja arvioita syntyville aksiaalijännityksille. Kun menetelmiä edelleen sovellettiin HDR-testilaitoksen geometrialle sekä vaihtuville lämpöjännityskuormille, havaittiin niiden käyttäytymisessä kuitenkin selkeitä eroja. Lämpötaivutuksiin perustuvan menetelmän huomattiin soveltuvan käytettäväksi ainoastaan tilanteissa, joissa tuentaolosuhteet sallivat putken kiertymät molemmissa päissä. Lämpötilajakauman erittelyyn perustuvan menetelmän puolestaan todettiin antavan suhteellisen tarkkoja arvioita putken jännitystilasta selvästi laajemmalla joukolla tuentaolosuhteita. Menetelmän käyttö vaatii kuitenkin jännityskomponenttien vaikutuskertoimien optimoinnin ja tämän lisäksi käyttäytyminen todenmukaisella yhdyslinjageometrialla täytyy vielä varmistaa jatkotutkimuksilla.

Avainsanat Lämpötilakerrostuma, Lämpöjännitykset, Painevesireaktori, Yhdyslinja

Preface

This Master's thesis is designed to be extension to my Bachelor's thesis written roughly two years ago. The topic of thermal stratification is of high importance in nuclear power plant design and, since multiple publications have been released on the topic, there is urge need for all around comparative work to harvest all of this knowledge. Comparison is especially needed for simple analytical formulas that could provide measures for fast engineering approximations. Together with clarifying fundamentals behind this multiphysical phenomenon, comparing and defining analytical quick assessment methods was thus chosen as the main objective of this thesis. This thesis was funded by Finnish Radiation and Nuclear Safety Authority (STUK). In addition, computational resources where provided by the IT Center for Science LTD (CSC).

First of all the author would like to acknowledge both Finnish Radiation and Nuclear Safety Authority (STUK) and IT Center for Science LTD (CSC) for their contribution to the framework of this work. Particularly, compliments to M.Sc. Petri Vuorio, thesis advisor M.Sc. Yrjö Hytönen, M.Sc. Jukka Mononen and D.Sc. Mika Bäckström from STUK for providing guidance, knowledge and favorable circumstances for the work. The author is also grateful for the support and time given by thesis supervisor Prof. Luc St-Pierre and D.Sc. Tommi Mikkola from Aalto University. Finally, honest appreciation to everyone contributing to the completion of this thesis.

Espoo 5.4.2019

Matti Hautala

Contents

Symbols

Latin alphabet

A	[m^2]	area
C	[J/kg·K]	specific heat of the wall
D_i	[m]	pipe inner diameter
D_m	[m]	pipe middle diameter
D_o	[m]	pipe outer diameter
D_{ref}	[m]	reference pipe diameter
E	[Pa]	Young's modulus
F_T	[N]	thermal normal force
H	[m]	mixing layer height
I	[m^4]	moment of inertia
M_T	[N·m]	thermal bending moment
S_u	[Pa]	ultimate tensile strength
T	[°C]	temperature
T_0	[°C]	zero thermal strain reference temperature
T_b	[°C]	linear portion of temperature profile
T_C	[°C]	temperature of lower stratification layer
T_H	[°C]	temperature of upper stratification layer
T_p	[°C]	nonlinear portion of temperature profile
T_m	[°C]	average portion of temperature profile
ΔT	[°C]	temperature difference
ΔT_3	[°C]	temperature difference between stratification layers
U	[m/s]	velocity
V	[°C]	variation of linear portion in temperature decomposition
att	[ ]	attenuation factor
f	[1/s]	frequency of fluid temperature oscillation
g	[m/s^2]	gravitational acceleration
g'	[m/s^2]	reduced gravitational acceleration
h	[W/ m^2 K]	heat transfer coefficient
l	[m]	characteristic length
n_1	[ ]	effectiveness factor for wall thickness
n_2	[ ]	effectiveness factor for mixing layer thickness
t	[m]	pipe wall thickness
y	[m]	vertical position in pipe cross section

Greek alphabet

α	[1/K]	coefficient of thermal expansion
ς	[rad]	radial positon of stratification
κ	[m^2/s]	thermal diffusivity
λ	[W/m·K]	thermal conductivity
ρ	[kg/ m^3]	density
σ	[Pa]	stress
σ_b	[Pa]	bending stress
σ_m	[Pa]	membrane stress
σ_p	[Pa]	peak stress
φ	[rad]	radial position, neutral point at the pipe top
φ_1	[rad]	radial position of the mixing layer upper limit
φ_2	[rad]	radial position of the mixing layer lower limit
χ	[m]	penetration of thermal oscillation

Abbreviations

ASTM	American Society for Testing and Materials
CFD	Computational Fluid Dynamics
CFL	Courant-Fridrich-Lewy (condition)
CSC	IT Center for Science LTD.
DES	Detached Eddy Simulation
DOF	Degrees of Freedom
EPR	European Pressurized Water Reactor
FEM	Finite Element Method
FE	Finite Element
FSI	Fluid-Structure Interaction
FVM	Finite Volume Method
FV	Finite Volume
HDR	Heißdampfreaktor
LES	Large Eddy Simulation
NEA	Nuclear Energy Agency
NOC	Normal Operating Conditions
NS	Navier-Stokes (equations)
OECD	Organization for Economic Co-operation and Development
PNAE	Pravila i Normi v Atomnoi Energetike (Правила и нормы в атомной энергетике)
RANS	Reynold's-averaged Navier-Stokes (equations)
RCC-M	Règles de Conception et de Construction des Matériels Mècaniques des Ilots Nucléaires
RPV	Reactor Pressure Vessel
SST	Shear Stress Transport
STUK	Radiation and Nuclear Safety Authority
TSP	Thermal Stress Parameter
TSR	Thermal Shock Ratio
USNRC	United States Nuclear Regulation Commission
VVER	Vodo-vodjanoi energetitšeski reaktor (Водо-водяной энергетический реактор)

1 Introduction

Design of nuclear power plant is one of the most legislated processes in any field of engineering. Legislation is typically enforced by design standards such as ASME, RCC-M or PNAE. With high conservatism, these standards aim to eliminate possibility of failure even during abnormal or unanticipated operational conditions. However, these standards feature few well known unclarities such as assessment of thermal stratification in long horizontal pipelines. This phenomenon was first observed in 1988 at Trojan nuclear power plant in the United States of America (Bulletin 88-11) and thereafter multiple failures, such as leakages and pipe support ruptures, have been observed world wide (OECD-NEA 2005).

In thermal stratification, temperature dependent density variation drives fluid flow inside horizontal pipes into state where upper and lower parts are occupied with fluids on different temperatures. Furthermore, due to uneven thermal expansion, there are two main features that promote failure. Displacements and bending moments are caused by global stratification, where as local temperature loads are induced from fluctuation of stratification layer called thermal striping. Each of these features have reached relatively wide research interest and both experimental and numerical studies have been conducted. Due to low velocities and high temperature differences surge line of pressurized water reactor is favorable location for stratification to occur. In addition, common surge line designs include long vertical portions which in worst case could undergo stratification with length of meters.

The primary objective of this thesis is to clarify key aspects of thermal stratification and methods for assessment of structural response due to induced thermal stresses. The secondary objective is to continue previous work and study the accuracy of empirical formulas for peak stresses gleaned in Hautala (2017). Ultimately, the aim is to develop simplified method for broad conservative structural assessment. In this research, coupled numerical fluid-structure interaction model created with commercial simulation software STAR-CCM+ (13.04.011-R) will be utilized. Due to high computational demand Reynold's averaged turbulence models will be used and consequently, scope of the thesis will be limited to only consider global stratification as only the average fluid motion is solved. In normal operational condition the pressure inside primary piping is designed to maintain cooling water in liquid state. Therefore, in this thesis only one-phase flows are addressed. Even though, for some abnormal operating conditions also two-phase flows are possible. Initial plan was to perform studies on realistic surge line geometry of a Finnish nuclear power plant. However, due to computational complexity, this was found to be excessively laborious for the framework of this thesis and these studies were deliberately postponed.

In the first chapter current state of knowledge, experiences and management measures are summarized to give reader insight into the topic. After this introductory part, numerical simulations for both thermal-hydraulic heat transfer and solid stress are performed and validated with experimental results. In chapter 5 formulas of quick structural assessment are first presented and used for rough estimations. The objective of chapters 3, 4 and 5 is to validate the modelling and calculation procedures. Finally, in chapter 6 parametric study on thermal stratification is performed together with application of quick assessment formulas. The reader of this thesis is assumed but not required to have basic knowledge in working principles of pressurized water reactors and buoyancy driven flows.

2 Current State of Knowledge

The issuance of bulletin 88-11 was the turning point for the research of thermal stratification in the field of nuclear power. During that time computational capabilities for fluid dynamics were still relatively limited and therefore mainly experimental studies were conducted until the end of 20th century. German HDR program, which will also be used as numerical validation reference on this thesis, is a prime example of these tests as the experiments were performed in full scale plant unit. These researches, together with newer computational studies, have enlighten the phenomenon of thermal stratification significantly and the objective of this chapter is to give overview of the knowledge relevant for the assessment of surge line stratification.

2.1 Brief Introduction to Thermal Stratification and PWRs

In stratification fluids with different densities tend to flow into state of equilibrium where fluid with lower density is on the top of fluid with higher density. This is caused by differences in buoyant forces, which promote natural convection. If the density differences are related to the temperature of the fluid, the phenomenon is called thermal stratification. From the force balance point of view, in this situation buoyant forces dominate viscous and inertial forces. In this thesis, the medium of interest is water and main parameters affecting the magnitude of these forces are flow velocity and temperature difference between hot and cold regions. The increase in velocity will promote turbulence and tend to mix up the stratification, whereas increase in temperature difference will make the layers more stable.

In the design of pressurized water reactor, surge line is the component that connects the pressurizer into the primary loop (Figure 2). In ideal operating conditions there are no flows inside the surge line, but whenever there is a need to regulate primary loop pressure, flows will be induced also into the surge line. According to the direction, these flows are often characterized as in and out surge (Figure 1).
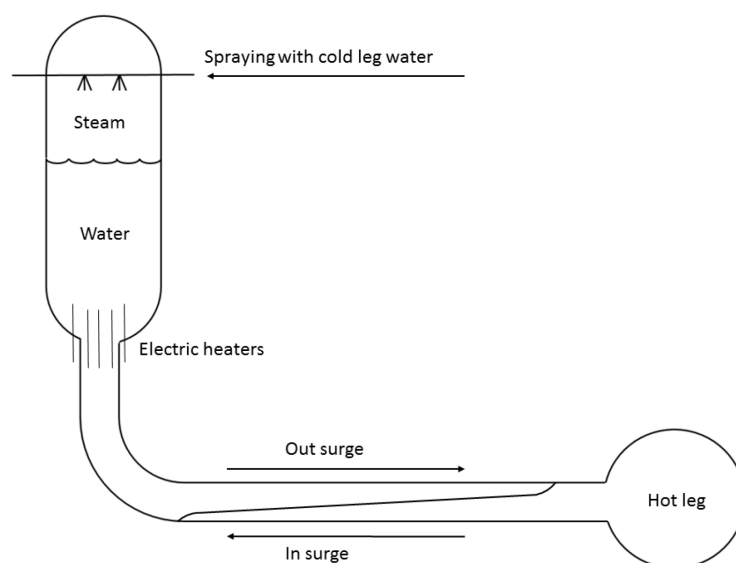

Figure 1: Schematic of thermal stratification in PWR surge line. (Hautala 2017)

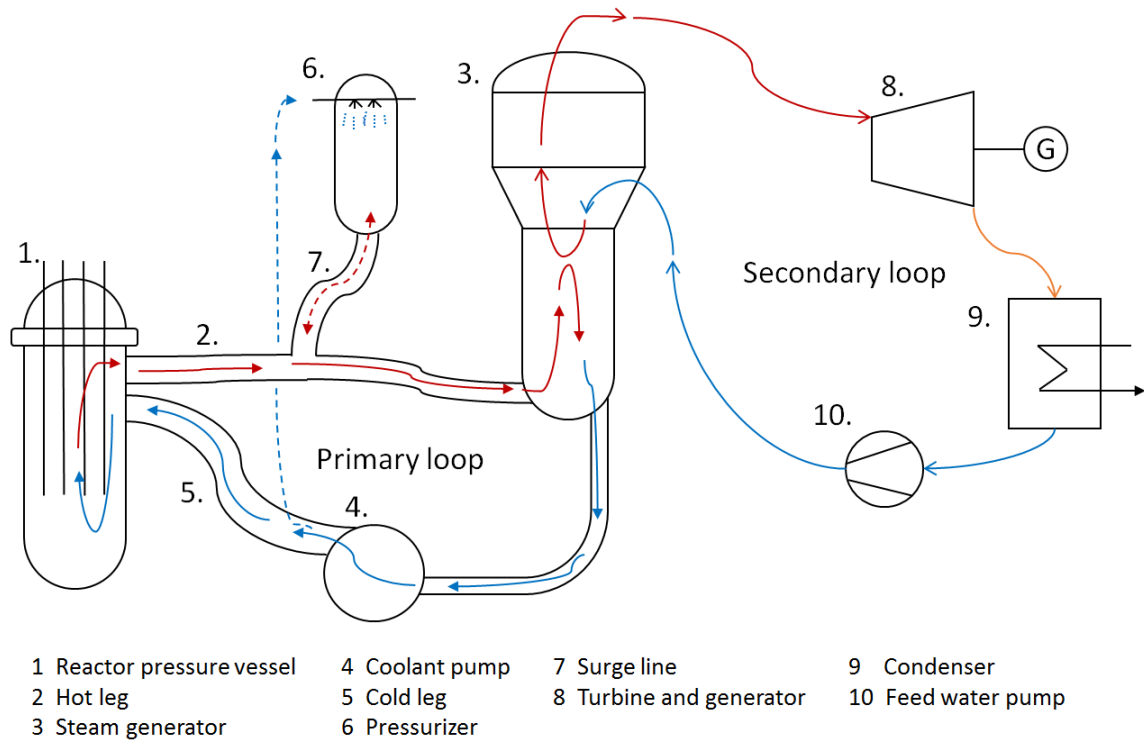|			
1 Reactor pressure vessel	4 Coolant pump	7 Surge line	9 Condenser
2 Hot leg	5 Cold leg	8 Turbine and generator	10 Feed water pump
3 Steam generator	6 Pressurizer		

Figure 2: Simplified process diagram for Pressurized Water Reactor.

Since pressurizer is filled with water in both liquid and gas phases, elevated temperature is required in comparison to primary loop, in which water is maintained at liquid state. During normal operating condition, this temperature difference is more or less 30 °C, whereas on course of start up or shutdown values as high as 180 °C are plausible (Bieniussa and Reck 1999). Such a temperature difference pose severe threats especially if combined with periodic surge flows. Simplified process diagram for generalized pressurized water reactor, shown in Figure 2, is now exploited to illustrate how in and out surges are formed.

The root cause of surge flows is closely linked into pressure regulation mechanism of the pressurizer (6) and fill level variation. Pressure regulation via fill level variation is needed when disturbances, including deviations of reactor core heat removal (1) and secondary loop power generation process, are encountered in operating conditions. Furthermore, since the heat removal capacity of the secondary loop is altered (3, 8, 9, 10), these disturbances also affect coolant temperature and trigger thermal expansion or contraction of the working medium. These changes in fluid volume, drive flows to and fro surge line (7) as the fill level of the pressurizer (6) varies. Similar filling level movement also follows from pressure adjustment, which is performed either by condensing steam with cold leg (5) water spraying or evaporating water with electric heaters. Even during normal operating conditions, small spraying is typically maintained and thus constant out surge will be formed. Thermal-hydraulic behavior of the surge line (7) is thus complex and in some degree random process for which forecasting of exact condition is no easy matter. For design purposes, in a field with high safety margins, it is often common to play with the extremes. The maximum amplitude of temperature fluctuation in side surge line is explicitly limited by pressurizer (6) and hot leg (2) temperatures. For the number of stratification occurrences there however is no evident upper limit, which inflicts design challenges.

2.2 Measures of Continuous Stratification

As it has already been stated, thermal stratification is characterized by the balance between buoyant, viscous and inertial forces. The ratio of these ultimately defines the stability of stratification and can be explicitly expressed with use of nondimensional quantities. The most used relations are Froude and Richardson numbers, which both concern inertial and buoyant forces. Froude number is defined as

$$Fr = \frac{U}{\sqrt{g'l}} \tag{1}$$

where $g' = g(\rho_2 - \rho_1)/\rho_1$ is the reduced gravity. U it the velocity, g is the gravitational acceleration, ρ_2 is the density of lower fluid, ρ_1 is the density of upper fluid and l is characteristic length. Richardson's number is defined in opposite manner with buoyant forces at numerator and inertial forces at denominator

$$Ri = \frac{g'l}{U^2} \tag{2}$$

(Kundu et al. 2008, p. 292-293).

Both of these commonly used measures are defined for discrete stratification layers. However, for thermal stratification such discrete layers are impossible because heat conduction will diffuse rapid variations effectively. This can be realized with simple numerical simulation of Fourier's law such as the one performed by Hautala (2017). On the other hand, such simulation will also show that speed of heat conduction will decrease significantly as the temperature gradient is reduced. Therefore, use of these simple nondimensional quantities is still possible and in fact used in multiple researches. If more detailed analysis is needed, continuous stratification can be assessed with gradient based Richardson's number

$$Ri(z) = -\frac{g(d\rho/dz)}{\rho_0(dU/dz)^2} \tag{3}$$

for which threshold value of 0.25 can be determined analytically. If the value of Richardson's number surpasses this condition for the whole domain, the flow is considered to be stable everywhere. In practical applications the threshold value may vary from one type of flow to another and therefore this should not be threaded as exact criterion. (Kundu et al. 2008, p. 493-504) Use of these measures is particularly useful for the evaluation and examination of both experimental and numerical studies along with data extracted from in service monitoring systems.

2.3 Thermal Striping

When stratification is considered to be stable, two separate layers of fluids are formed. Furthermore, these two layers will often have different velocities which will produce shear forces near the interface. If no or insufficient balancing forces are present, self-supporting feedback loop will occur and cumulatively these two layers will form larger rotating structures that finally mix together. This is well known phenomena known as Kelvin-Helmholtz instability (Kundu et al. 2008). For thermal stratification, such accumulative process will of course not happen as stable stratification is maintained by buoyant forces. However, in favorable conditions, prior signs of similar wave structures will be observed. This wave motion is called thermal striping, for which illustration is presented in Figure 3. The illustration was produced with CFD simulation by Timperi (2010) and it shows that striping does not occur uniformly in the mixing layer. Striping is spatially and temporally varying phenomenon and therefore probable loading conditions are often estimated with the use of stochastic methods (Radu 2015).
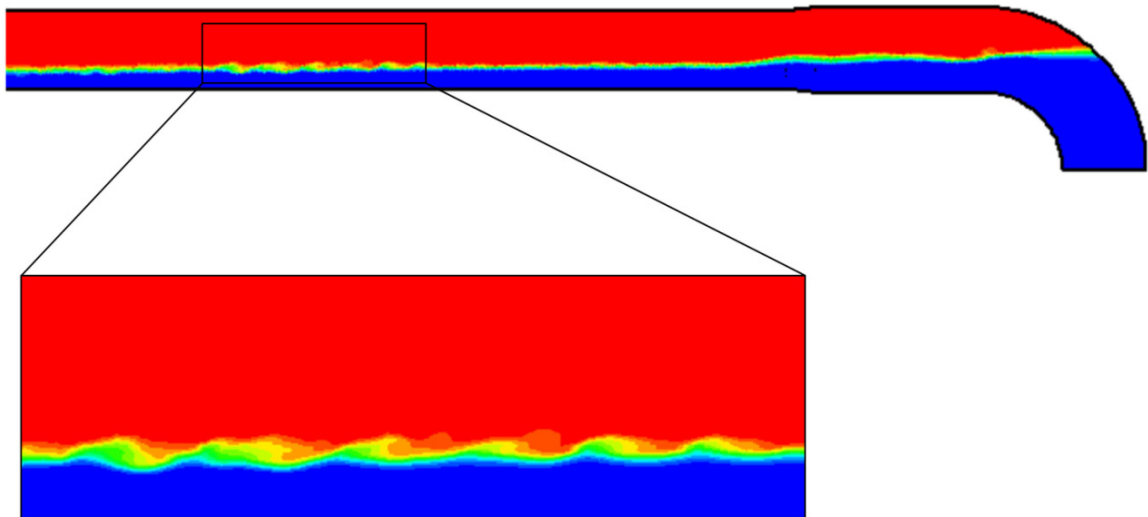

Figure 3: Simulation of thermal striping in a HDR experiment (Timperi 2010)

From the design point of view, undesired consequence from thermal striping is the formation of multiple small fatigue cracks due to thermal fatigue, which is mainly driven by the range of temperature fluctuation. In conservative assessment, this range may be assumed to be equal to maximum temperature difference between stratification layers ΔT. However, based on the experimental results from Talja (1988), this approach might lead to severe over estimation. In that study, considerably smaller temperature differences at pipe surfaces were observed and in addition, dependency in relation of flow velocity was found. With average cross-sectional velocities of 200 mm/sec maximum ranges of 0.35 ΔT was recorded and with slower velocity of 100 mm/sec maximum range was reduced to 0.15 ΔT.

When estimates of fluid temperature variation are known, factors effecting thermal fatigue, including fluctuation range and depth of penetration in the pipe material, may be calculated based on aspects such as heat transfer properties and fluctuation frequency. Assessment of these factors will be covered in section 5.5.

2.4 Thermal Stresses and Strains

When steel component is subjected to changes in temperature thermal expansion will occur. Furthermore, if the expansion is restricted, mechanical stresses will be induced. These stresses can be classified into internal and external stresses in accordance to the type of restraint. For piping parts, external stresses are those imposed by supports and internal stresses are those related to pipe geometry and local nonlinearities in temperature. The amount of thermal stresses induced, and susceptibility of each material to fail under thermal loading, can be characterized with quantities such as Thermal Shock Parameter and Thermal Stress Ratio. These quantities are defined as

$$TSP = \frac{S_u \sqrt{\kappa}}{\alpha E} \tag{4}$$

$$TSR = \frac{S_u}{\alpha E}, \tag{5}$$

where S_u is the ultimate strength, α is the thermal expansion coefficient, E is Young's modulus and κ is the thermal diffusivity. As can be seen, these two parameter are only separated by addition of square root of thermal diffusivity $\sqrt{\kappa}$. This addition takes into account the ability of material to spread thermal energy and reduce temperature gradients during rapid changes. For both TSP and TSR higher the values are, the better resistance material will have against thermal loading. (Barron and Barron 2011)

Stable stratification will cause uneven thermal expansion as the lower part of the pipe contracts and upper part of the pipe expands. For straight horizontal pipe, assessment of stresses associated with of such loading is relatively straightforward and can be performed by decomposition of the temperature profile (Figure 4).
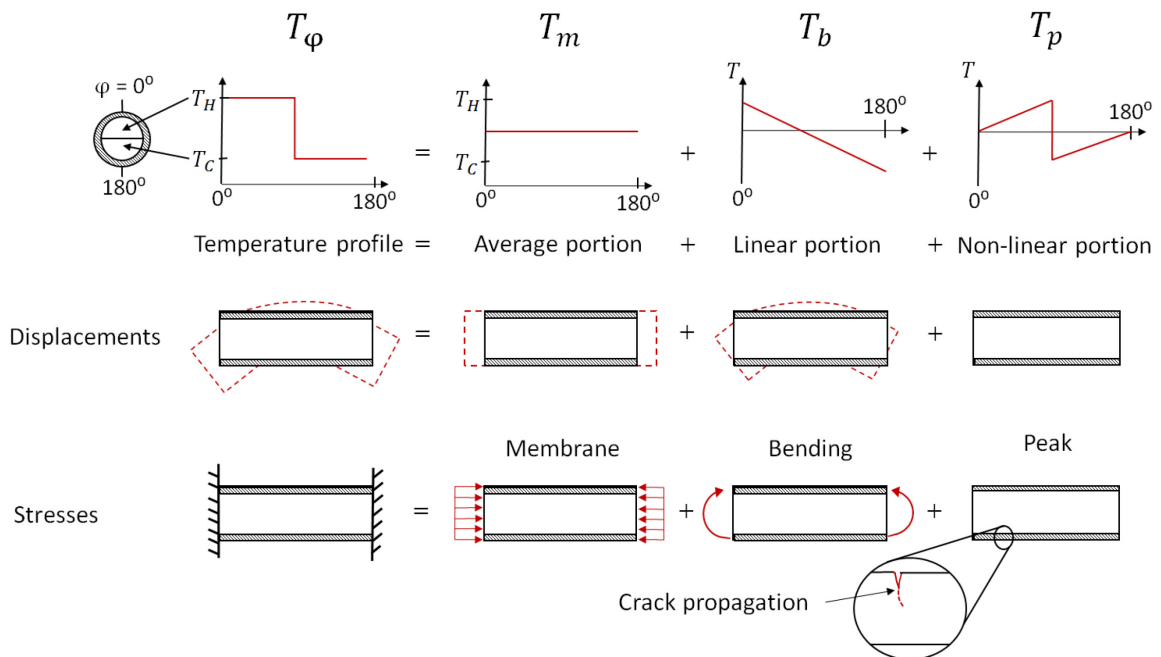

Figure 4: Decomposition of stratified temperature distribution (Hautala 2017).

The main idea in the decomposition is to classify stresses into membrane, bending and peak stresses. Membrane and bending stresses are the production of average and linear parts of the temperature profile respectively. These stresses are associated with global deformations and require external constraints. In the surge line design, the affect of these two is considered by including multiple bends and by designing supports to allow free expansion into all plausible deformed shapes. The last part of the decomposition, the nonlinear part, is simply what is left after subtraction of average and linear portions. These stresses are independent of external restrains and only compensate the thermal expansion. They can be classified as internal stresses and are often incorporated with crack propagation. Assessment of both external and internal stresses will be covered in sections from 5.1 to 5.4.

2.5 Experiences with Thermal Stratification in PWR Surge Line

According to OECD-NEA's (2005) survey among member countries surge line is one of the components most affected by thermal stratification. Furthermore, stratification may occur during all operational stages, namely start up, normal operation and shut down. Therefore, multiple loading cycles will be produced during the life time of the power plant and significant contribution to the overall fatigue will be accumulated. This statement is supported by the study of Myung and Young (2008) which implies that the magnitude of thermal loading cycles is much higher than those imposed by the internal pressure load. The most severe cycles are encountered during start up and shut down. If thermal expansion is restricted, deformation during these conditions could (and have) tear off pipe supports and caused significant plastic deformation (U.S. NRC., 1988). However, in terms of fatigue, number of these cycles is limited by plant lifetime and therefore failure would have to occur in low cycle fatigue regime with stresses over the plastic limit. For normal operational conditions the temperature fluctuations are much more moderate, around 25-35 ℃, and will not result in stresses high enough to cause yielding. Since annular operation cycles are limited to low number of repetitions, periodic variations are needed to introduce enough cycles for high cycle fatigue. Such conditions have been observed by Boros and Asz´odi 2007. Their study concluded that location of the stratified zone during NOC shifts periodically in synch with pressurizer filling level. Furthermore, observed periodic time of approximately 45 min indicates that the number of loading cycles will be large enough for high cycle or mixed cycle fatigue failures to be plausible.

The pre-mentioned survey was subjected to total of 11 countries and only USA reported that PWR specific surge line incidents due to thermal stratification have occurred in their plants. Their answer comprised of two incidents that both dealt with significant deformation. In Trojan plant, permanent deformation, caused by stresses over the yield strength, were introduced by excessive bending moments. In addition, also crushed insulation, rupture restraint gap closing and increased pipe support loads were observed. In the other incident, at Beaver Valley 2, piping displacements resulted in stroke out of snubbers. Even thought, based on this survey the number of incidents occurred at surge line appears to be relatively small, multiple countries did state that they have observed stratification in their plant units. For example, in the Slovakian Bohunice power plant, these observations lead to component replacement as the calculated cumulative fatigue factor had surpassed the threshold value. (OECD-NEA 2005)

2.6 Thermal Cycling Management

As it was previously shown in section 2.2, thermal stratification can be characterized with use of nondimensional quantities. These quantities include the most important parameters related to the issue and offer evident solutions for operational management. Therefore, it is no surprise that multiple solutions and guidelines related to altering either velocities, densities or length scale have been proposed.

One of these solutions is the calculated increase of surge line flow velocities suggested by Baik et al. (1998, p. 177-182). In principal, higher velocities should promote turbulence and thus efficiently break the stratification. However, as it was demonstrated by Cai et al. (2017), the functionality of this solution is arguable. Their study showed that in cases where insufficient amount of turbulence is produced, the increase in velocity might magnify local temperature differences. Yet another downside of this solution is the overall influence it might have. Altering surge line velocity might influence the overall primary loop flow and could in worst case trigger some other known or unknown issue. Baik et al. (1998, p. 177-182) did also propose another more subtle measure of introducing minor slope into horizontal parts of the pipe. Even minor slope of few degree was found to effectively reduced the area exposed to stratification. This measure is also commonly utilized in surge line design. The last parameter included in both Froude and Richardson's number is the characteristic length. For this quantity there are multiple practical definitions and one of them is pipe diameter. Intuitively small pipelines should be relatively insensitive to stratification since effects of thermal conductivity will be magnified. This assumption have been confirmed by Schüman (1998, p. 162-167), who by means of numerical simulation showed that pipelines with nominal diameter under 25mm will not produce significant stresses when exposed to environment susceptible to thermal stratification. For surge line design, this result has only minor significance since possibility to have such small diameter is limited. However, in terms of larger scope, this result enables operators to prioritize surveillance and monitoring of initiating thermal fatigue into larger pipelines.

Due to complexity and diversity of factors involved in buoyancy driven flows, it is practically impossible to prefigure flow behavior inside the surge line during design phase. For example, small changes in operating conditions during start up might have major impact to development of temperature differences, or minor deviation of pressurize spraying might create periodic loading. All of these features contribute to the degradation of the pipe material and the accuracy of initial data is a vital part of reliable life cycle management procedures, such as fatigue calculations. Use of stratification surveillance and monitoring systems is therefore arguably the most important aspect of thermal cycling management and can not be over emphasized. Especially in western plant units, monitoring is often performed with the Fatigue Measuring System FAMOS developed by Siemens. For stratification measurements, at each cross-section, FAMOS uses seven thermocouples distributed evenly along the pipe outer surface. Furthermore, when multiple cross-sections of surge line are monitored, insight into the overall loading conditions are revealed (Golembiewski and Kleinöder 2000). Based on the obtained temperature data, the operator is able to adapt and improve operating procedures, even without fatigue calculations. For example, in the study of Hudcovsky and Slanina (2001), this possibility of optimizing transients was found to be effective way to limit the influence of thermal stratification on the total lifetime of VVER 440 type PWR's.

2.7 Trends in Computational Modelling of Thermal Stratification

In the late-80s, when first numerical studies of thermal stratification were conducted, simulations were without exception strictly limited to simple cases. However, recent development in computer science have enabled and accelerated the use of computational methods. Multiple publications of fluid dynamical and structural simulations have been released during past few years with constant pace towards larger and more complex models. For example, the idea of solving random patterns of turbulent flow was unthinkable in the late-80s, while at the present it is state of art research topic.

In numerical thermal-hydraulic studies, use of turbulence resolving methods such as Large Eddy Simulation or Detached Eddy Simulation enables modelling of random flow patterns and thermal mixing. Both flow patterns and mixing are known to significantly contribute to thermal fatigue of nuclear piping components (Radu 2015, Kamaya and Nakamura 2011, Hannink and Blom 2010). Furthermore, according to OECD-NEA (2005) broad research interest should aim towards understanding these features of thermal stratification, since global features of stratification are considered to be relatively comprehensively known. Modelling of chaotic processes require extensive computational resources. In addition, due to random nature these simulation often require multiple runs, with different initial conditions, before valid conclusions can be made. Therefore, use of simplified methods for turbulence, such as Reynold's-averaged Navier-Stokes equations, are still effective for cases where only average flow behavior is needed. Study of global stratification is a good example of such case and it will be covered later in chapter 6.

From structural side, assessment of thermal stratification is in much more mature state and less limited by restrictions imposed by computational capabilities. This is well documented in the study of Myung and Jhoun (2008), which showed that even simplified beam or shell models can provide sufficiently accurate results when their limitations are realized. For example, at pipe elbows shell models produced results similar to solid model, whereas at more complicated geometries, such as nozzles, simplification led to significant difference. Since the numerics of structural calculations are already well handled, the main issue for structural simulations is the accuracy of initial conditions. Therefore, many of recent publications have tried to solve this issue by coupling CFD and structural simulations. Simulation of Fluid-Structure Interaction offers new possibilities especially for study of fatigue. When temperature variation spectrum is known detailed stochastic analysis can be performed for more reliable fatigue life estimates. Performing such FSI simulations is however currently mainly limited to research purposes. Addition of time dependent structural simulation into already laborious task of solving the fluid motion creates computations that can not be solved in reasonable time without use of supercomputer. To represent this limitation, computation of relatively simple FSI simulation, presented in chapters 3 and 4, took roughly two days with above average multicore (Intel i7-8th generation, 8 cores) consumer workstation.

3 Numerical Simulation of Thermal-Hydraulics

The German HDR program offers valuable experimental data for the study of thermal stratification. These results are especially useful for the validation of numerical model as was done in the study of Timperi (2008). In the upcoming chapters, Test Group TEMR and experiments T33 are used as reference for validation of both thermal-hydraulic and solid stress model. Results of T33 experiments are summarized by Talja (1988) and Häfner (1990) as part of HDR Sicherheitsprogramm Evaluation Reports. The schematics of the HDR test setup is presented in Figure 5 and the measurement cross-sections are shown in Figure 6. Initially the whole domain is filled with hot water and thermal stratifications is generated into the horizontal part of the pipe line leading to pressure vessel by feeding colder water with constant velocity. The specific experiment simulated here is T33.19 and initial conditions for this test are presented in Table 1.

Table 1: Experiment conditions for test T33.19 (Talja 1988).

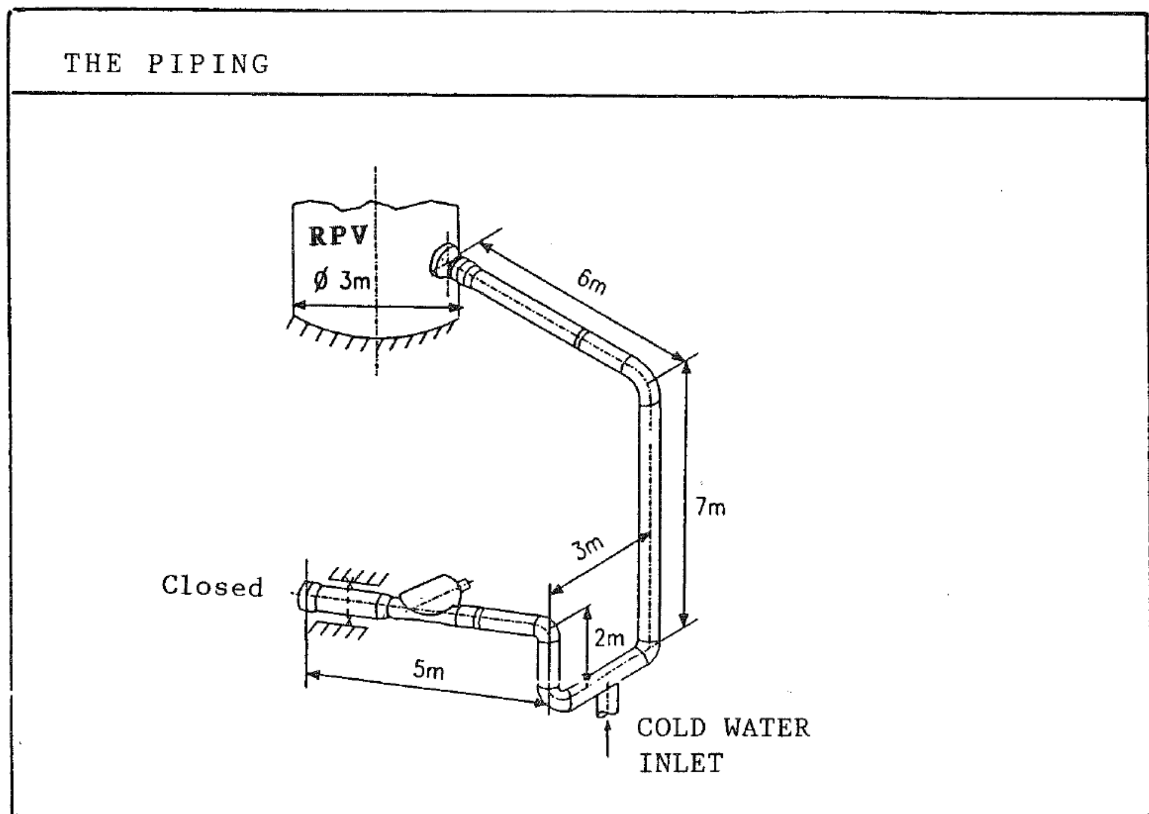| p (bar)	T_H (°C)	T_C (°C)	ρ_H (kg/m^3)	ρ_C (kg/m^3)	v (m/s)
22.4	214.0	54.5	848.3	987.0	0.104

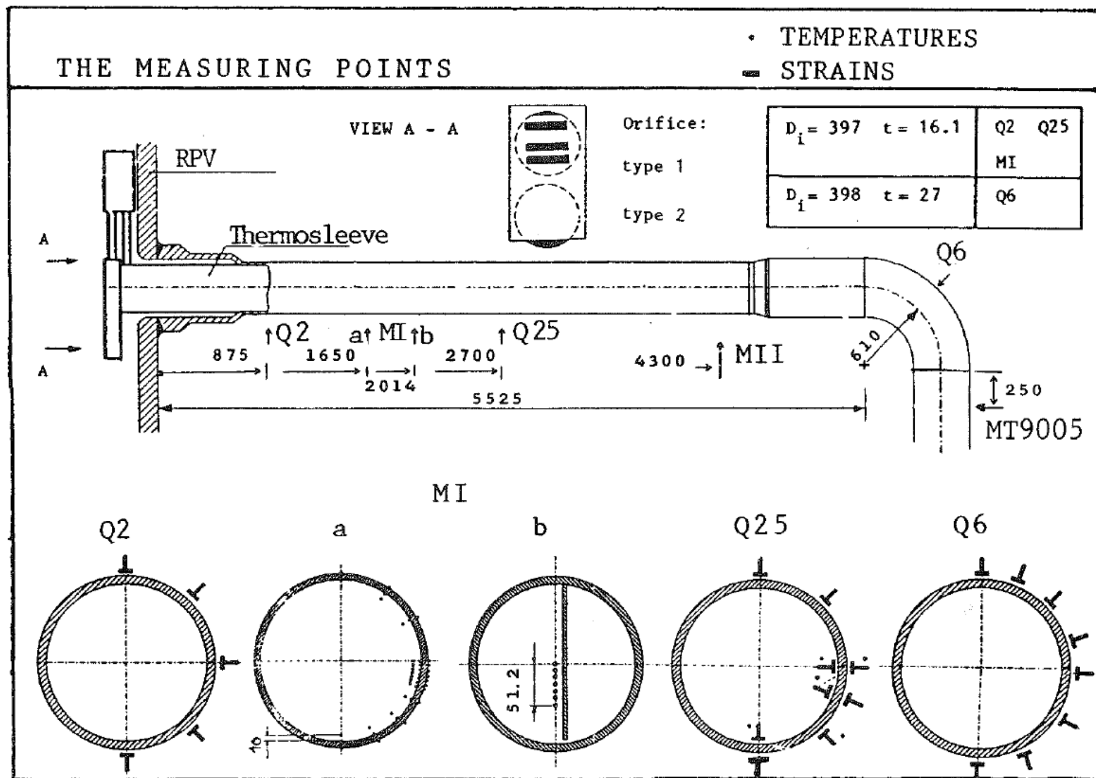*Figure 5: Geometry of HDR experimental setup (Talja 1988).*

Figure 6: Measuring points for HDR experiments (Talja 1988).

3.1 Modelling Approach

In terms of thermal stratification only the horizontal part of the test setup along with sufficiently large section of the first bend and pressure vessel are relevant. Therefore, in order to save computational resources, the numerical model is simplified to only consider these parts. This simplification procedure might lead into scenario where domain boundaries interact with the flow and produce inconsistent results. To exclude possibility of boundaries affecting the results the size of computational domain is extended in verification studies. Since the inlet boundary is defined into vertical part of pipe, the buoyant forces will naturally drive the flow into approximately constant cross-sectional velocity and temperature profile. This allows use of simple boundary condition assumptions without significantly affecting the results. Finally, since the model is symmetrical, only half of it will be modelled and symmetry conditions will be applied.

Even though flow velocities required for thermal stratification to occur are quite small, turbulent features are still present and there is a need for a turbulence model (OECD-NEA 1998). Cai et al. (2017) have studied applicability of Reynolds averaged turbulence methods for modelling of thermal stratification by comparing computed temperature profiles into experimental data. Their study demonstrated that Shear Stress Transport model (SST k-omeaga) provides solution with good agreement to experimental results, whereas k-epsilon and RMS models under and overshooted temperature values respectively. However, compared to k-epsilon model, SST k-omega model is significantly more demanding in terms of computational resources and numerical stability. Therefore, in this study both of these models will be used and their suitability compared.

The ability of solid pipe to store thermal energy influences fluid temperatures near the pipe. Consequently, the pipe acts as heat battery or sink and alters the flow behavior via buoyancy forces. Therefore, the conjugate heat transfer between fluid and solid should be modelled accurately as have been demonstrated by Cai et al. (2017). For the buoyant forces, temperature dependent density model is needed and in this study, Star-CCM+ build-in model for water properties, defined according to IAPWS-IF97 (1997), is used. Thermal properties of the bainitic steel, 15NiCuMoNb5 at 200 °C, pipe are 510 $\frac{J}{kg\,K}$ and 46.4 $\frac{W}{K\,m}$ for specific heat and thermal conductivity respectively (Schygulla 1986).

3.2 Case Setup

The heat transfer simulations are solved with Finite Volume Method. The numerical accuracy of Finite Volume solver is highly dependent on different aspects of case setup such as computation grid, boundary conditions and simulation models. Also the level of details included in the geometry may influence the obtained results. In the previous HDR simulations performed by Timperi (2008), fine details, including thickness variation and thermal sleeve, were modelled. However, the computational domain of this study is more simplified and only the main geometrical features are included. The validity of this simplification will be demonstrated later.

Discretization of the geometrical model into FV-mesh was done with the *directed mesh* utility of Star-CCM+ which allows creation of semi structured mesh. For this operation 2D mesh, presented in Figure 7, was defined and swept along the pipeline geometry. For the pressure vessel, similar approach was taken and the consistency in regards of cell size was ensured. The number of cells used at each region is shown in Table 2.

Table 2: Number of cells used in Finite Volume model.

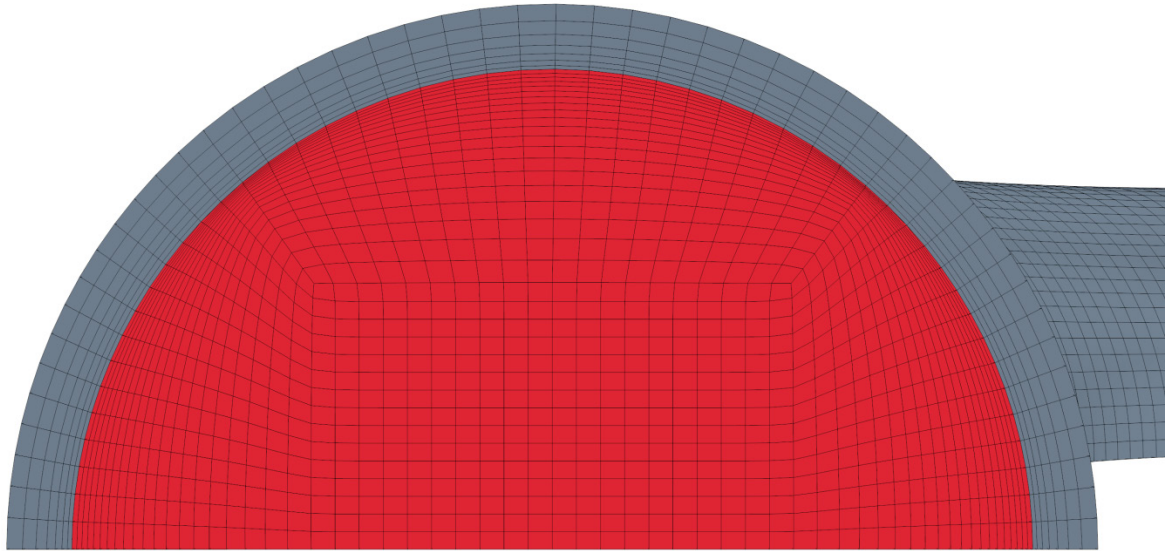|	Cells in 2D cross section	Number of cross sections	Number of cells
Pipeline: Fluid	1 300	300	390 000
Pipeline: Solid	350	300	105 000
Pressure vessel: Fluid	1 900	20	38 000
Pressure vessel: Solid	1 00	6	6 000
Totals	-	-	539 000

Figure 7: 2D cross-section of directed mesh in Finite Volume model.

Use of *Directed mesh* utility provides excellent control for meshing of swept geometries. This allows user to define consistent good quality mesh. Typically, mesh quality is realized from measures such as Cell quality, Volume change and Skewness angle. Threshold values for these quantities, in regards of code performance, are defined in Start-CCM+ user manual (CD-adapco 2018). The worst cell values of 0.259, 0.383 and 70 for Cell quality, Volume change and Skewness angle are clearly above these recommendations and therefore over all mesh quality is sufficient in terms of code performance. Overview of the mesh is presented in Figure 8.

From the modelling point of view, the domain includes four different boundaries. These boundaries are: Inlet of cold water, Outlet at pressure vessel end, solid-fluid interface and solid outer surface. Within these boundaries, the initial pressure was defined as uniform and *zero gradient pressure* condition was applied at the pressure vessel outlet. The velocity at solid-fluid interface was subjected to *no slip* condition with *Dirichlet boundary condition* at the cold fluid inlet. For temperature, *Dirichlet boundary condition* at the cold water inlet, perfect insulation with *Neumann boundary condition* (zero gradient) at the solid outer surface and conjugate heat transfer at solid-fluid interface were applied. Boundary condition are illustrated in Figure 9.
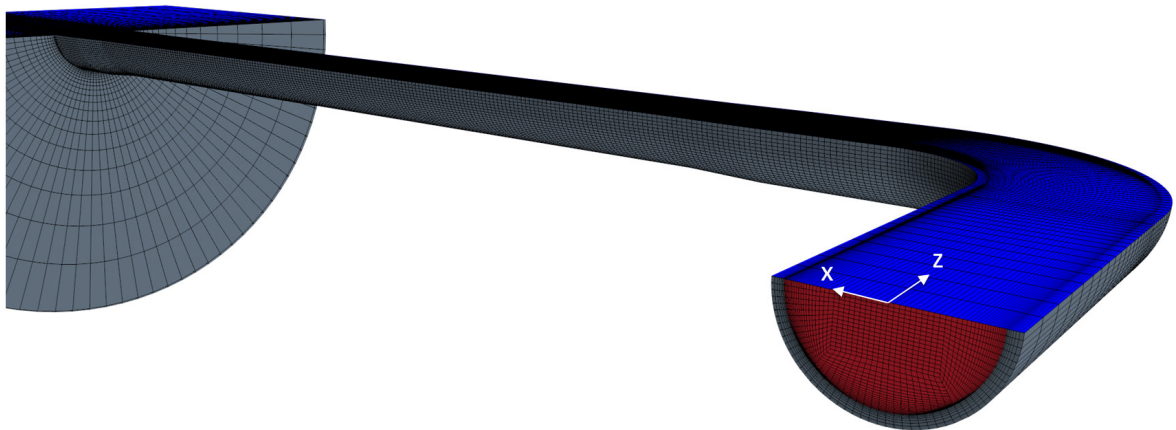

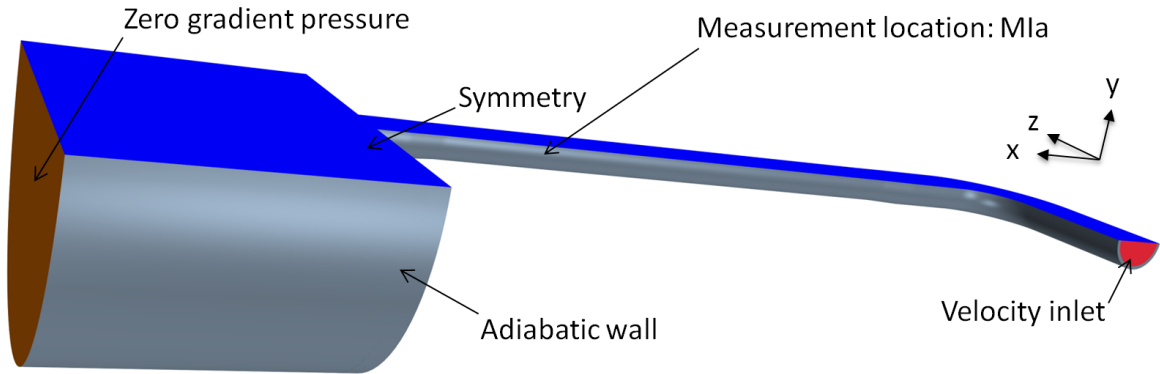*Figure 8: Overview of the computational domain for Finite Volume model.*

Figure 9: Boundary conditions for Finite Volume solver.

For the case setup, last important aspect is the selection of physical models. As the phenomenon of thermal stratification is highly dependent of buoyant forces and turbulent mixing, the choices of physical models are at high importance. For turbulence, *SST k-omega* and *Realiziable k-epsilon Two-layer* models were both used and at the near wall regions these were complemented with *All y+ wall treatment*. Star-CCM+ offers *segregated* and *coupled* solvers for Navier-Stokes equations, which both have their advantages. Computationally less expensive *segregated* solver is preferred choice for models where weak link between velocity and pressure is enough. However, in the modelling of stratification natural convection is the dominant feature and thus tight link is needed. Therefore, *coupled* solver with 2nd order temporal scheme and *implicit* time discretization was used. The number of iterations was set to 5 and size of time steps was defined by Star-CCM+ build in *convective CFL* and *energy* based controllers.

3.3 Verification

For CFD simulations verification of the results is of high importance. The outcome of simulation might be affected by poor convergence, bad mesh resolution and time step choices or unsound boundary conditions. Therefore, the objective of this section is to prove that results obtained here are numerically consistent.

Judging convergence of transient simulation requires considerably more effort compared to steady state simulation. For steady state model, solution is considered to be converged when both residuals and quantities of interest have reached asymptotic state. However, in transient simulations residuals fluctuate from one time step to another and the number of iterations needed for convergence might vary considerably. The default number of inner iterations in STAR-CCM+ is 5, which is sufficient for most of the cases. For this study, the number of iterations was determined by running the simulation with 10 iterations at the time instance featuring most significant changes in field variables. Largest changes are most likely to occur when cold water penetrates into horizontal pipeline, and thus that time instance was used. Based on this study, it was found that near asymptotic state is reached after 3-5 iterations and thus use of 5 iterations was adopted.

The next part of verification process is to ensure sufficient mesh resolution and time steps size. Both of these quantities have significant affect to the computational cost and should therefore be chosen as coarse as possible. For the time step control, Courant-Friedrichs-Lewy condition determines ratio between velocity, time step and mesh size. If CFL number is below unity, flow quantities are moving less than one cell per time step and the opposite is true for values above unity. Typically it is desired to keep CFL number below unity to ensure numerical stability. However, since implicit time integration scheme is used, larger steps may be taken with expense of accuracy in physical time. The default average CFL number for STAR-CCM+ time step control is 5. To check that sufficient time accuracy is reached, the simulation was run from start until time instance $t = 5$s, with neutral point set to the moment when cold water reaches cross section MIa (Figure 6). Fluid temperatures at the bottom of the pipe were then compared between runs and when sufficient CFL number was found, similar study was also conducted for mesh refinement.

Results for both time step and mesh dependency studies are presented in Figure 10. From Figure 10, it is clear that sufficient convergence have been reached for both time step and mesh resolution with values of 5 and 500 000 respectively. Based on the time step study CFL number could be increased. However, this was not possible due to numerical instability.
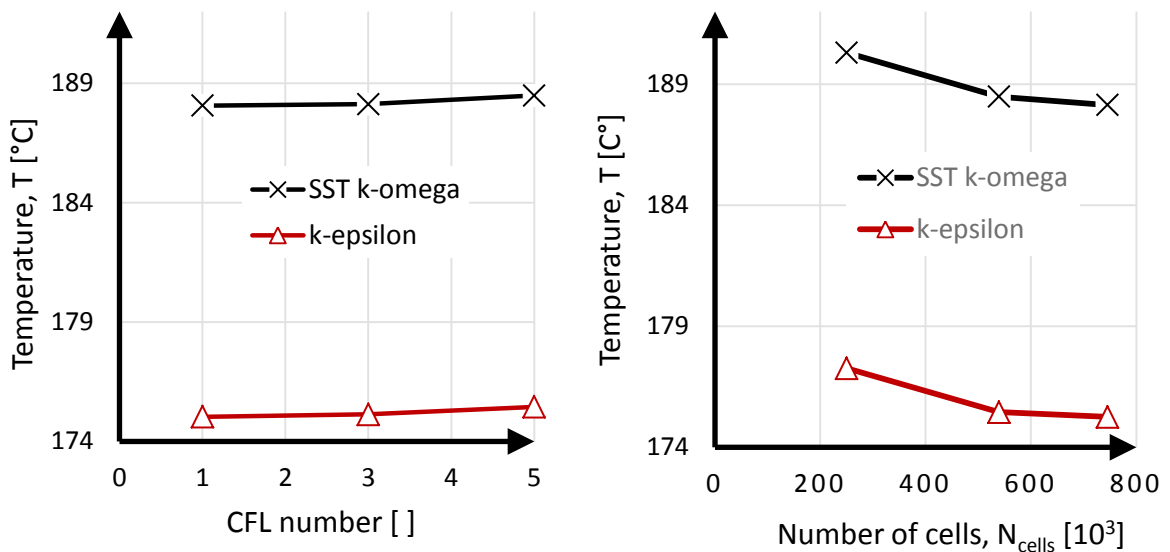

Figure 10: Study of time step and mesh dependency for Finite Volume solver.

Last part of the verification process is to study boundary conditions and their affect to the results. For example, if either inlet or outlet is defined too close, result will be altered. At the inlet, flow quantities are assumed to be close to uniform distribution and therefore no significant affect is expected from moving the boundary further away. Same can not be ruled for the outlet, for which too close proximity would influence pressure field and thus the whole solution. Therefore, outlet boundary was moved 0.5m furher away to ensure consistent results. Since early stages of the solutions were found to be unchanged, results were considered to be independent of boundary conditions.

Verification studies conducted here are relatively laborious, but if multitude of similar simulations will be performed optimizing these quantities is highly recommended. Even small increase in cell size will not only reduce computations needed during each iteration, but also increase the size of plausible time steps. This is because larger cells permit faster velocities for the same CFL number. In this study number of simulations performed is relatively small and thus no significant advantage would have been gained from the reduction of computational time. Therefore, only numerical consistency was studied. Based on this study sufficient consistency have been reached and the model is considered to be numerically sound.

3.4 Validation

Since simulation results were found to be numerically consistent, the last issue is to ensure that results agree with physical world. For example, choice of turbulence model may lead to fictitious results that might be numerically sound, yet have not much to do with actual thermal-hydraulic behavior. In this study, validation is performed by comparing results to those recorded at HDR facility.

In Figure 11 and Figure 12, simulation results are plotted together with HDR measurements. As can be seen, relatively large differences are found between numerical solution and experimental measurements. For the SST k-omega turbulence model, there is too much mixing between hot and cold regions, which is evident from the almost linear cross-sectional temperature profile in Figure 12. In contrast, k-epsilon model seems to give relatively accurate cross-sectional temperature distribution, but features almost $100\,°C$ temperature deviation for the development of temperature at $100°$ measurement point. This error can be reasoned with shifted mixing layer position. In HDR measurements, mixing layer is located at $94°$, whereas based on the k-epsilon model it would form into $100°$. Thus the solution obtained from the k-epsilon model appears to be relatively close to experimental values, with small exception on the mixing layer location. In the structural assessment of chapter 5 it will be shown that stresses induced by stratification are much less sensitive to deviations of mixing layer position compared to mixing layer height or maximum temperature difference. Therefore, k-epsilon model is considered to approximate real world with feasible accuracy and based on this study it should be used over SST k-omega model. Also, it can be noted that geometrical simplifications made, did not appear to affect the outcome of thermal-hydraulics. For more detailed validation, larger number of measurements locations and time instances should be investigated. However for this study, such information was unfortunately not available. Illustration of the flow and temperature fields for k-epsilon model are presented in Figure 13.
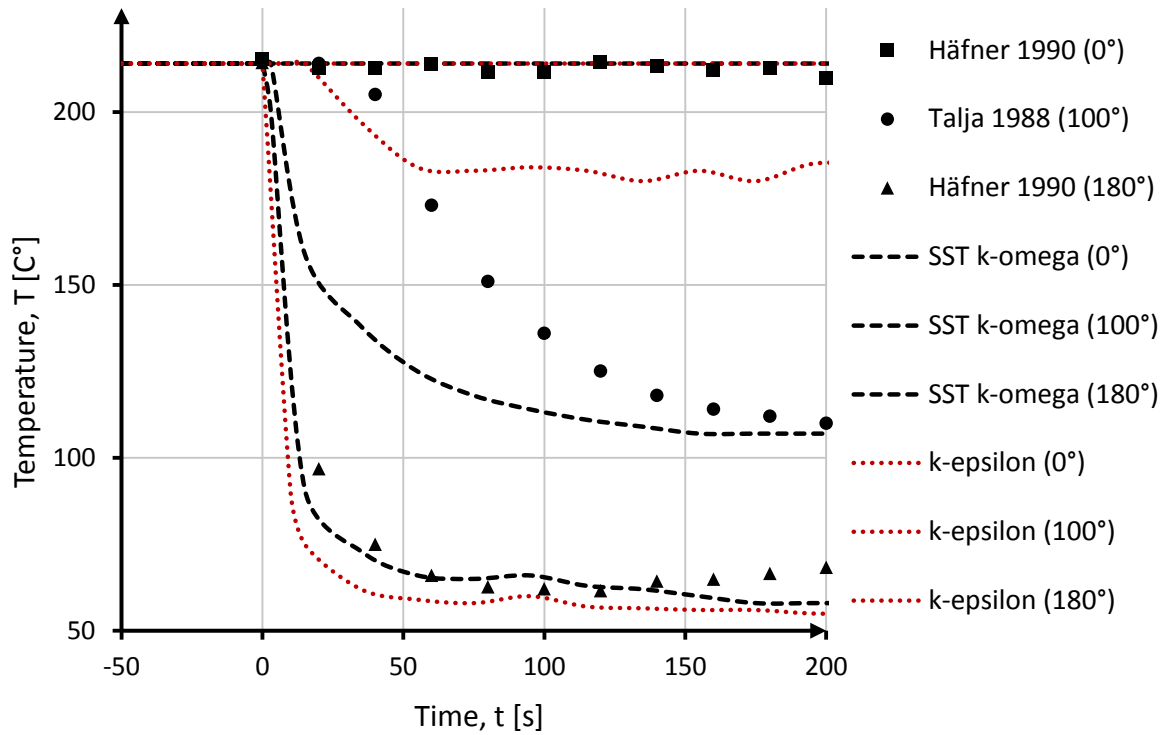
Figure 11: Validation of CFD simulation with results recorded at HDR facility.
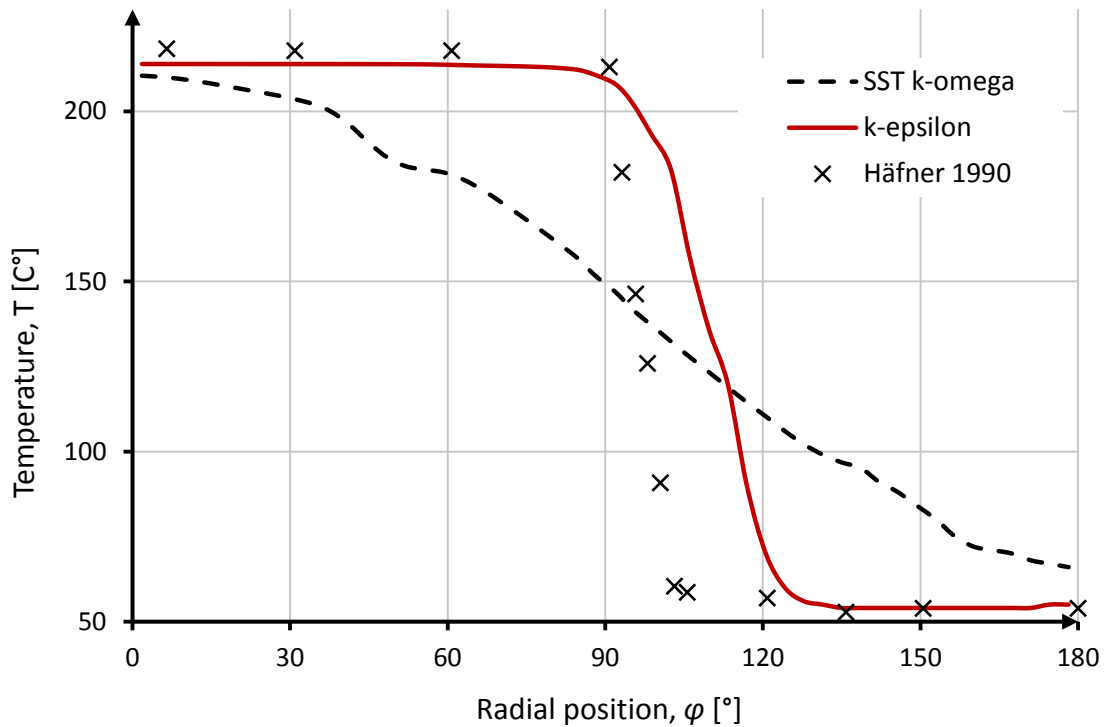

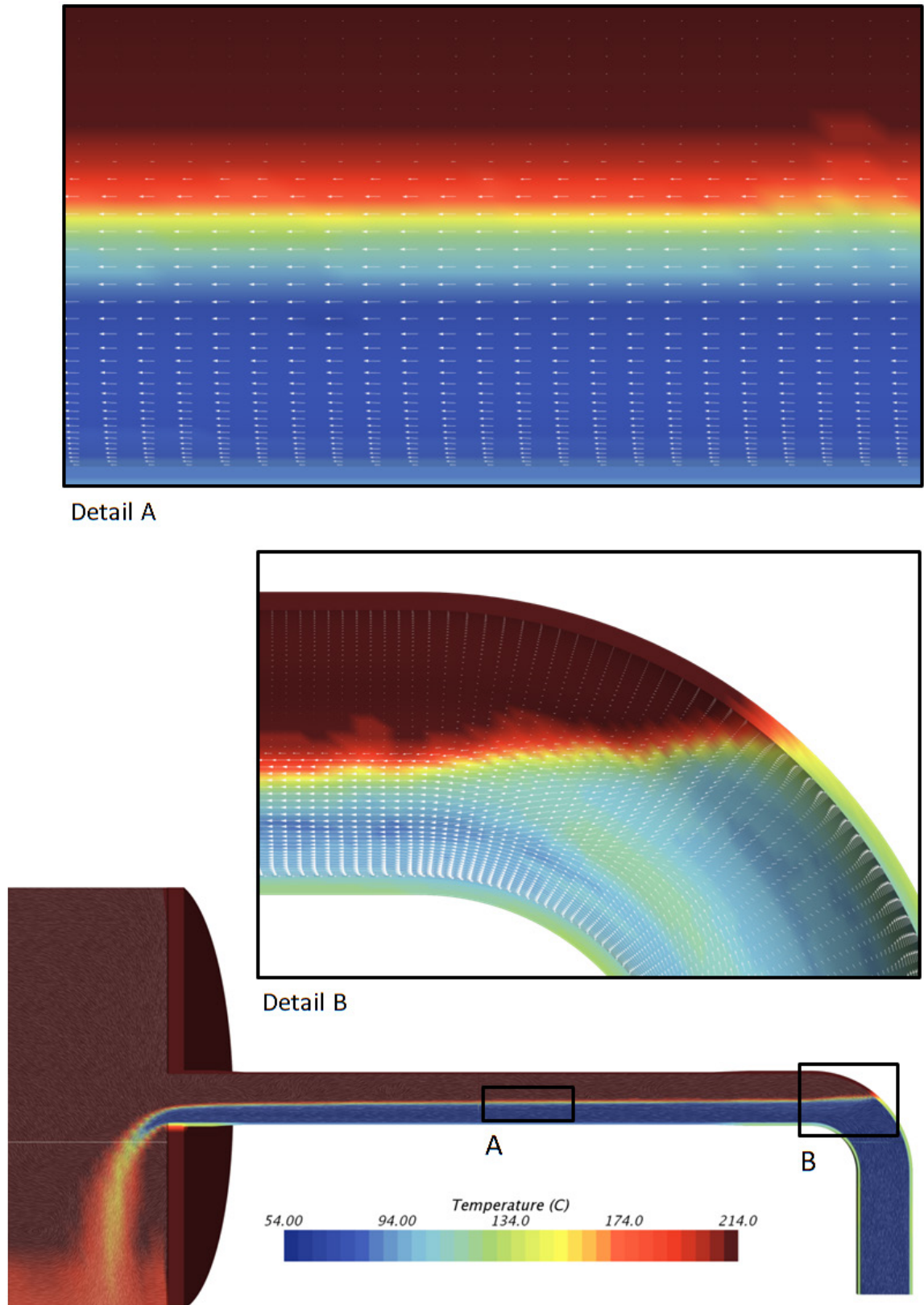*Figure 12: Q25 cross-sectional fluid temperature profile at t = 100s.*

Detail A

Detail B

Figure 13: Velocity and Temperature fields at t = 100s, k-epsilon model.

3.5 Simplified Models for Buoyant Forces

Numerical simulation of buoyancy driven flows with small velocities might pose stability issues, especially when long pipes are modelled. One significant source of instability is poor pressure field initialization, which often triggers unnatural convective flows. Instability of CFD simulations is closely linked into the complexity of model used to calculate temperature dependent fluid properties, such as density. The aim of this section is to study the accuracy of polynomial density and Boussinesq models for simulations where either enhance of numerical stability or reduction of computational cost is required.

In previous simulations, IAPWS-IF97 model was used to model density and other physical properties of water as function of both temperature and pressure. In STAR-CCM+, IAPWS-IF97 is the most realistic model for buoyant forces, but it is also most prone to diverge. To enhance numerical stability, complexity of buoyant force model can be reduced by only modelling changes in density and approximating it as polynomial function of temperature alone. In this polynomial model, Navier-Stokes equations are still solved fully and the only simplification is related to calculations of density changes. If even further simplifications are needed, the last option is to use boussinesq approximation. In Boussinesq approximation, changes in density are ignored in NS equations except when they are multiplied with gravitational acceleration. Essentially, this means that inertia driven buoyant forces are assumed to be negligible compared to those induced by gravity. In Boussinesq model, density differences are calculated based on volumetric expansion coefficient and it can be used for moderate temperature variations. (Bergman et al. 2011, p. 597-598)
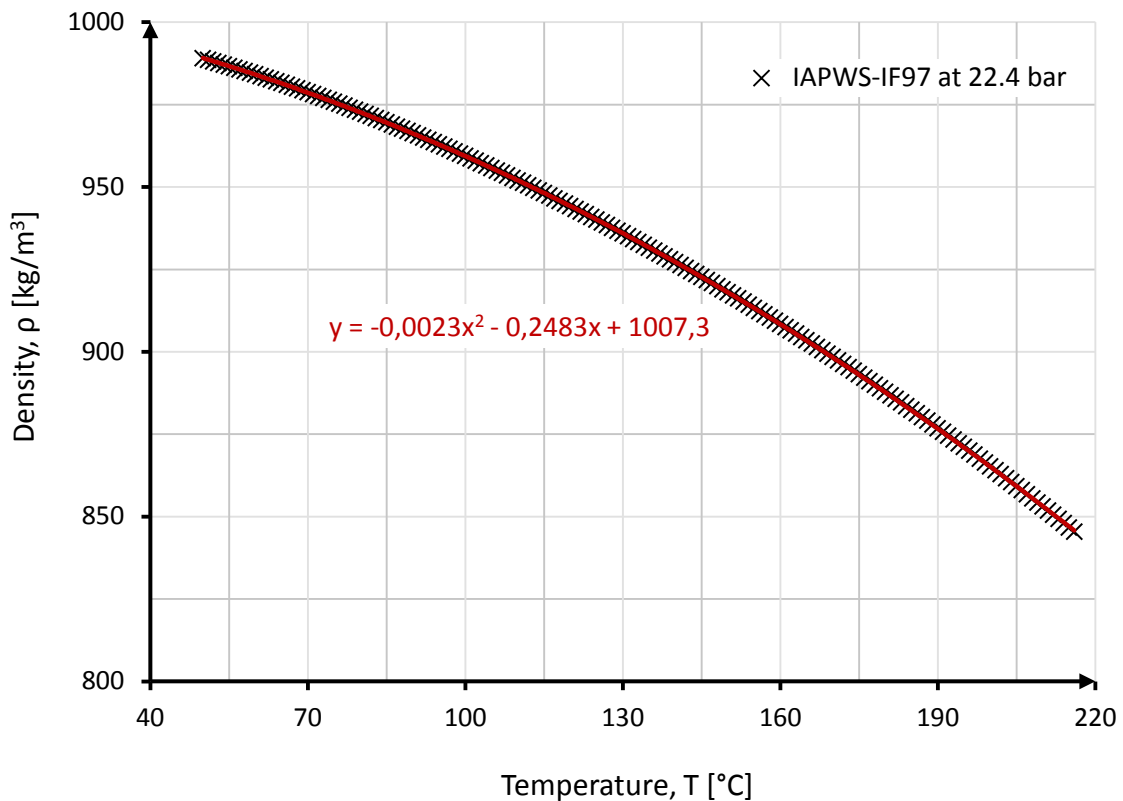

The plotted data is labelled "IAPWS-IF97 at 22.4 bar" and the fitted curve is $y = -0{,}0023x^2 - 0{,}2483x + 1007{,}3$. The axes are Density, ρ [kg/m^3] versus Temperature, T [°C].

Figure 14: Polynomial approximation of density variation at 22.4 bar (IAPWS-IF97 1997).
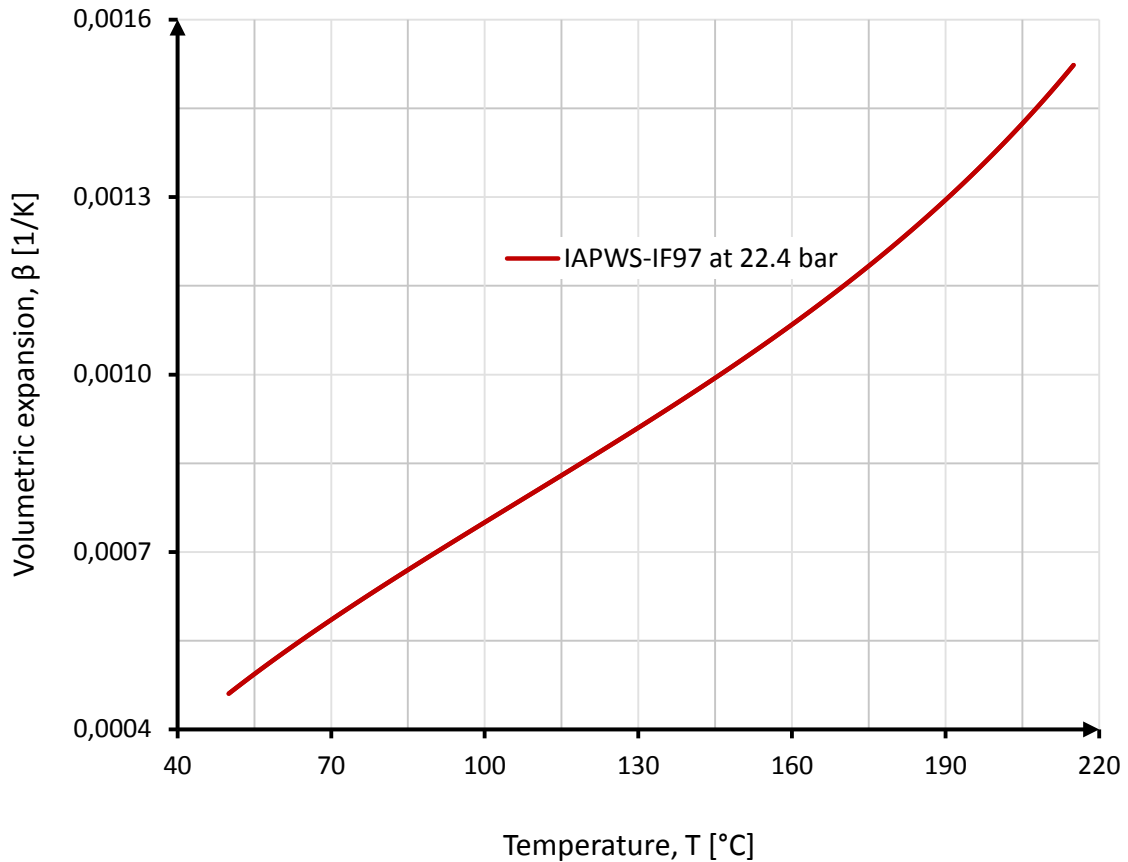
Figure 15: Volumetric expansion coefficient at 22.4 bar (IAPWS-IF97 1997).

To study the effect of density model simplification, polynomial density and volumetric expansions coefficients are defined according to IAPWS-IF97 (1997). They are shown in Figure 14 and Figure 15 respectively. Based on Figure 14, second order polynomial function appears to fit the density variation data and can thus be implemented into STAR-CCM+. Contrary, significant temperature dependency for the volumetric expansion coefficient is evident (Figure 15). Therefore, approximate value, $\beta = 0.001$ 1/K, is adopted. Finally, since the k-epsilon model was found to be more sufficient, it will be also applied in this study. Other model features are kept as before.

Validation results for all buoyant models are presented in Figure 16 and Figure 17. Based on Figure 16, in contrast to experimental measurements, clear pattern between model accuracy and simplicity is found. However, the same can not be ruled for the cross-sectional temperature profiles in Figure 17. In fact the opposite seems to be true. Yet another trend to be noticed is that the error between best fitted numerical solution and experimental measurements is larger than that between any pair of numerical solutions. Therefore, it could be argued that any of these models may be used for qualitative study on primary flow behavior and trends. For such conclusion, there should however be multiple studies and thorough investigation of flow, temperature and pressure fields at multiple spatial and temporal instances. Furthermore, based on STAR-CCM+ user guide (2018) accuracy of boussinesq model can not be ensured for temperature differences of this magnitude.
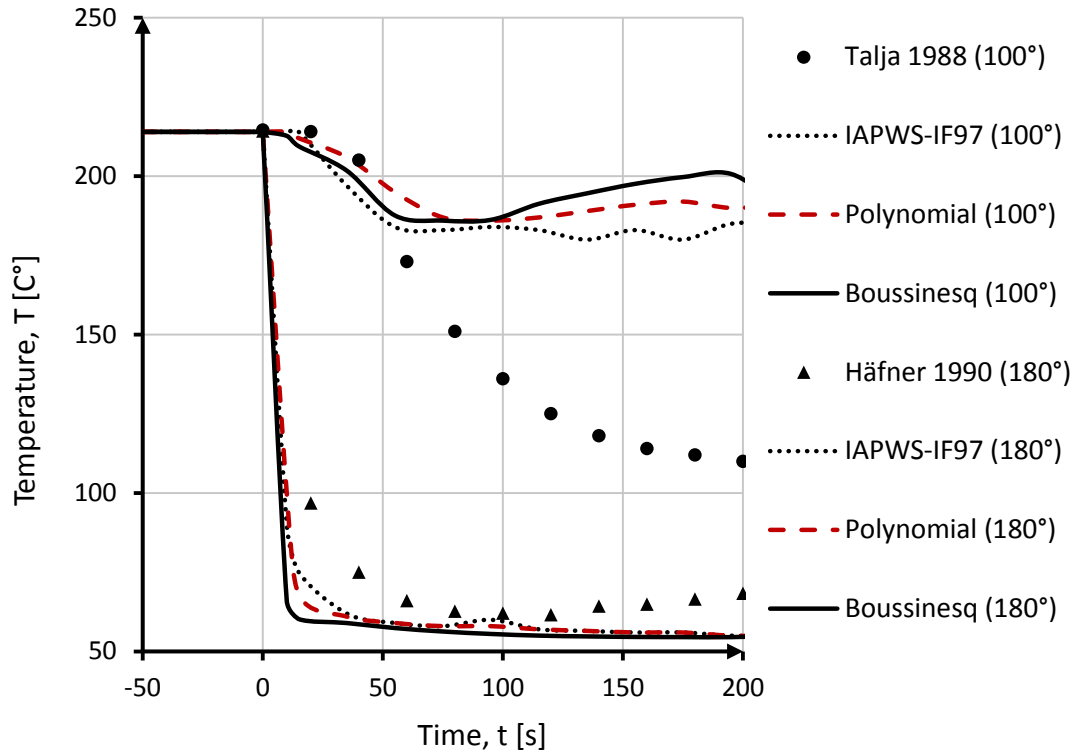
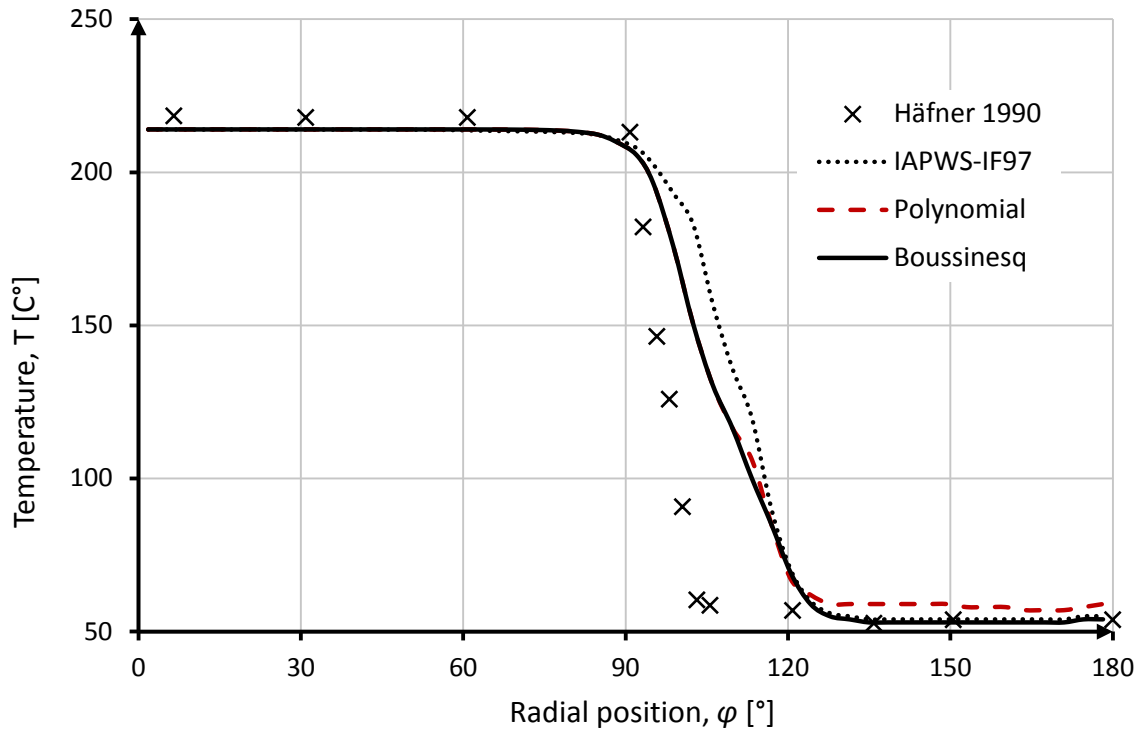*Figure 16: Temperature profiles for different buoyancy models.*

Figure 17: Q25 fluid temperature profile for different buoyancy models at t=100s.

4 Numerical Simulation of Thermal Stresses

The solution obtained from thermal-hydraulic model in preceding chapter can be further utilized as temperature load on solid stress calculations. Due to thermal expansion, the pipe geometry might undergo large deformations, which could affect flow patters and consequently alter thermal-hydraulic behavior. Modelling of such two-way linkage is computationally expensive since both models are solved simultaneously and thus parallel iterations are required. Therefore, in the following calculations the deformation of the pipeline due to thermal expansion is assumed to have negligible influence on the fluid flow. This assumption allows use of one-way interaction where heat transfer model is used only as input on structural model without feedback loop. Even thought this approach might appear to be drastic, similar assumption has been used also in other studies such as Kim et al. (2013) and Kang et al. (2011). The HDR experiment T33.19, used for validation of thermal-hydraulic model also includes measurements of structural response, which will be used to validate results obtained here for thermal stresses.

4.1 Modelling Approach

The approach chosen for solid stress modelling is relatively straight forward. The geometry for the solid stress model is identical to the solid part of the thermal-hydraulic model and the mapping of temperature load is handled by means of Star-CCM+ *data mapper* utility. Since the structural model is separated from the heat transfer model, previously used Finite Volume Method is replaced by Finite Element Method, as it is recommended and widely used in structural models. If the temperature input data from thermal-hydraulic model is available for each time step, one-way FSI linkage offers possibility of performing structural computations completely independently. This further enables running and optimizing the model in terms of aspects such as constraints and mesh refinement, with the expense of increased demand of memory needed to store temperature data for each time step. The alternative approach would be to solve structural model simultaneously with the heat transfer model. Since the models are solved simultaneously, current solution for temperature can be used for the solid stress model. This removes the need of extensive storing of temperature data. Considering the recourses available for this study, computational time is notably more limited than memory capacity. Thus saving temperature data until some extend was possible. Therefore, as compromise, temperature data was saved in intervals of 5 second. Furthermore, since only discrete instances of temperature history are stored, the structural model should be threated as series of static simulations performed in isolation of each other. This simplification from transient to static simulation is supported by the fact that temperature changes in solid are relatively slow and thus dynamic aspects are likely to be negligible.

The model will only consider thermal loads transported from thermal-hydraulic model, which means that other loads, such as internal pressure and gravity, will not be included. This is inline with measurements procedure followed in HDR experiments, where zero strain reference point was set to the time instance just before stratified flow reaches horizontal part of the pipeline (Talja 1988). Mechanical properties of the bainitic steel (15NiCuMoNb5) pipe used in the model are given in Table 3.

Table 3: Mechanical properties of 15NiCuMoNb5 at 220 °C (Schygulla 1986).

	E (GPa)	ρ (kg/m^3)	α (1/K)
15NiCuMoNb5	203	7850	$12.5 \cdot 10^{-6}$

4.2 Case Setup

For static structural simulations choice of element type, mesh resolution and constraints might have significant impact on results. The aim of this section is to present and give reasoning for modelling choices made during the case setup.

According to STAR-CCM+ user manual (CD-adapco 2018) use of hexahedral elements have multiple advantages over tetrahedral, wedged and pyramid elements including more compact stiffness matrix and higher accuracy for thin members under bending load. In STAR-CCM+ there are both linear (Hex8) and quadratic (Hex20) elements available. Quadratic elements have more degrees of freedom and are therefore typically more accurate than linear elements. However, increase in accuracy comes with the downside of increased degrees of freedom and thus computational cost. For thermal stresses, stress variations are likely to be moderate and therefore use of linear elements should provide sufficient accuracy. In this study Hex8 elements will be used and their suitability will be verified in section 4.3.

The mesh resolution needed for sufficient accuracy is closely linked into element type used. In general, more linear elements are needed for the same accuracy that is obtained with quadratic elements. Similarly fewer hexahedral elements are needed in contrary to tetrahedral elements. As for the thermal-hydraulic model, the mesh generation is once again carried out with STAR-CCM+ *directed mesh* utility. For the pipeline, 7, 50 and 300 elements are used in thickness, radial and axial directions respectively. Illustration and details for the mesh are given in Table 4 and Figure 18.

Table 4: Number of elements used in Finite Element model.

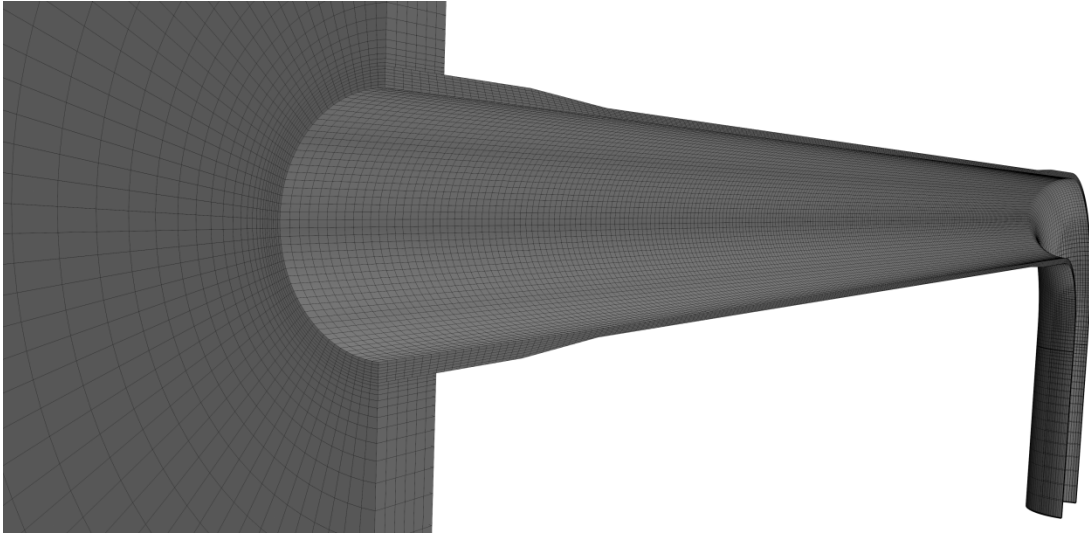|	Elements in 2D cross section	Number of cross sections	Number of elements
Pipeline	350	320	112 000
Pressure vessel	1000	6	6 000
Totals	-	-	118 000

Figure 18: Overview of the computational domain for Finite Element model.

In section 2.4, it was noted that thermal stresses can be divided into external and internal stresses according to their origin. Setup used in the HDR facility certainly poses restrictions for thermal expansion and thus both internal and external stresses will arise. Finding the exact support configuration is a difficult task that would require multiple runs and adjustments to constraints accordingly. Therefore, for this study alternative path is taken and extremes are modelled by selection of lightly constrained and fully constrained conditions. In all of these conditions, all degrees of freedom are restricted on the outer edge of pressure vessel, whereas Fixed, Slider or Free supports is defined at the pipe inlet (Figure 19 and Appendix 1). Zero thermal strain temperature is set to the initial temperature of 214 °C. This choice will pose unrealistic thermal stresses into constrained pipe inlet as the cross section is not allowed to expand. However, according to Saint-Venant's principle stress peaks will redistribute, and if the results are collected sufficient far away, stress field should not be influenced.
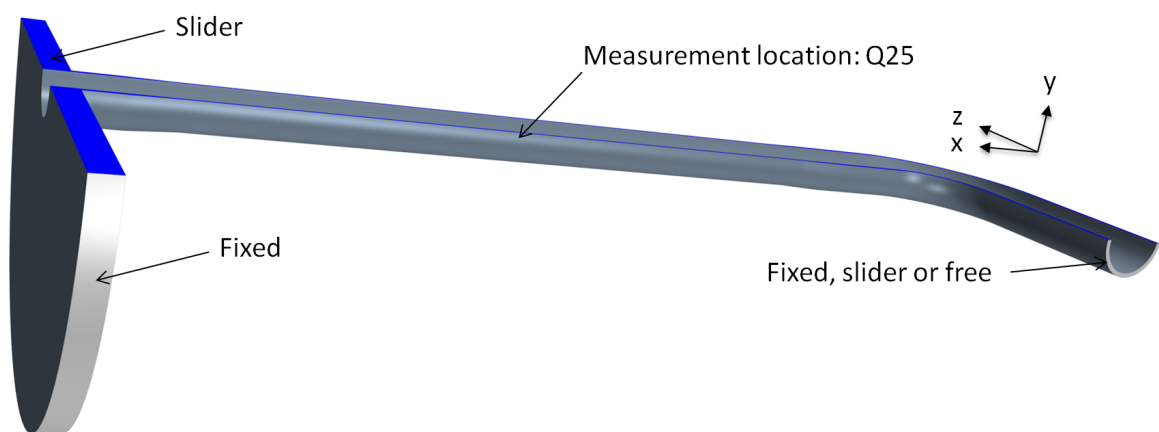

Figure 19: Mechanical constraints for Finite Element solver.

4.3 Verification

Numerical consistency of the structural model is ensured with combination of mesh refinement, element type and iteration convergence studies. Mesh refinement and element type studies are conducted only for the most severe time instance, where as convergence of solver residuals is confirmed for each static simulation.

If mesh resolution is gradually increased, results should approach state of convergence. Preferably simulations should be run with as coarse mesh as possible for efficient calculations and therefore gradual refinement was applied to define this resolution. Time instance of 200 *s* was selected for this study as it contains largest temperature differences and thus most likely requires finest resolution. Results for maximum stresses at cross-section Q25 (Figure 19) are shown in Figure 20 for both Hex8 and Hex20 elements. Based on this study, total of 118 000 elements is found to be sufficient for linear Hex8 elements. Results are also found to be consistent with those obtained for quadratic Hex20 elements.
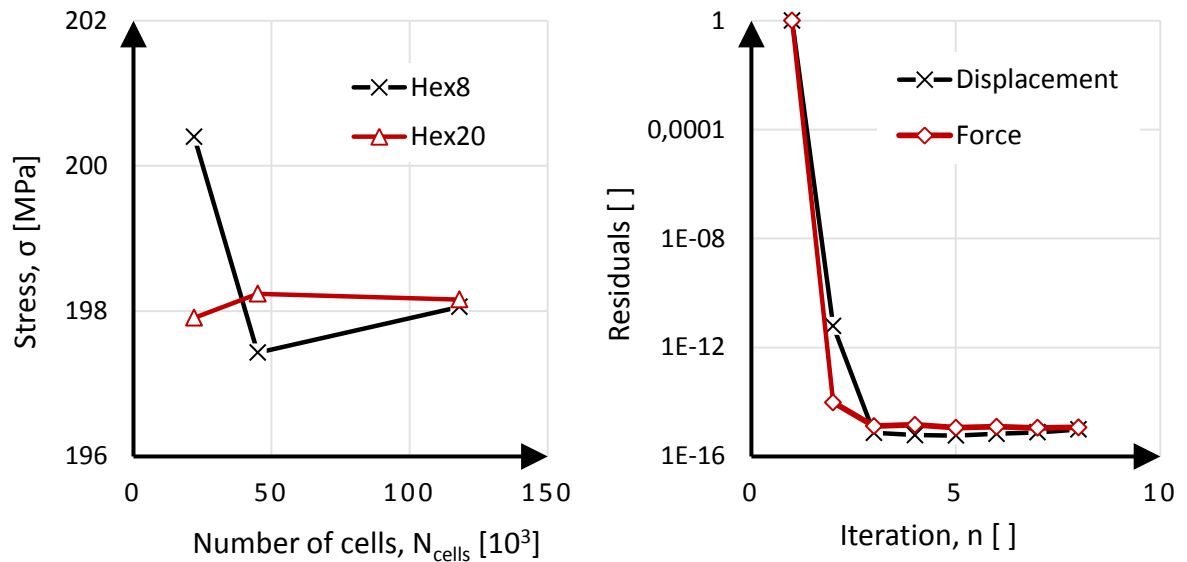

Figure 20: Mesh refinement and convergence at t = 200s for FE solver, Fixed support.

The last part of the verification of structural model is to ensure that solver has converged. In general, convergence is assumed to be reached when asymptotic line is normalized for both solver residuals and quantities of interest. For this study, convergence is ruled based on displacement and force residuals, and maximum stress at cross-section Q25. In Figure 20, convergence for time instance 200s is realized. Similar fulfilment will be required for all static simulations.

4.4 Validation

Since the structural response obtained from the Finite Element solver was found to be numerically consistent, the next step is to ensure validity. In Talja (1988), stresses have been extracted from strain gauge measurements. These values are presented for cross-section Q25 at time instance of 200s. The validity of structural model is studied here by comparing simulation results into those values.

In Figure 21, FEM solution is presented for three different support conditions at pipe inlet. The results are found to be fairly close to the experimental values when slider support condition is applied. Furthermore, as could be expected, minor over shooting is obtained with conservative fixed support, and relatively large under shooting with free support. The exact constrain conditions are therefore realized somewhere between these two extremes and slider constraint seems to simulate this conditions with feasible accuracy. From Figure 21, it should also be noted that compared to the HDR experiment stress peaks for the FEM solutions are slightly shifted. Since similar shift was also evident for the location of stratification layer, this behavior is caused by the error induced during thermal-hydraulic calculations. This shift was presented earlier in Figure 12 of section 3.4, where the cross-sectional temperature profile was compared to experimental data. The FEM model is therefore found to be sufficiently accurate for assessment of thermal stresses induced into horizontal pipelines due to thermal stratification. As it was previously noted during validation of thermal-hydraulic model, if available, larger quantity of experimental data should have been used also for the validation of the structural model. Deformed geometries and temperature profiles for different support conditions are presented in Figure 22.
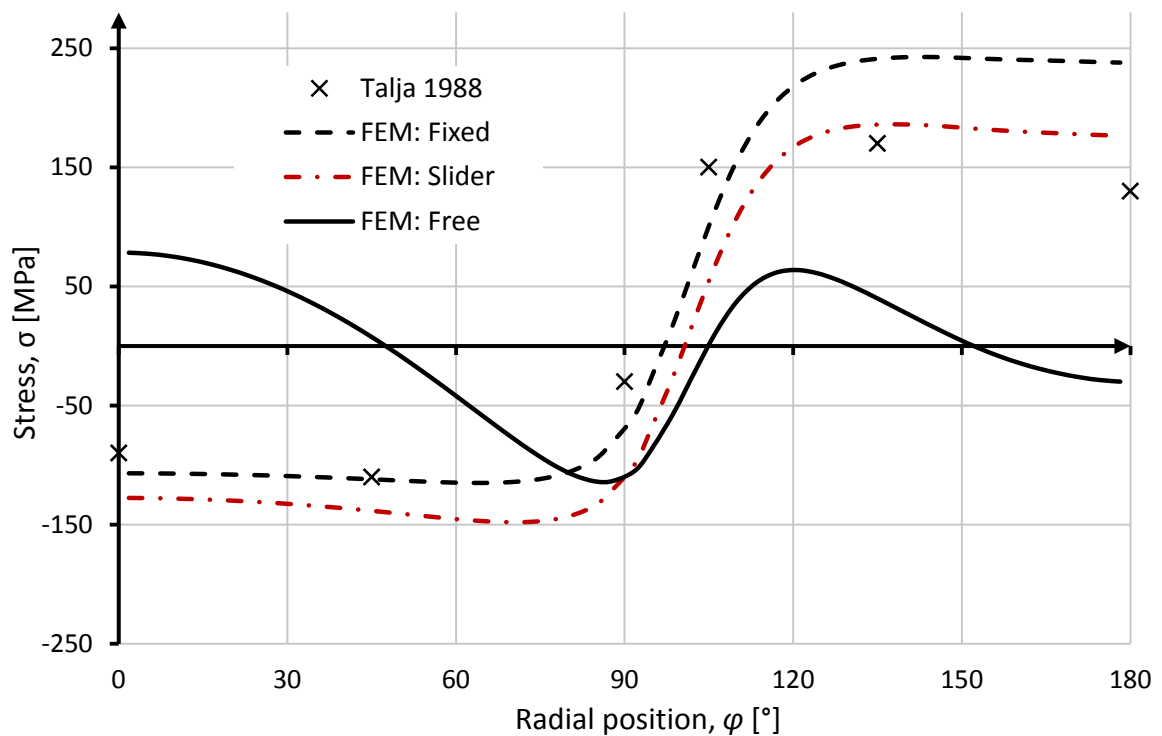

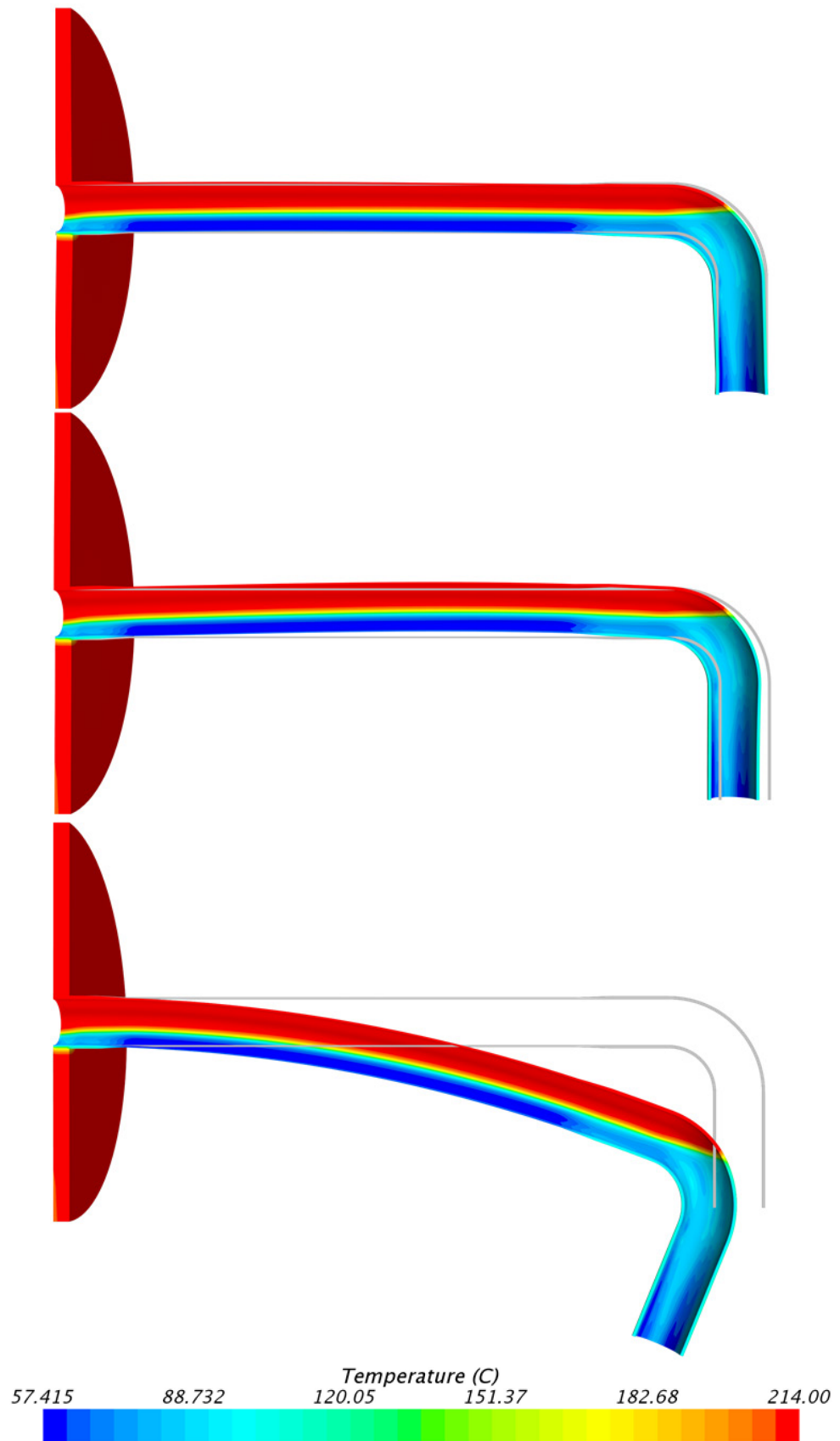*Figure 21: Stresses at outer surface of cross-section Q25 at t = 200s.*

Figure 22: Deformed geometries and pipe temperature at t = 200s for fixed, slider and free supports at cold water inlet, Displacements scaled with factor of 10.

5 Methods for Quick Assessment

Practical aspects, such as time and resources, often limit or even exclude the use numerical simulation for the assessment of thermal stratification. Moreover, rationalizing simulation results from complex multiphysical phenomena is often no easy matter. To address this issue, methods for quick assessment have been gathered up into this chapter.

Methods presented here will mainly focus on technique of temperature profile decomposition, which was earlier displayed in section 2.4 and reillustrated in Figure 23. In addition, alternative formula for simply supported pipe will be derived and consideration of random temperature fluctuations given. The only type of stresses typically associated with thermal stratification not considered here are tangential stresses. Tangential stresses originate from light bulb shaped deformation of the pipe cross-section. This is caused by expansion of the upper pipe segment and contraction of the lower one. Multiple publications, including Talja (1988) and Kumar et al. (2014), have shown that the magnitude of tangential stresses is notably smaller than axial stresses. Therefore, assessment of these stresses have been excluded from this thesis. The formulas presented hereafter are based on assumption of linear mixing layer between hot and cold regions (Figure 24). Based on the temperature distribution obtained from HDR simulations, this assumption is proven to be relatively accurate approximation of the actual temperature profile.
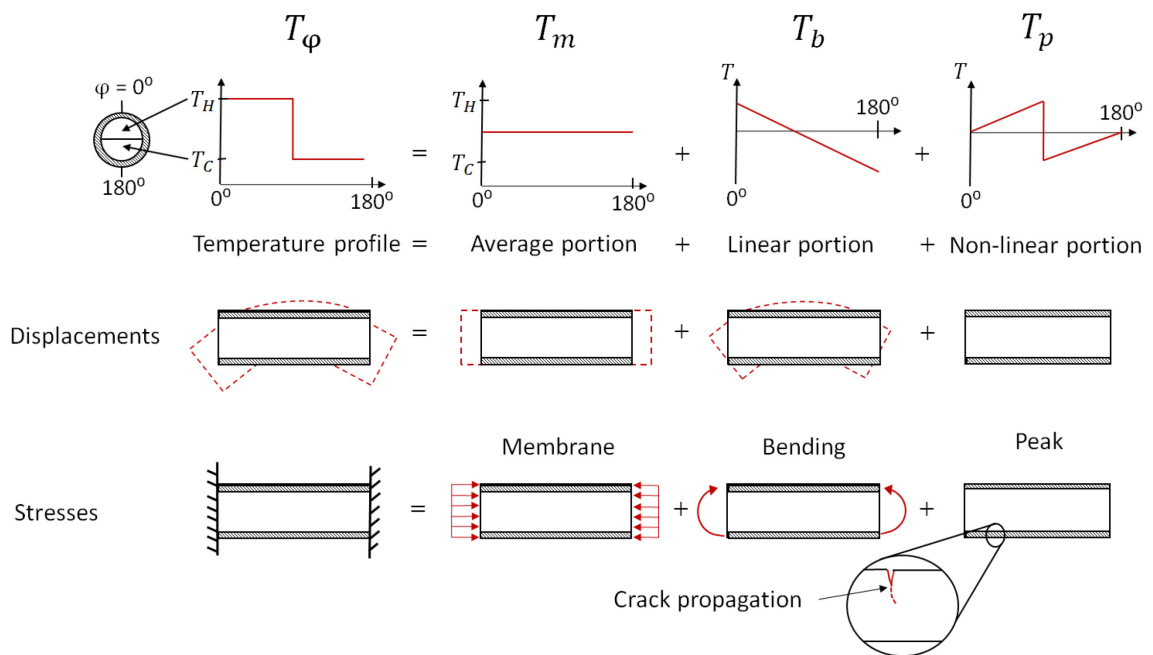

Figure 23: Decomposition of stratified temperature profile (Hautala 2017).

5.1 Decomposition method

In decomposition method stresses are calculated based on decomposed temperature profile and idealized stresses. In this section calculation of membrane, bending and peak stresses are presented. The overall stress state is the sum of these components.

5.1.1 Membrane Stresses due to Average Temperature Portion

The first set of stresses in the decomposition method are membrane stresses. Calculation of membrane stresses is straight forward and follow law of thermal expansion. If longitudinal expansion is fully restricted stresses are computed from (Santaoja 2017, p. 78)

$$\sigma_m = \pm E\alpha T_m \,, \tag{6}$$

where plus sign is used if reference temperature $T_0 = T_H$ and minus if $T_0 = T_C$. T_m is the average portion of temperature profile. It is defined as (ASME 2007)

$$T_m = \frac{1}{l} \int_{-l/2}^{l/2} T(y)\, dy \,, \tag{7}$$

where l is the wall thickness and $T(y)$ is the temperature profile as function of position. For piecewise linear temperature profile and curved geometry, integration of average temperature simplifies into

$$T_m = \frac{(T_H - T_C)(\varphi_1 + \varphi_2)}{2\pi} \,, \tag{8}$$

where φ_1 and φ_2 are the radial position of mixing layer upper and lower limits respectively in radians. T_H is the tempeture at upper region and T_C is the temperature at lower region. These quantities are illustrated in Figure 24.
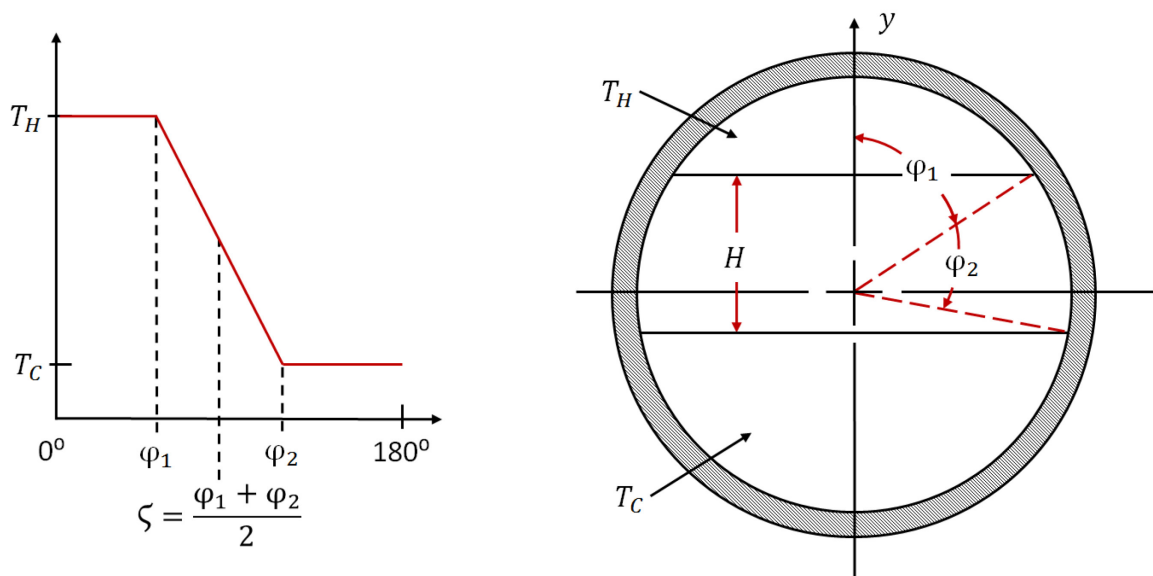

Figure 24: Mathematical formulation of stratified temperature profile.

5.1.2 Bending Stresses due to Linear Temperature Portion

The second set of stresses in the decomposition method are bending stresses. These stresses are related to linear temperature profile with zero average value. Linear temperature variation is given by (ASME 2007)

$$V = \frac{12}{l^2} \int_{-l/2}^{l/2} y \, T(y) \, dy \,. \tag{9}$$

When piecewise linear temperature profile assumption is applied, variation simplifies into

$$V = \frac{(T_H - T_C)(4\varphi_2^2 + 4\varphi_1\varphi_2 - 6\varphi_2\pi - 2\varphi_1^2 + 3\pi^2)}{\pi^2} \,. \tag{10}$$

Temperature profile and bending stresses associated with variation V are then given by

$$T_b = \frac{V}{2} - \frac{\varphi}{\pi} \cdot V \tag{11}$$

$$\sigma_b = \pm \frac{4E\alpha \cos(\varphi) \, V}{\pi^2} \,, \tag{12}$$

where plus sign is used if $T_0 = T_H$ and minus if $T_0 = T_C$. Validation of formulas for membrane and bending stresses are done with comparison of results into finite element code (STAR-CCM+). Membrane and bending stresses are extracted by subtracting FEM results for cantilever beam from pipe with both ends fixed (Appendix 1). In the case of cantilever beam, there are no restrictions for thermal expansion and thus only internal stresses are induced. When both pipe ends are fixed also external stresses are induced and thus desired stresses can be extracted based on superposition. FEM model and initial conditions are same as those presented in Appendix 2, for the validation of alternative formula presented in section 5.4. Similarly, derivation of σ_b follows steps analogous those presented in Appendix 2. As can be seen from Figure 25, correlation between stresses calculated with decomposition method and FEM is found to be evident.
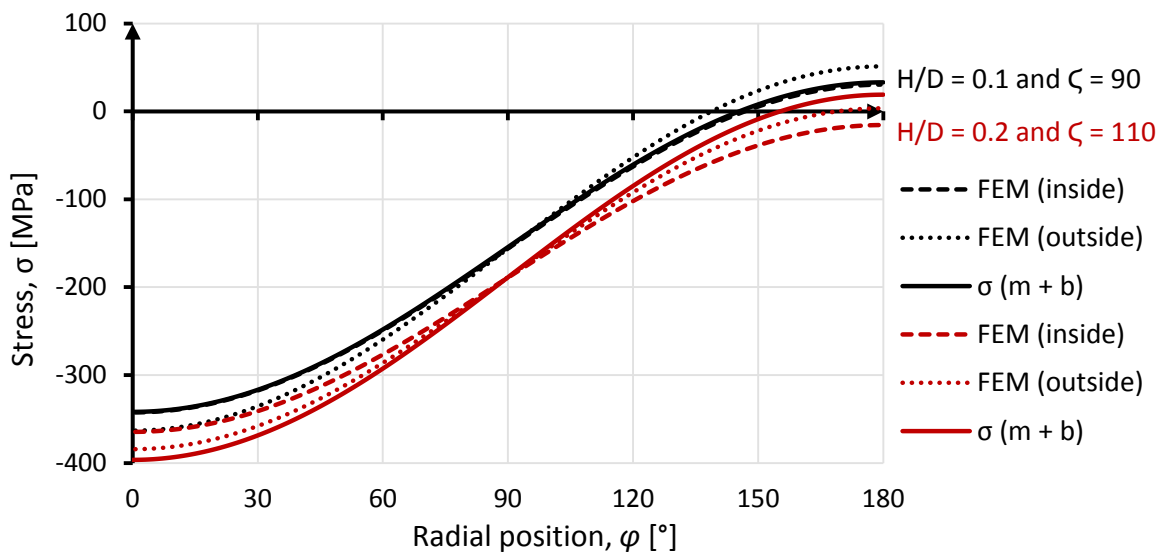

Figure 25: Membrane and bending stresses according to decomposition method and FEM.

5.1.3 Peak Stresses due to Nonlinear Temperature Portion

In addition to global membrane and bending stresses, stratification also induces peak stresses, which are the third and last set of stresses in the decomposition method. These are generally considered as stresses that remain after idealized global stresses are extracted from the true stress state. Multiple formulas have been proposed for evaluation of peak stresses, including Kumar et al. (2014), Kweon et al. (2008) and Bieniussa and Reck (1999). These have been compared in previous work (Hautala 2017). Based on that study, formulas from Kumar et al. (2014) and Kweon et al. (2008) are considered here since they were found to be most suitable.

According to Kweon et al. (2008) peak stresses can be evaluated from

$$\sigma_p = \left(0.1174\frac{D_i}{D_{ref}} - 0.4606\frac{t}{D_{ref}} + 1.5003\right)E\alpha T_p \,, \tag{13}$$

where $D_{ref} = 254$ mm and nonlinear portion of temperature profile T_p can, if needed, be approximated with

$$T_p = \left(0.0871 + 0.7455e^{-3.6474\left(\frac{H}{D_i}\right)}\right)\Delta T_3 \,. \tag{14}$$

For convenience, charts for nondimensional effectiveness factors n_1 and n_2 may also be utilized (Appendix 3)

$$n_1 = 0.1174\frac{D_i}{D_{ref}} - 0.4606\frac{t}{D_{ref}} + 1.5003 \tag{15}$$

$$n_2 = T_p = 0.0871 + 0.7455e^{-3.6474\left(\frac{H}{D_i}\right)} \,. \tag{16}$$

The other formula, given by Kumar et al. (2014), is defined as

$$\sigma_p = n_2 E\alpha T_p \,, \tag{17}$$

where effectiveness factor n_2 is found at Appendix 3 or calculated from

$$n_2 = 1.218 - 2.847\left(\frac{H}{D_m}\right) + 4.16\left(\frac{H}{D_m}\right)^2 - 2.531\left(\frac{H}{D_m}\right)^3 \,. \tag{18}$$

If $T_0 = T_H$ is chosen as reference temperature, additional minus sign will be introduced to formulas of σ_p. Validation of these formulas is once again done by means of FEM model and since only internal stresses are now considered, cantilever beam is used. Based on Figure 26 and Figure 27, qualitative correlation is realized in comparison to FEM results. However, Kweon et al. (2008) is found to overshoot mixing layer values and undershoot boundary values, whereas more precise results where obtained with Kumar et al. (2014). Therefore, use of Kumar et al. (2014) is adopted hereafter with notion that some degree on nonconservatism might exist.
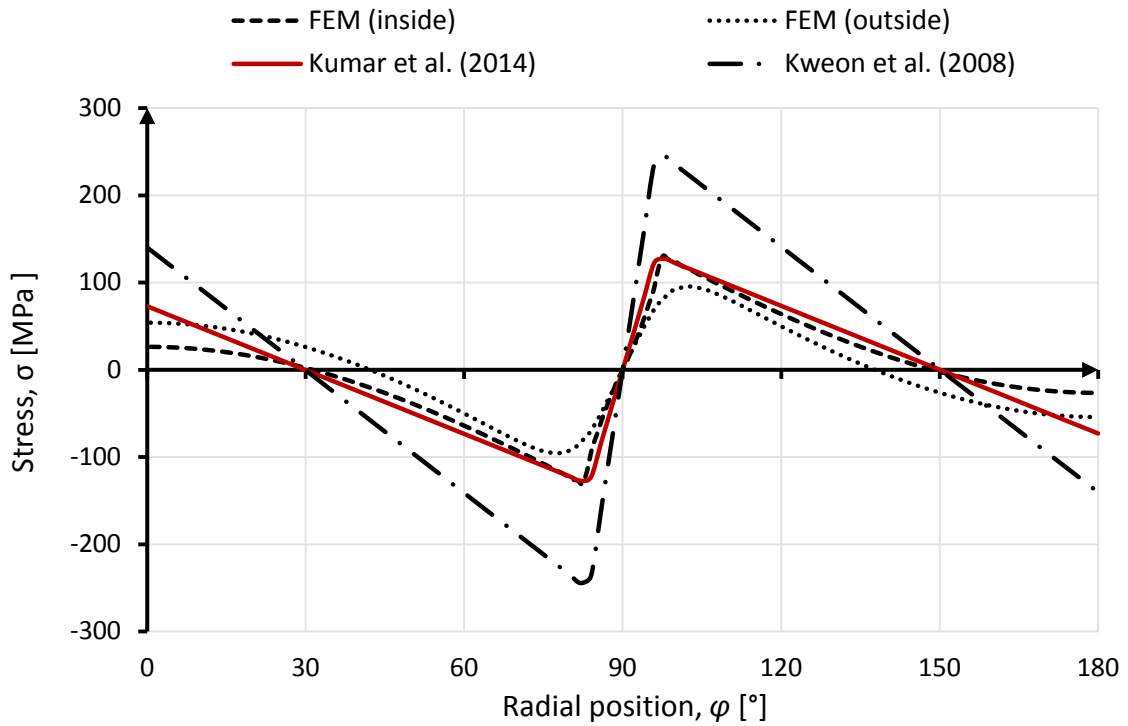
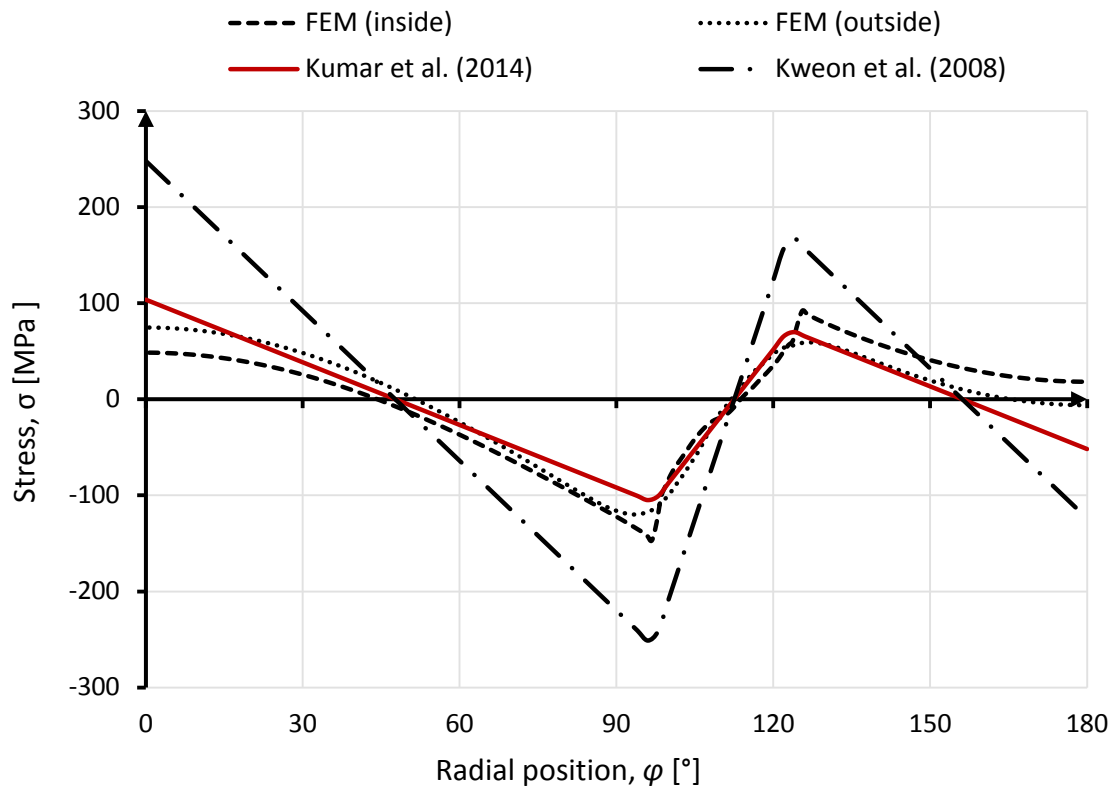*Figure 26: Peak stresses according to simple formulas and FEM, H/D = 0.1 and ς = 90°*

Figure 27: Peak stresses according to simple formulas and FEM, H/D = 0.2 and ς = 110°

5.2 Thermal Bowing Method for Simply Supported Pipes

In addition to the decomposition method presented in previous sections, alternative method suitable for analysis of simple supported pipes will be described here. This method, referred as thermal bowing method, is derived based on analytical formulas.

Pipelines subjected to stratified temperature loads are not solely limited to nuclear engineering. For example, these are typical design loads for cryogenic process pipes that are used as partially filled. Barron and Barron (2011) have derived formulas for stresses in thin-walled cryogenic pipelines under these circumstances. Similar derivation may also be adopted for typical stratified temperature profiles occurring in PWR surge lines. To maintain fluent progression, detailed derivation of stress distribution is bypassed here and presented in Appendix 2. Stresses induced into simply supported (Appendix 1) straight pipelines are formulated, with following approximations and assumptions, as

1. Pipe is considered to be thin-walled ($t \ll D$)
2. Pipe inside and outside temperatures are equal
3. Piecewise linear temperature load (Figure 24)
4. Material properties are independent of temperature

$$\sigma = \sigma_m + \sigma_b = \frac{F_T}{A} - \alpha E \Delta T(\varphi) + \frac{M_T y}{I} \tag{19}$$

$$\sigma_m = \frac{\alpha E \Delta T_3}{\pi}\left(\varphi_1 + \frac{\varphi_2 - \varphi_1}{2}\right) - \alpha E \Delta T(\varphi) \tag{20}$$

$$\sigma_b = \frac{2\alpha E \Delta T_3}{\pi}\cos(\varphi_1)\left(\sin(\varphi_1) - \frac{\cos(\varphi_1) - \cos(\varphi_2) + \varphi_1 \sin(\varphi_2) - \varphi_2 \sin(\varphi_2)}{\varphi_1 - \varphi_2}\right), \tag{21}$$

where α is the thermal expansion coefficient, E is the Young's modulus and I is the area moment of inertia. F_T and M_T are the force and moment due to thermal expansion. Temperature difference $\Delta T_3 = T_H - T_C$ and $\Delta T(\varphi)$ is defined as deviation from reference temperature $T_0 = T_C$ as function of radial position. If T_H is chosen as the reference temperature, additional minus should be introduced to the obtained stresses and radial locations should be flipped around at the end of calculations. Quantities of stratification location, φ_1 and φ_2, are illustrated in Figure 24. In this formulation, peak stresses present in the decomposition method are included in membrane and bending stresses.

The stress extremes will occur at the ends of mixing layer, at φ_1 and φ_2. This notion allows plotting of maximum and minimum stresses as function of mixing layer location. Since it is often more convenient to describe mixing layer as function height H and central position $\varsigma = (\varphi_1 + \varphi_2) / 2$, these two are utilized in Figure 28, where nondimensionalized stress extremes are plotted. If only maximum and minimum stresses are concerned, calculation of equation 19 can be simplified by scaling nondimensional stress values accordingly.
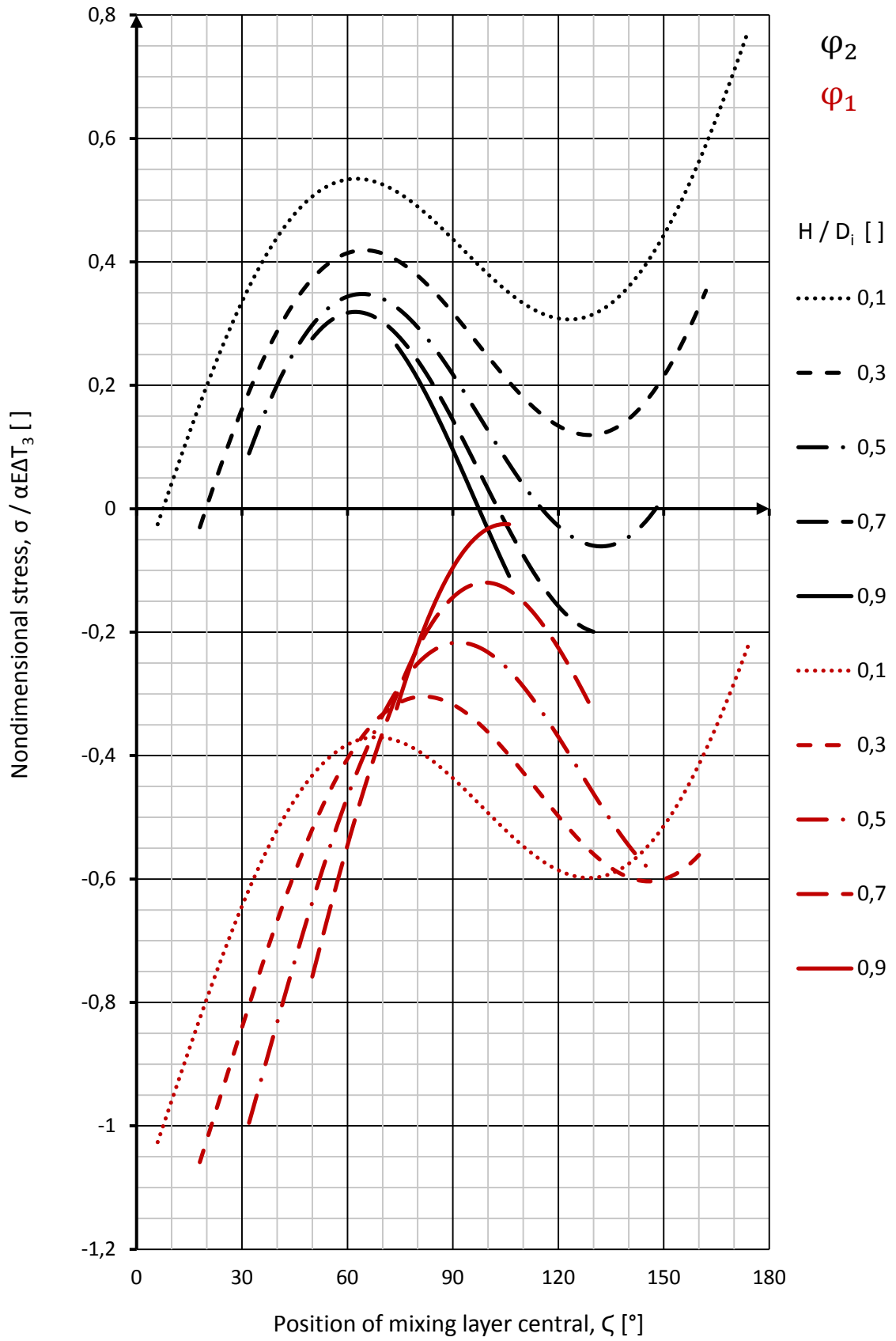
Figure 28: Nondimensional axial stress extremes for simply supported pipeline.

5.3 Random Fluctuations and Thermal Striping

The last subject considered here is the stresses related to thermal striping. Striping induces random thermal oscillations into inner surface of the pipeline near the mixing layer. Temperature fluctuation is a common cause of high cycle fatigue and, as has been stated in section 2.3, it is characterized by two factors: attenuation factor and depth of penetration. Formulas for both of these factors are retrieved from Parras et al. (1979) and are used for the consideration of pipeline's mechanical response during thermal striping.

Attenuation factor is influenced by the profile of fluctuation. Theoretically, for thermal striping this shape is relatively close to sinusoidal profile. For sinusoidal fluctuations, attenuation factor will take the following form

$$att = \left[1 + 2 \left(\frac{\pi f \lambda \rho C}{h^2} \right)^{1/2} + 2 \left(\frac{\pi f \lambda \rho C}{h^2} \right) \right]^{-1/2}, \qquad (22)$$

where f is the frequency of fluid temperature, h is the heat transfer coefficient and ρ, C and λ are density, specific heat and thermal conductivity of the wall respectively.

For the Depth of penetration of thermal oscillation, approximation of temperature profile is also needed. When similar sinusoidal assumption is exploited, it can be formulated as

$$\chi = 1.6 \left(\frac{\pi \lambda}{\rho f C} \right)^{1/2}. \qquad (23)$$

For both of these factors, it should be noted that the assumption of sinusoidal function is not the most conservative one. For example, discrete step function, with values alternating between 0 and 1, would results in much more severe mechanical response. However, such temperature fluctuation would be blatantly unphysical.

These factors are used as input on thermal fatigue calculations and are thus essential for analysis of thermal striping. In conservative assessment, temperature fluctuation range needed for stress calculations can be approximated as temperature difference between stratification layers reduced by attenuation factor. Furthermore, depth of penetration gives the maximum depth for the cracks that can be initiated by thermal striping. In this thesis, loads due to random temperature oscillation are not considered, and therefore detailed calculation of stresses associated with thermal striping are excluded.

5.4 Quick Assessment of HDR Experimental Results

In section 4.4, FEM results for cross sectional axial stresses were found to be well in line with experimental values. Defining such model with realistic thermal load is however relatively laborious task. Therefore, especially when only key features of the stratified temperature load are known, assessment methods presented in this chapter are respectable alternative for stress assessment. Here example calculations for axial stresses of cross-section Q25 at $t = 200\ s$ are demonstrated for both decomposition and thermal bowing methods.

According to Talja (1988), at time instance $t = 200$ s, stratification layer is located at radial positions of $\varphi_1 = 80°$ and $\varphi_1 = 108°$. Temperature difference between hot and cold regions is 144 °C. Based on CFD simulation the mixing layer height is roughly 10 mm, which equals to $H/D \approx 0.25$. Material parameters and dimensions are the same as presented in sections 3 and 4. Reference temperature is set to $T_0 = T_H$.

Beginning with the decomposition method, membrane stresses are calculated as (eq. 6 and 8)

$$\varphi_1 = 80° = 1.391 \text{ rad}$$

$$\varphi_2 = 108° = 1.889 \text{ rad}$$

$$T_m = \frac{(T_H - T_C)(\varphi_1 + \varphi_2)}{2\pi} = \frac{(144\ °C)(1.391 + 1.889)}{2\pi} = 75.2\ °C$$

$$\sigma_m = E\alpha T_m = 203 \cdot 10^9 \text{ MPa} \cdot 1.25 \cdot 10^{-5} \cdot \frac{1}{°C} \cdot 75.2\ °C = 191 \text{ MPa},$$

bending stresses at mixing layer interface as (eq. 10 and 12)

$$V = \frac{(T_H - T_C)\left(4\varphi_2^2 + 4\varphi_1\varphi_2 - 6\varphi_2\pi - 2\varphi_1^2 + 3\pi^2\right)}{\pi^2} = 144°C \cdot 1.51 = 217.4\ °C$$

$$\sigma_b\left(\varphi_1\right) = -\frac{4E\alpha \cos(\varphi)V}{\pi^2} = -\frac{4 \cdot 203 \cdot 10^9 \text{ MPa} \cdot 1.25 \cdot 10^{-5} \cdot \frac{1}{°C} \cdot \cos(1.391) \cdot 217.4\ °C}{\pi^2} = -40 \text{ MPa}$$

$$\sigma_b\left(\varphi_2\right) = -\frac{4E\alpha \cos(\varphi)V}{\pi^2} = -\frac{4 \cdot 203 \cdot 10^9 \text{ MPa} \cdot 1.25 \cdot 10^{-5} \cdot \frac{1}{°C} \cdot \cos(1.889) \cdot 217.4\ °C}{\pi^2} = 70 \text{ MPa}$$

and peak stresses at mixing layer interface as (eq. 11, 17 and 18, and Appendix 3)

$$n_2(0.25) = 0.735$$

$$T_p(\varphi_1) = T_\varphi - T_m - T_b = 144°C - 75.2°C - \left(\frac{217.4\,°C}{2} - \frac{1.391}{\pi} \cdot 217.4°C\right) = 56.4\,°C$$

$$T_p(\varphi_2) = T_\varphi - T_m - T_b = 0°C - 75.2°C - \left(\frac{217.4\,°C}{2} - \frac{1.889}{\pi} \cdot 217.4°C\right) = -53.2°C$$

$$\sigma_p(\varphi_1) = -n_2 E\alpha T_p = 0.735 \cdot 203 \cdot 10^9 \text{ MPa} \cdot 1.25 \cdot 10^{-5} \cdot \frac{1}{°C} \cdot 56.4°C = -105 \text{ MPa}$$

$$\sigma_p(\varphi_2) = -n_2 E\alpha T_p = 0.735 \cdot 203 \cdot 10^9 \text{ MPa} \cdot 1.25 \cdot 10^{-5} \cdot \frac{1}{°C} \cdot (-53.2°C) = 99 \text{ MPa}.$$

Membrane and bending stresses are constraint dependent. Since both expansion and bending are not fully restricted, values obtained here are highly conservative. Therefore, factors for constrain severity are induced to reach reasonable results. Since compression is assumed to be relatively nonconstrained, only 10 % of membrane stresses will be considered. Bending on the other hand confronts much more significant restrictions and therefore factor of 0.8 will be used. Peak stresses are independent of global restrains and thus accounted fully. When these factors are applied, following maximum stresses are obtained.

$$\sigma(\varphi_1) = 0.1 \cdot \sigma_m + 0.8 \cdot \sigma_b(\varphi_1) + \sigma_p(\varphi_1)$$

$$= 0.1 \cdot 191 \text{ MPa} - 0.8 \cdot 40 \text{ MPa} - 105 \text{ MPa} = -118 \text{ MPa}$$

$$\sigma(\varphi_2) = 0.1 \cdot \sigma_m + 0.8 \cdot \sigma_b(\varphi_2) + \sigma_p(\varphi_2)$$

$$= 0.1 \cdot 191 \text{ MPa} + 0.8 \cdot 70 \text{ MPa} + 99 \text{ MPa} = 174 \text{ MPa}.$$

The second quick assessment technique is the thermal bowing method. For this method, stresses can be calculated based on nondimensional stresses that can be extracted from Figure 28.

$$\varsigma = \frac{\varphi_1 + \varphi_2}{2} = \frac{80° + 108°}{2} = 94°$$

$$\frac{\sigma(\varphi_1)}{\alpha E \Delta T_3}(H/D = 0.25, \varsigma = 94°) = 0.32$$

$$\sigma(\varphi_1) = -\left(0.32 \cdot 203 \cdot 10^9 \text{ MPa} \cdot 1.25 \cdot 10^{-5} \cdot \frac{1}{°C} \cdot 144°C\right) = -117 \text{ MPa}$$

$$\frac{\sigma(\varphi_2)}{\alpha E \Delta T_3}(H/D = 0.25, \varsigma = 94°) = -0.36$$

$$\sigma(\varphi_2) = -(-0.36 \cdot 203 \cdot 10^9 \text{ MPa} \cdot 1.25 \cdot 10^{-5} \cdot \frac{1}{°C} \cdot 144°C) = 132 \text{ MPa}.$$

For both of these methods, spreadsheet calculation for stresses as function of radial position have been performed to obtain cross-sectional stress distribution. These distributions are presented in Figure 29. Experimental results from the HDR measurements (Talja 1988) are also presented in the same figure.

Based on Figure 29, decomposition method seems to give accurate estimations for stresses, whereas slightly too small values are obtained with thermal bowing method. However, values obtained with decomposition method are significantly influenced by the choice of constrain severity factors. Furthermore, since selection of these factors is an engineering task, large variations from person to person are expected. The accuracy of this method is thus highly influenced by personal proficiency and experience. For thermal bowing method the opposite is true, since this method provides explicit results for simply supported pipes. However, restriction of support conditions introduces another engineering task. This task is to judge whether the simple support conditions are realized or not. Overall, if support conditions are approximated with reasonable accuracy, both of the presented methods should provide measures for rough structural assessment. They are especially useful in situations where limited amount of initial information is available.
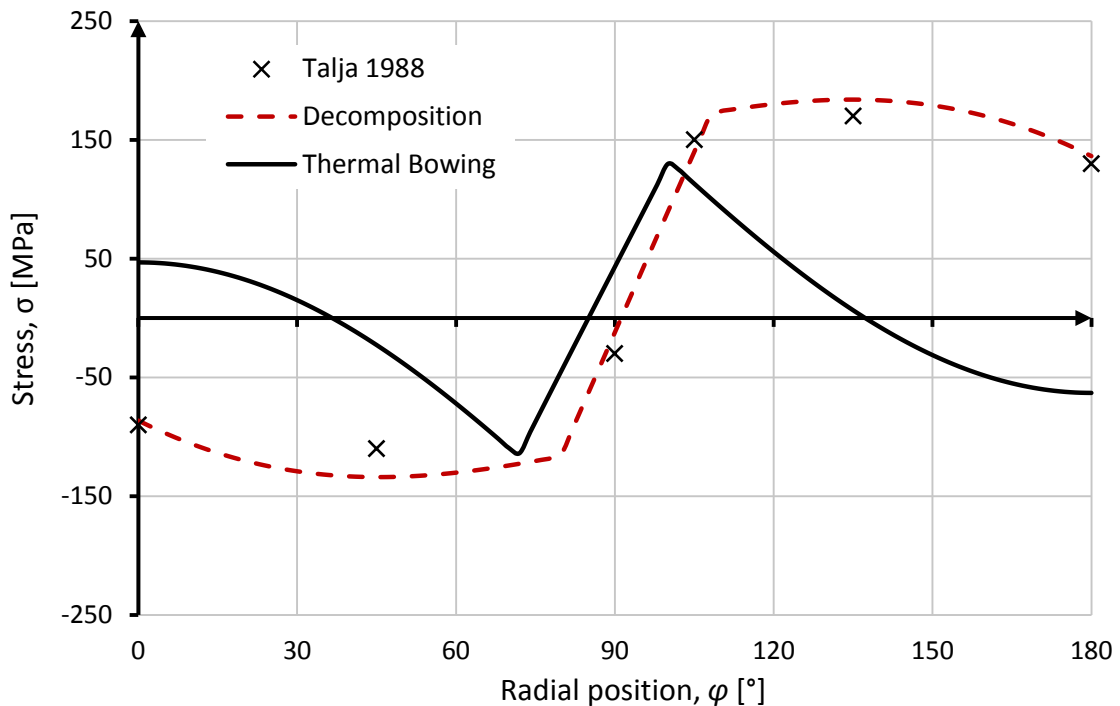

Figure 29: Calculated stresses at outer surface of cross section Q25 at t = 200s.

6 Parametric Study on Thermal Stratification

In this thesis, thermal stratification has been considered in terms of fundamentals, experiences, numerical modelling and structural assessment. These all form foundation for parametric study performed hereafter for HDR piping. The study consists of multiple one-way coupled CFD-FEM simulations for different in surge conditions. Afterwards, notions will be made based on the knowledge of previous chapters and the accuracy of quick assessment formulas will be tested.

6.1 Modelling Approach and Test Matrix

The modelling approach and computational domain used for the parametric study are practically identical to those presented in chapters 3 and 4 for thermal-hydraulic and solid stress models respectively. The only modification will be made to buoyant force model, where polynomial density model will be used together with k-epsilon model for turbulence. Based on the evidence shown in section 3.5, use of IAPWS-IF97 model for buoyant forces did not produce significantly more accurate results over polynomial model. Therefore, with the limitations posed by resources available, use of a simpler buoyant model is an efficient maneuver for preservation of computational resources. In section 4.4, slider constraint at cold water inlet was found to be most accurate and it is thus applied in this study.

The parametric study on HDR geometry comprises of multiple simulations with wide range of Richardson's numbers. In surge velocities and temperatures are chosen to be as close as possible to actual PWR surge line conditions. These conditions, presented in Table 5, form 3 by 2 matrix with varying inlet velocity and temperature. Presented Richardson's numbers are calculated according to equation 2, where pipe diameter is used as characteristic length and densities are calculated based on IAPWS-IF97 (Figure 14). For example, calculation of Richardson's number for $v = 54.5\,°C$ and $T_C = 0.052\,\text{m/s}$ is preformed as

$$Ri = \frac{g(\rho_2 - \rho_1)/\rho_1 l}{U^2} = \frac{9.81\,\frac{\text{m}}{\text{s}^2} \cdot \left(\frac{987\,\frac{\text{kg}}{\text{m}^3} - 848\,\frac{\text{kg}}{\text{m}^3}}{848\,\frac{\text{kg}}{\text{m}^3}}\right) \cdot 0.397\,\text{m}}{\left(0.052\,\frac{\text{m}}{\text{s}}\right)^2} = 236\,.$$

Initial pressure and temperature for all cases are 22.4 bar and 214 °C respectively. In the parametric study, pipeline material is the same as is chapters 3 and 4, but for additional structural assessment, case with inlet velocity of 0.104 m/s and temperature of 54.5 °C will be resimulated after material is altered to 15NiCuMoNb5. Material properties for both of these materials are presented in Table 6.

Table 5: Test matrix and calculated Richardson's numbers for the parametric study.

	$v = 0.052\,\text{m/s}$	$0.104\,\text{m/s}$	$0.207\,\text{m/s}$
$T_C = 54.5\,°C$	236	59.0	14.9
$T_C = 100\,°C$	188.5	47.1	11.9

Table 6: Material properties for VVER 1200 simulations (PNAE 1989, Schygulla 1986).

	S_u (MPa)	E (GPa)	α (1/K)	C (J/kg K)	λ (W/m K)	κ (m^2/s)
08Cr18Ni10Ti	412	185	$17.4 \cdot 10^{-6}$	530	19.0	$44.8 \cdot 10^{-5}$
15NiCuMoNb5	450	203	$12.5 \cdot 10^{-6}$	510	46.4	$1.17 \cdot 10^{-5}$

6.2 Notions on Thermal-Hydraulic Behavior

In this section, notions will be made for the changes in behavior and formation of thermal stratification when flow conditions are altered. First, notions common to all simulations will be made and then correlation between Richardson's number and quantities describing thermal stratification will be studied. Finally, increase of turbulent intensity will be examined.

The first notion, common to all of the simulated cases, is the inefficiency of thermal conductivity in water. This feature of thermal stratification was already mentioned in section 2.2 and can now be visualized with passive scalar. Passive scalar can be considered as dye that will not alter flow fields and only marks the convection of new fluid into the domain. If passive scalar has value of unity, fluid in that region is from the cold water inlet. When passive scalar has value of zero, the opposite is true. For intermediate values, some mixing between new and old fluid have occurred. The catch is that, since no conduction is modeled for passive scalar, if the obtained scalar field is similar to temperature field, no conduction have occurred. In Figure 30, fields for both passive scalar and temperature profile are presented for arbitrarily chosen case and time instance. Since the fields are practically identical, temperature variations are mainly due to convection. Use of phrasing "mainly" is needed because of numerical diffusion, which produces slight conduction also into the passive scalar field.
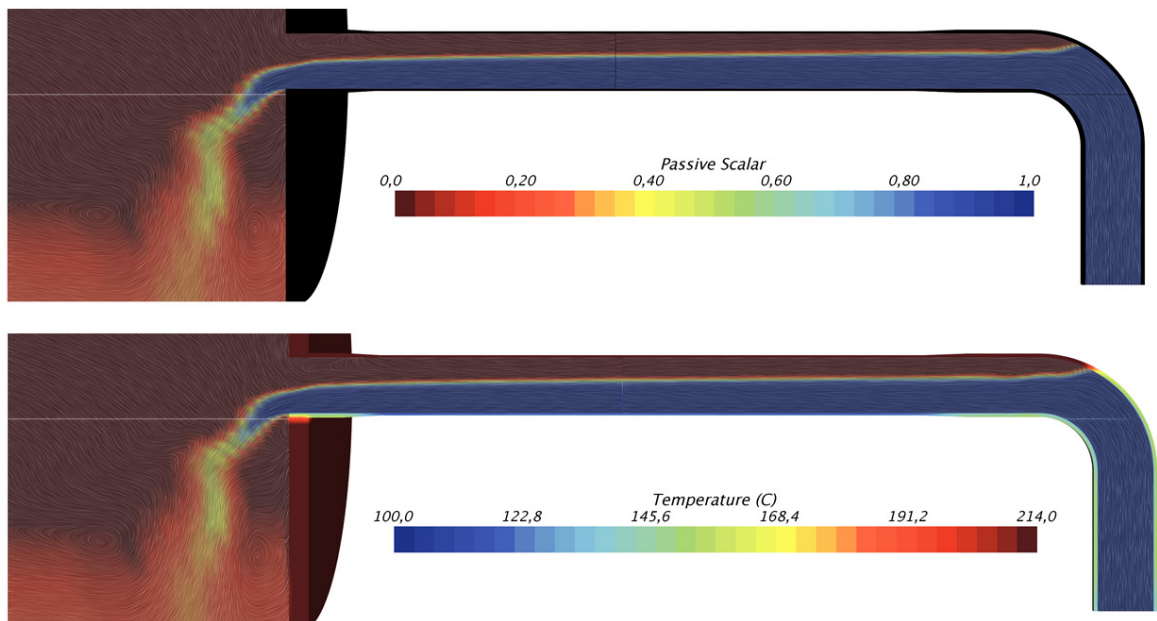

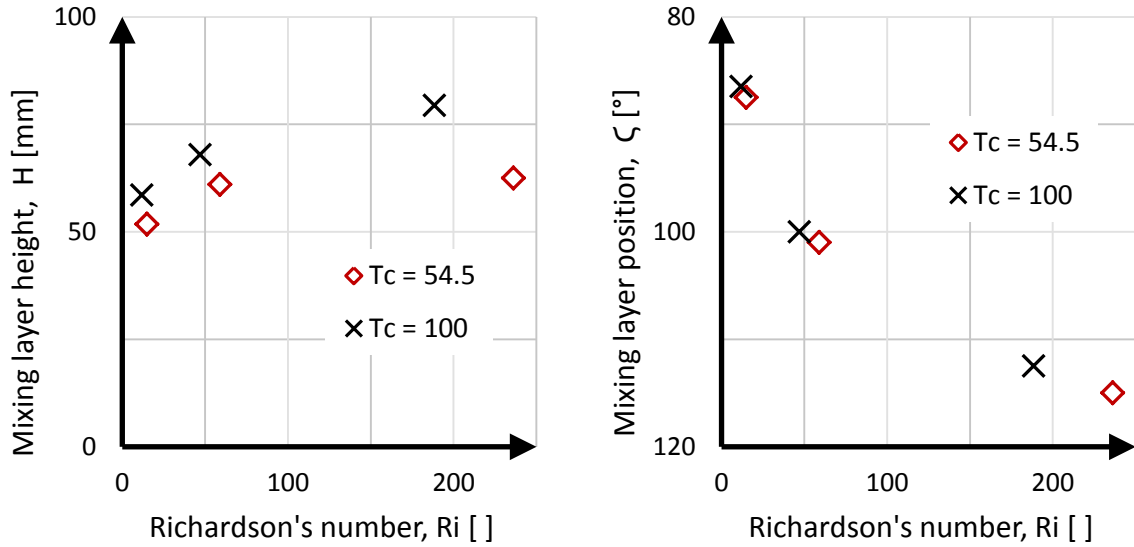*Figure 30: Passive scalar and temperature at t = 100s, v = 0.207m/s and Tc = 100°C .*

Figure 31: Richardson's number and stratification parameters at t = 200s.

In fluid dynamics, dynamical similarity between flows is often described with non-dimensional quantities. Furthermore, if the nondimensional quantity is defined correctly, clear correlation between flow features and nondimensional quantity should be realized. For description of thermal stratification, the most important features are mixing layer position and height. In Figure 31, these two values have been plotted as function of Richardson's number and modest correlation is realized for both of these features. For mixing layer position, there is evident positive trend and this correlation can be reasoned with flow physics. With high Richardson's number, buoyant forces dominate viscous and inertial forces and should therefore squeeze incoming cold flow into as narrow strip as possible. This squeezing is illustrated in Figure 32 where temperature fields for simulations with the largest and smallest Richardson's number are presented. In Figure 32a, only thin cold layer is able to penetrate into the pipe filled with hot water. On the contrary, significantly larger portion of the pipe is instantly filled with cold water when flow velocity is increased and temperature difference decreased (Figure 32c).

In section 2.2, increase of Richardson's number was also associated with the stability of stratification. By intuition, one could assume that for stable stratification mixing layer should be thinner as the buoyant forces are more dominant. However, based on this study the opposite seems to be true as negative trend between mixing layer height and Richardson's number is realized. This behavior could be explained with circulation and mixing inside stratification layers. When flow velocities are higher also the circulation and mixing inside a stratified layer is enhanced and consequently a larger portion of both cold and hot regions are at constant temperature. For mixing layer height, it should also be noted that Richardson's number seems to be not enough for predictions as values for different temperature differences are separated. Therefore, mixing layer height is likely to be function of both Richardson's number and temperature difference, whereas Richardson's number alone seems to be sufficient for description of mixing layer position. Overall, in terms of thermal-hydraulics, this parametric study has provided proof for the suitability of diameter based Richardson's number to be used to describe and estimate the behavior of thermally stratified pipe flow.

To further illustrate changes observed in thermal-hydraulic behavior, Figure 32 will be used. Comparison of temperature fields for simulations with the largest and smallest Richardson's number illustrate how turbulent intensity and overall flow energy are increased for more unstable stratification conditions. Increase of turbulence is most evident from the flow structures at the pressure vessel inlet. In Figure 32b, clean and straight fall is formed for high Richardson's number flow, whereas chaotic and wriggling decent, in Figure 32d, is caused by increased turbulence. Yet another sign of increased flow energy can be seen from the first time instances when the penetration of cold water begins. For high energy flow (Figure 32c), cold water is able to fill most of the first bend before running out of momentum. On the contrary, straight horizontal mixing layer is formed for low energy flow with high Richardson's number (Figure 32a). Finally, in Figure 32c, signs of thermal striping, caused by increased shear forces, clearly indicate that forces promoting mixing have strengthened for the flow with low Richardson's number. Since thermal striping is characterized by random and chaotic flow behavior, it should be reminded that Reynold's averaged turbulence model have been used in this study. RANS models filter most of the random flow structures and therefore the field presented here is the average solution. Consequently, in reality interface between hot and cold regions might be much more unstructured. For the same reason, even though thermal striping was not discovered for cases with larger Richardson's numbers, random oscillations might also be possible for more stable stratification conditions.
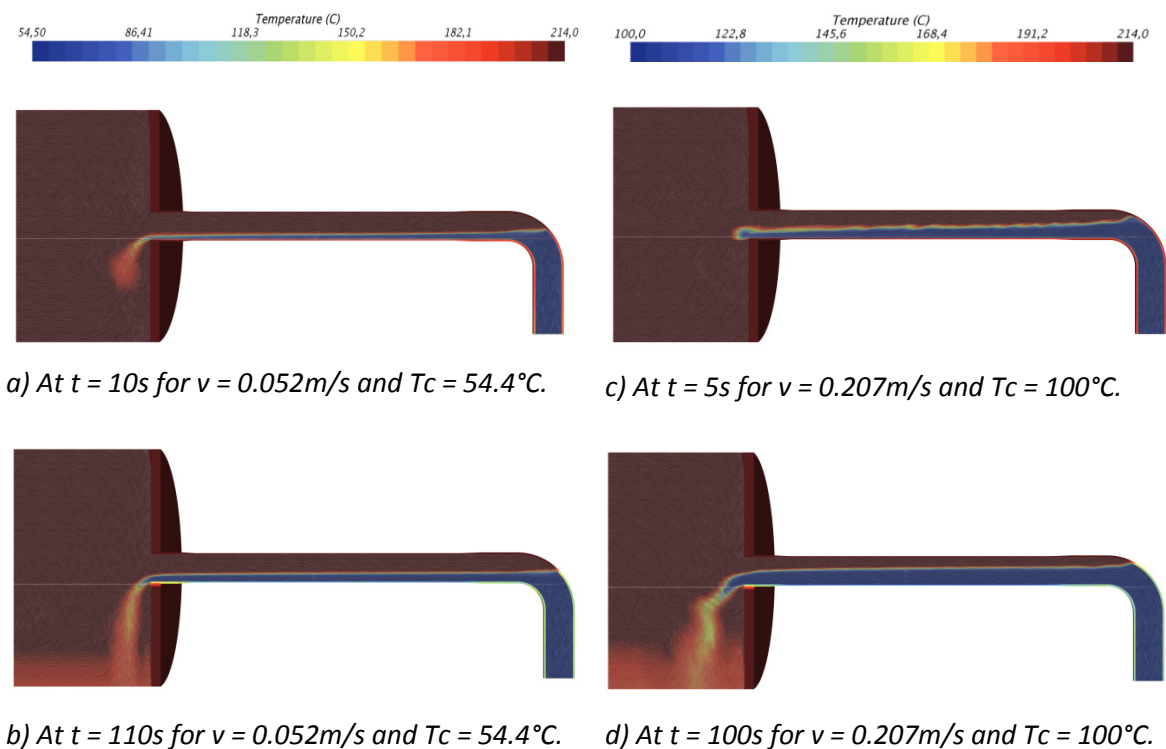

a) At t = 10s for v = 0.052m/s and Tc = 54.4°C.

c) At t = 5s for v = 0.207m/s and Tc = 100°C.

b) At t = 110s for v = 0.052m/s and Tc = 54.4°C.

d) At t = 100s for v = 0.207m/s and Tc = 100°C.

Figure 32: Development of stratification for cases with extreme Richardson's numbers.

6.3 Comparison of Mechanical Responses

This section covers results for mechanical simulations. First, overall trends and plausible correlations are discussed followed by study of pipe material choice. For the discussion on material choice, use of Thermal Shock Parameter and Thermal Stress Ratio, introduced in section 2.4, will also be presented. In addition, development of maximum stresses as function of time will be considered.

The mechanical response caused by thermal stratification load is mainly characterized by height and the location of the mixing layer. In the previous section, correlation was found between these two factors and the Richardson's number. Since such correlation exist, similar dependency might also be realized for stress extremes caused by the stratification. To further study whether such dependency exists or not, maximum and minimum stresses for cross-section Q25 have been calculated and plotted as function of Richardson's number. These correlations are presented in Figure 33. For isothermal simulations, both maximum and minimum stresses seem to feature correlation with Richardson's number. Since the magnitude of thermal stresses is mainly dictated by temperature differences, such dependency was expected.

Based on the results of this parametric study, if two stratification cases are similar in terms of temperature extremes, features such as mixing layer position and height begin to distinguish stress states from each other. In addition to notion on Richardson's number correlation, these results also exhibit another interesting feature concerning the range between maximum and minimum stresses. For isothermal simulations this range is found to be near to constant. For cases with high Richardson's numbers maximum stresses are higher and at same time compressive stresses start to diminish. Similarly, the opposite is true for low Richardson's number flows. Reason for such behavior is unknown, but could be due to changes in membrane stresses. Membrane stresses are dependent of stratification location and have tendency to increase or decrease overall stress state. To conclude, based on the results obtained from this parametric study, stress range within a cross-section is found to be in correlation with Richardson's number and consequently mixing layer height and position.
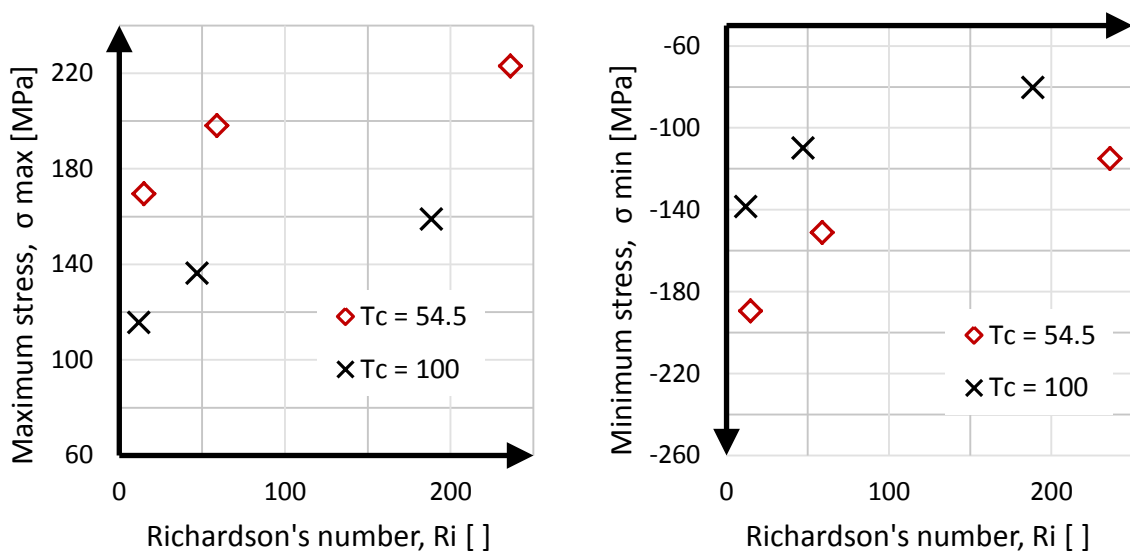

Figure 33: Correlation between Richardson's number and stresses at Q25, t = 200s.

For pipelines under thermal loading material choice has significant impact on the magnitude of developing stresses. To ease comparison between materials, two parameters, Thermal Shock Parameter and Thermal Stress Ratio, were previously introduced in section 2.4. For 15NiCuMoNb5, the material used in HDR piping, these two are

$$TSP = \frac{S_u\sqrt{\kappa}}{\alpha E} = \frac{450 \text{ MPa} \cdot \sqrt{1.17 \cdot 10^{-5} \text{ m}^2/\text{s}}}{12.5 \cdot 10^{-6}\frac{1}{K} \cdot 203 \text{ GPa}} = 0.61 \frac{\text{m} \cdot \text{K}}{\sqrt{\text{s}}}$$

$$TSR = \frac{S_u}{\alpha E} = \frac{450 \text{ MPa}}{12.5 \cdot 10^{-6}\frac{1}{K} \cdot 203 \text{ GPa}} = 177.34 \text{ K}.$$

And for 08Cr18Ni10Ti, pipeline material defined according Russian standard PNAE, these are

$$TSP = \frac{S_u\sqrt{\kappa}}{\alpha E} = \frac{412 \text{ MPa} \cdot \sqrt{44.8 \cdot 10^{-5} \text{ m}^2/\text{s}}}{17.4 \cdot 10^{-6}\frac{1}{K} \cdot 185 \text{ GPa}} = 2.71 \frac{\text{m} \cdot \text{K}}{\sqrt{\text{s}}}$$

$$TSR = \frac{S_u}{\alpha E} = \frac{412 \text{ MPa}}{17.4 \cdot 10^{-6}\frac{1}{K} \cdot 185 \text{ GPa}} = 128.0 \text{ K}.$$

For both of these quantities, higher values are associated with better resistance against thermal loading. Thus, values obtained for TSP suggest that 08Cr18Ni10Ti should perform significantly better under sudden temperature variations, such as thermal striping, but is inferior when it comes to static loading conditions. To test how these assumptions hold, original HDR experiment T33.19 was resimulated with properties of 08Cr18Ni10Ti and maximum stresses were calculated for all of the recorded time instances. Development of the maximum stresses for both of these cases are presented in Figure 34.
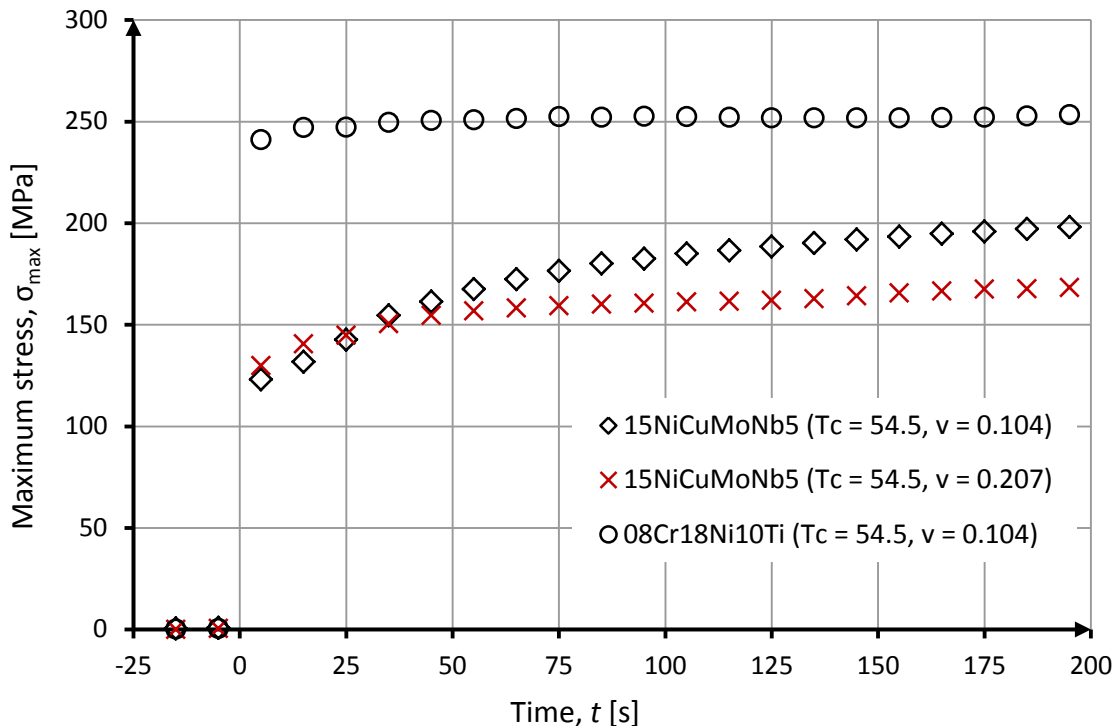

Figure 34: Development of maximum stresses at cross-section Q25.

Based on Figure 34, the maximum stresses are in sync with values of TSR as significantly larger stresses have developed into the alternated pipe material. These stresses in 08Cr18Ni10Ti also reach the maximum value almost immediately which is a sign of efficient redistribution of temperature and stresses. This is the feature measured with TSP. Therefore, both of these parameters have shown their potential as assistance in early design and assessment of material choice. In terms of static thermal loading, original HDR pipe material 15NiCuMoNb5, seems to be clearly more suitable for surge line material, since smaller stresses are induced. However, in the choice of pipe material, also other loads such as internal pressure and thermal striping have to be taken into account and therefore ruling 15NiCuMoNb5 as superior over 08Cr18Ni10Ti is not possible.

In Figure 34, there is also plot for stresses for simulation with higher fluid velocity. For higher velocity Richardson's number is lower and thus, based on previous results, stress levels are smaller. Even thought, this can be clearly seen from the development of maximum stresses, the stresses for the simulation with higher velocity rise more rapidly than for the one with lower velocity. This is caused by the increase of heat transfer between fluid and the pipe, which is proportional to the fluid velocity. Therefore, for faster flow velocities random temperature oscillations, such as thermal striping, are more severe. Furthermore, because signs of thermal striping were only observed for the cases with higher velocities, increase of flow velocities can not be considered as solution to thermal stratification. In the worst case such measure could promote high cycle fatigue.
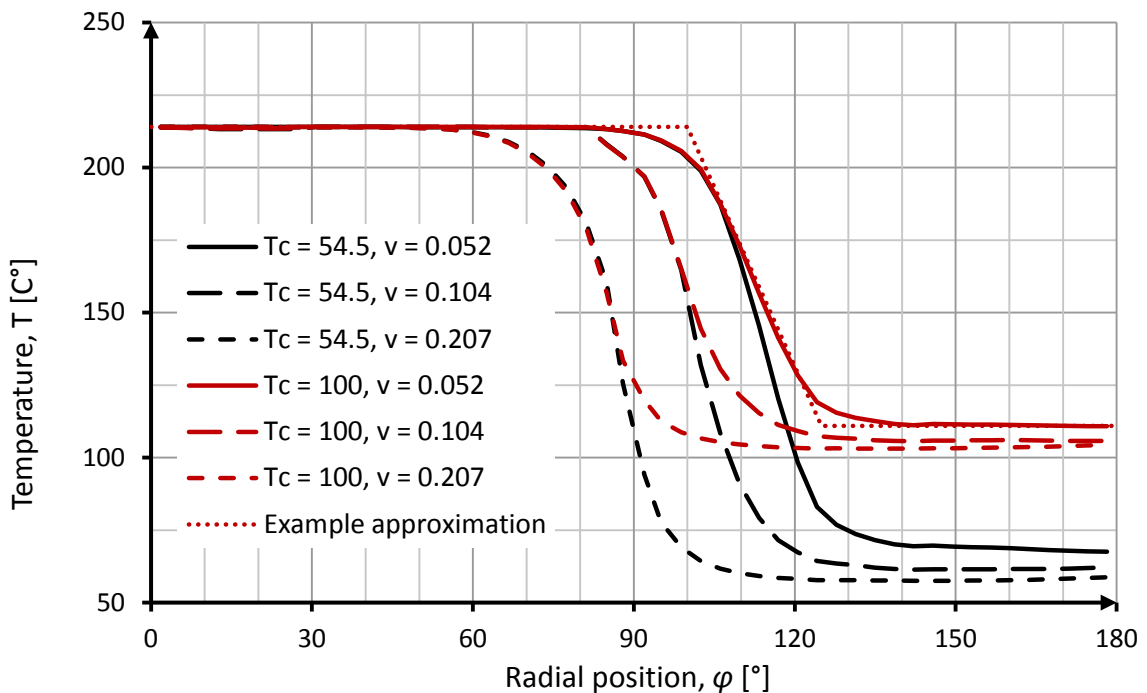

Figure 35: Q25 inner wall temperature profile at t = 200s.

6.4 Accuracy and Sensibility of Quick Assessment Formulas

Numerical results obtained for structural response required relatively high computational resources and work hours for setting up the models. Furthermore, if a study similar to this would be performed for real surge line geometry with length of 10 to 15 meters, getting results would likely take relatively long time. If the quick assessment formulas presented in this thesis are suitable for rough estimates, they should provide results that are consistent for wide range of flow conditions. Therefore, the maximum stresses for the parametric study are calculated with both decomposition and thermal bowing methods. These estimates are then compared to FEM solutions for consideration of model accuracy and sensibility.

For quick assessment, cross-sectional temperature profile describing stratification conditions is needed. In this study, these profiles are extracted from numerical simulations, but for operating power plant, this data can be obtained from temperature surveillance and monitoring system, such as FAMOS. Therefore, in practical applications use of these formulas can be independent of thermal-hydraulic simulation. The temperature profiles used in the calculations are presented in Figure 35. In Figure 35, there is also an example on how the piecewise linear temperature profile is approximated. After the stresses are estimated with quick assessment formulas, the deviation from the FEM results is defined. These calculations and initial conditions are presented in Table 7.

In section 5.6, both decomposition method and the thermal bowing method were found to give results with reasonable accuracy. For decomposition method, the accuracy was introduced with correct selection of scale factors for membrane and bending stresses to correspond actual support condition as accurately as possible. This step includes certain level of arbitrariness and, in ideal conditions, values for the scale factors should be optimized before applying the assessment method. In this study, calculations performed in section 5.6 served as calibration since the values for scale factors were chosen to match with stresses recorded at HDR facility. Based on Table 7, deviation of results obtained with decomposition method in contrast to the FEM solution is at its' highest, about 30%, for minimum stresses. Slightly smaller maximum deviation of 16% is found for maximum stresses. Furthermore, for both of these errors the magnitude and direction is consistent. Consistent error implies that the analytical formula is providing consistent results and performs as expected.

For the thermal bowing method much larger deviation is found together with clear inconsistency. The error recorded from the FEM simulations range from 75% to -60% and the sign of the error varies from case to case. All together, this is a clear indication of insufficient support condition approximation. Thermal bowing method offers no possibilities for support condition optimization and is therefore rigid in terms of scenarios where it can be applied. When support condition for the pipe can not be described with simple support assumption, inconsistent and bad approximation are obtained. Furthermore, judgement of scenarios where this model can be applied into actual pipeline geometry is a challenge. Therefore, use of the decomposition method has proven to be more suitable measure for quick assessment. Based on this study, if scale factors for decomposition are optimized, it will produce consistent results with relatively good accuracy. However, further studies are still needed on realistic surge line geometry. The main objective should be to study how features, such as the bends and other changes in geometry, affect performance and reliability of the analytical model.

Table 7: Stress extremes for parametric study with quick assessment formulas.

		$T = 54.5$ $v = 0.052$	$T = 54.5$ $v = 0.104$	$T = 54.5$ $v = 0.207$	$T = 100$ $v = 0.052$	$T = 100$ $v = 0.104$	$T = 100$ $v = 0.207$
H/D	( )	0.16	0.15	0.13	0.20	0.17	0.15
ζ	( )	115	101	88	113	95	87
ΔT_3	(°C)	146	153	156	103	108	111

Parameters for thermal stratification

T_m	(°C)	93.5	85.6	76.0	64.5	57.2	53.3
V	(°C)	247.9	237.0	233.2	173.4	164.3	164.9
$T_p\,(\varphi_1)$	(°C)	74.9	69.9	67.5	49.4	46.7	46.7
$T_p\,(\varphi_2)$	(°C)	-46.7	-59.6	-69.6	-31.8	-43.6	-48.8
n_2	( )	0.86	0.87	0.91	0.79	0.84	0.88
σ_m	(MPa)	237.3	217.2	193.0	163.6	145.0	135.2
$\sigma_b\,(\varphi_1)$	(MPa)	70.4	9.5	-41.4	34.4	-14.3	-35.0
$\sigma_b\,(\varphi_2)$	(MPa)	142.5	82.4	20.7	99.4	43.3	14.5
$\sigma_p\,(\varphi_1)$	(MPa)	-164.1	-154.3	-156.2	-99.6	-99.2	-104.3
$\sigma_p\,(\varphi_2)$	(MPa)	102.3	131.5	161.1	64.2	92.6	109.0
σ_{min}*	**(MPa)**	**-84.1**	**-124.9**	**-170.0**	**-55.7**	**-96.1**	**-118.8**
σ_{max}*	**(MPa)**	**240.0**	**219.1**	**197.0**	**160.1**	**141.8**	**134.1**
e_{min}**	**(%)**	**-27 %**	**-17 %**	**-10 %**	**-31 %**	**-13 %**	**-14 %**
e_{max}**	**(%)**	**8 %**	**11 %**	**16 %**	**1 %**	**4 %**	**16 %**

Estimates for stress extremes according to decomposition method.

$\dfrac{\sigma(\varphi_1)}{\alpha E \Delta T_3}$	( )	-0.54	-0.46	-0.41	-0.51	-0.42	-0.39
$\dfrac{\sigma(\varphi_2)}{\alpha E \Delta T_3}$	( )	0.27	0.34	0.43	0.25	0.36	0.43
σ_{min}	**(MPa)**	**-201.6**	**-179.8**	**-161.0**	**-132.5**	**-114.6**	**-110.0**
σ_{max}	**(MPa)**	**100.6**	**130.9**	**171.5**	**64.3**	**99.2**	**120.2**
e_{min}**	**(%)**	**75 %**	**19 %**	**-15 %**	**65 %**	**4 %**	**-21 %**
e_{max}**	**(%)**	**-55 %**	**-34 %**	**1 %**	**-60 %**	**-27 %**	**4 %**

Estimates for stress extremes according to thermal bowing method.

* $\sigma_{min} = 0.1 \cdot \sigma_m + 0.8 \cdot \sigma_b + \sigma_p$ *** $e_{min/max} = (\sigma_{min/max} - \sigma_{FEM\ solution\ min/max})/ \sigma_{FEM\ solution\ min/max}$*

7 Conclusions

Thermal stratification has caused multiple failures in surge lines of pressurized water reactors around the world, but none of them have been severe or posed instant safety threat. Therefore, thermal stratification raises concern mainly in terms of fatigue. For stable stratification, with length of multiple meters and temperature difference over one hundred degrees, stresses high enough for plastic deformation are plausible. These loading condition are limited by the number of startups and shutdowns, but for life time of 50 to 60 years do still provide enough cycles for low cycle fatigue. In addition, there are also smaller stratification loads introduced during normal operational conditions. These loads are caused by periodic shifting of the stratification location and have enough occurrences for high cycle fatigue. To tackle these issues, power plant operators have introduced stratification monitoring and surveillance systems into the most critical parts of the surge line. These monitoring systems provide insight into the actual loading conditions and give operators possibilities to avoid conditions found to be favorable for stratification.

Accurate estimation of stresses induced by the thermal stratification form the base for fatigue calculations. These estimates can be obtained from numerical simulations and the results obtained from such models have been proved to be accurate in multiple studies. Similarly, when thermal-hydraulic and solid stress models were created in this thesis to simulate German HDR experiments, obtained results were found to be accurate. Furthermore, when these validated models were used for parametric study, multiple interesting features were observed. First of all, the height and the vertical position of the mixing layer were found to be in correlation with Richardson's number. For the position, Richardson's number alone was enough for the description, but for the height correlation was only realized for isothermal cases. Furthermore, similar isothermal positive trend was also observed for maximum and minimum thermal stresses.

In addition to the parametric study, change of pipe material from 15NiCuMoNb5 to 08Cr18Ni10Ti was also considered. Based on this study, both Thermal Shock Parameter and Thermal Stress Ratio were found to be useful tools for design phase assessment and comparison of material performance in terms of thermal stresses. Finally, for flows with higher velocity, thermal stresses were found to develop at much more rapid phase. When this notion was combined with the signs of thermal striping, captured only for high velocity cases, increase of flow velocities can not be considered as solution for thermal stratification. In the worst case such measure could promote high cycle fatigue.

One of the objectives of this thesis was to define a simplified method for broad conservative assessment. For this purpose two analytical models were introduced and compared. Based on the parametric study, decomposition method was found to be suitable and consistent for relatively accurate estimates. However, obtaining good quality results is highly dependent on the choice of scale factors for membrane and bending stresses. Due to limited time reserved for the thesis, and unexpected modelling and computer setbacks, the analytical models could not be verified with a real structure which would have been a surge line of a Finnish nuclear power plant. Therefore, further studies are still needed to validate model performance on realistic surge line geometry. These studies should include consideration of features such as bends and other changes in geometry, since their influence to the performance and reliability of analytical formulas used in decomposition method are still unknown.

References

ASME, 2007. Rules for Construction of Nuclear Power Plant Component: Subsection NB-3600 Piping Design. ASME B&PV Code, Section III, Subsection NB-3600.

BAIK, S.J., Y.I. IM ja T.S. RO., 1998. Specialists meeting on experience with thermal fatigue in LWR piping caused by mixing and stratification: Thermal stratification in the surge line of the Korean next generation reactor.

BARRON, R.F., BARRON, B.R., 2011. Design for Thermal Stresses. John Wiley & Sons, p. 528, ISBN 1118094530, 9781118094532.

BERGMAN, T.L., LAVINE, A.S., INCOPERA, F.P. and DEWITT, D.P, 2011. Fundamentals of Heat and Mass Transfer, 7th Edition. Wiley, p. 1048, ISBN 0470917857, 978-0470917855.

BIENIUSSA, K.W. and RECK, H., 1999. Piping specific analysis of stresses due to thermal stratification. Nuclear Engineering and Design, 190/1–2, p. 239-249, ISSN 0029-5493. DOI //dx.doi.org/10.1016/S0029-5493(99)00007-2.

BOROS, I., ASZ´ODI, A., 2007. Analysis of thermal stratification in the primary circuit of a VVER-440 reactor with the CFX code. Nuclear Engineering and Design, Volume 238, Issue 3, Pages 453-459, ISSN 0029-5493, https://doi.org/10.1016/j.nucengdes.2007.02.036.

CAI, B., GU, H., WENG, Y., QIN, X., WANG, Y., QIAO, S. and WANG, H., 2017. Numerical investigation on the thermal stratification in a pressurizer surge line. Annals of Nuclear Energy, 101, p. 293-300 ISSN 0306-4549. DOI //dx.doi.org/10.1016/j.anucene.2016.11.024.

CD-adapco, 2018. Simcenter STAR-CCM+ User manual. v13.06.

GOLEMBIEWSKI, H. and KLEINÖDER W., 2000. Monitoring for Fatigue − Examples for Unexpected Component Loading. International Conference, Nuclear Energy in Central Europe 2000. Bled, Slovenia. Siemens Nuclear Power GmbH.

HANNINK, M. and BLOM F., 2010. Numerical methods for the prediction of thermal fatigue due to turbulent mixing, Nuclear Engineering and Design, 241 (2011) 681–687.

HAUTALA, M., 2017. Lämpötilakerrostumat painevesireaktorin yhdyslinjassa, Thermal stratification in PWR surge line. Aalto University, Bachelor's Thesis. 30 p.

HUDCOVSKY, S. and SLINA M., 2001. Monitoring of Coolant Temperature Stratification at Piping Components of NPP VVER – 440. Smolenice, Slovakia.

HÄFNER, W., 1990. Thermische SchichtVersuche im horizontalen Rohr. Technischer Fachbericht PHDR 9289, HDR Sicherheitsprogramm, Kernforschungszentrum Karlsruhe.

IAPWS, 1997. Industrial Formulation 1997 for the Thermodynamic Properties of Water and Steam (IAPWS-IF97). The International Association for the Properties of Water and Steam, Lucerne, Switzerland.

JO, J.C., KIM, Y.I. and CHOI, S.K., 2001. Numerical Analysis of Thermal Stratification in a Circular Pipe. Journal of Pressure Vessel Technology, 123/4, p. 517 ISSN 0094-9930. DOI 10.1115/1.1388008.

KAMAYA, M. and NAKAMURA A., 2011. Thermal stress analysis for fatigue damage evaluation at a mixing tee, Nuclear Engineering and Design, 241 (2011) 2674– 2687.

KANG, D.G., JHOUNG, M.J. and CHANG, S.H., 2011 Fluid–structure interaction analsis for pressurizer surge line subjected to thermal stratification, Nuclear Engineering and Design, 241 (2011) 257–269.

KILPI, K., RINTAMAA, R. and TIMO, M., 1987. HDR-reaktoriturvallisuusohjelma. VTT/Ydincoimatekniikan laboratorio.

KIM, S., CHOI, J., PARK, J., CHOI, Y. and LEE, J., 2013. A coupled CFD-FEM analysis on the safety injection piping subjected to thermal stratification, Nuclear Engineering and Technology. Vol. 45, No. 2, April 2013.

KUMAR, R., JADHAV, P.A., GUPTA, S.K ja GAIKWAD, A.J., 2014. Evaluation of Thermal Stratification Induced Stress in Pipe and its Impact on Fatigue Design. ISBN 1877-7058. DOI //dx.doi.org/10.1016/j.proeng.2014.11.047.

KUNDU, P.K., AYYASWAMY, P.S., COHEN, I.M. and HU, H.H., 2008. Fluid mechanics, 4 edition. Burlington, Mass. Academic Press, ISBN 0-12-373735-4.

KWEON, H.D., KIM, J.S. ja LEE, K.Y., 2008. Fatigue design of nuclear class 1 piping considering thermal stratification. Nuclear Engineering and Design, 238/6, s. 1265-1274 ISSN 0029-5493. DOI //dx.doi.org/10.1016/j.nucengdes.2007.11.009.

MYUNG, J. J. and YOUNG, H. C., 2008. Surge line stress due to thermal stratification. Nuclear engineering and technology, vol.40, no.3 April.

OECD-NEA, 2005. Thermal Cycling in LWR Components in OECD-NEA Member Countries. NEA/CSNI/R(2005)8, NEA CSNI, CSNI Integrity and Ageing Working Group, Organization for Economic Co-operation and Development.

OECD-NEA, 1998. Specialists meeting on experience with thermal fatigue in LWR piping caused by mixing and stratification.

PARRAS, F., BOSSER, M., MILAN D. and BERTHOLLON, G., 1979. Heat Transfer in Pressurized Water Reactor Components Most Often Subjected to Thermal Shock. Nuclear Technology, Volume 47, July 6.

PNAE G-7-002-86, 1989. Regulations for Strength Analysis of Equipment of Atomic Power Plants. ENERGOATOMIZDAT p. 559.

RADU, V., 2015. Book of Stochastic Modelling of Thermal Fatigue Crack Growth, Volume 1. Springer International Publishing Switzerland. DOI: 10.1007/978-3-319-12877-1_6

SANTAOJA, K., 2017. Rasitusopin käsikirja, 3. uudistettu ja laajennettu painos. Taras. p. 495 ISBN 978-952-67899-4-1

SCHÜMAN, D., 1998. Specialists meeting on experience with thermal fatigue in LWR piping caused by mixing and stratification: Thermal stratification in Small Pipes with Respect to Fatigue Effects and so Called "Banana Effect". Division Energy and Systems Technology TÜV Nord e.V. Hamburg, Germany.

SCHYGULLA, U. and WOLF, L., 1986. Thermal stratification experiments in horizontal piping section. Design report, HDR Sicherheitsprogramm, Kernforschungszentrum Karlsruhe.

TALJA, A., 1988. Stresses in a Horizontal Pipe Line due to Thermal Stratification, Evaluation Report. HDR Sicherheitsprogram, Test Group TEMR, Experiments T33, July 1988. Nuclear Research Center Karlsruhe. 48p.

TIMPERI, A., 2010. The Finnish Research Programme on Nuclear Power Plant Safety 2007–2010 Interim Report, Chapter 26.2: Simulation of thermal striping in a HDR experiment. VTT, SAFIR2010/FRAS. ISBN 978-951-38-7267-0

TIMPERI, A., 2008. Numerical Simulation of Turbulent Buoyancy-Driven Flows. VTT, SAFIR2010/FRAS. 49p.

U.S. NRC., 1988. US Nuclear Regulatory Commission Bulletin 88-11, Pressurizer surge line thermal stratification.

Appendices

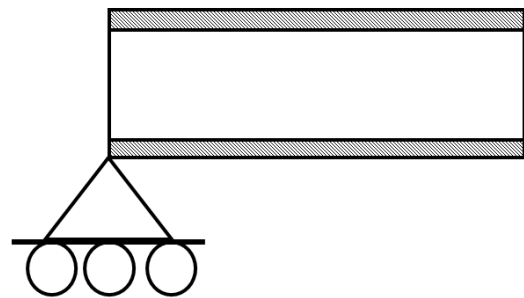## Appendix 1. Definitions for Mechanical Constraints
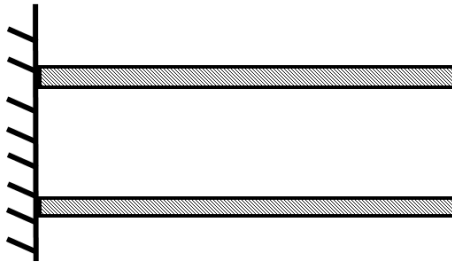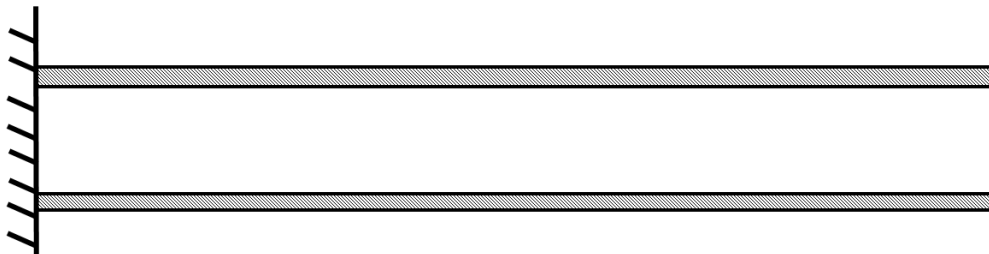
Fixed: 0 DOF.
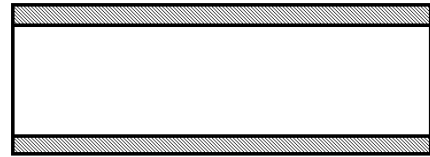
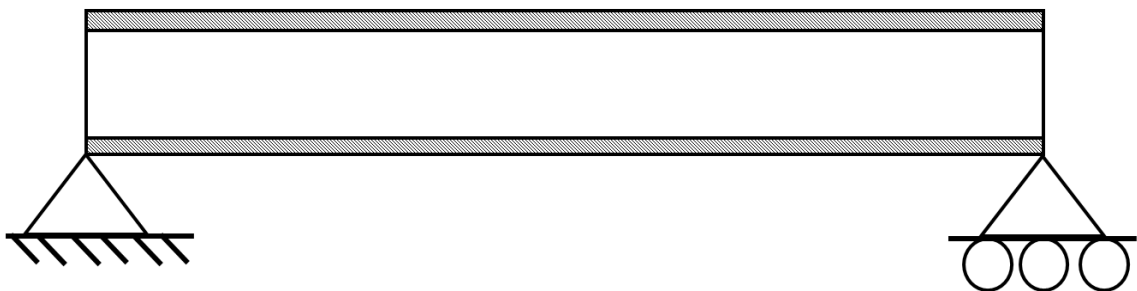Free: 6 DOF, Rotation and translation.
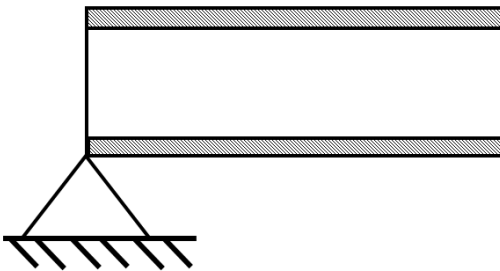
Pinned: 3 DOF, Rotation.

Slider: 5 DOF, Rotation and normal translation.

Cantilever beam: Fixed and free supports.

Simply supported beam: Pinned and slider supports.

Appendix 2. Derivation of Formulas for Thermal Bowing Method

In this appendix, formulas for membrane and bending forces, moments and stresses will be derived according to Barron and Barron (2011). Prepared formulas are then further validated with simple FEM model.

Thermal stresses at any point of simply supported pipe may be determined from (Barron and Barron 2011)

$$\sigma = \sigma_m + \sigma_b = \frac{F_T}{A} - \alpha E \Delta T(\varphi) + \frac{M_T y}{I}. \tag{1}$$

Assuming piecevise linear temperature profile, any stratified temperature profile may be expressed as

$$\Delta T(\varphi) = \begin{cases} T_H - T_C & 0 \le \varphi < \varphi_1 \\ (T_H - T_C)\dfrac{\varphi_2 - \varphi}{\varphi_2 - \varphi_1} & \varphi_1 \le \varphi < \varphi_2 \\ 0 & \varphi_2 \le \varphi \le 180 \end{cases} \tag{2}$$

In equation (1) thermal force and moment, F_T and M_T, are defined as

$$F_T = \alpha E \int \Delta T(\varphi)\, dA = 2\alpha E \int \Delta T(\varphi) \left(\frac{1}{2} D_m t\right) d\varphi \tag{3}$$

$$F_T = \alpha E D_m t \Delta T_3 \left(\varphi_1 + \frac{\varphi_2 - \varphi_1}{2}\right) \tag{4}$$

$$M_T = \alpha E \int y \Delta T(\varphi)\, dA = 2\alpha E \int \left(\frac{1}{2} D_m \cos(\varphi)\right)\Delta T(\varphi) \left(\frac{1}{2} D_m t\right) d\varphi \tag{5}$$

$$M_T = 2\alpha E D_m^2 t \Delta T_3 \left(\frac{\sin(\varphi)}{2} - \frac{\cos(\varphi_1) - \cos(\varphi_2) + \varphi_1 \sin(\varphi_2) - \varphi_2 \sin(\varphi_2)}{2(\varphi_1 - \varphi_2)}\right), \tag{6}$$

where following relations were applied

$$\Delta T_3 = T_H - T_C, \quad y = \frac{1}{2} D_m \cos(\varphi) \quad and \quad dA = \left(\frac{1}{2} D_m t\right) d\varphi. \tag{7}$$

If pipe is assumed to be thin-walled, simplified definition for moment of inertia may be applied together with definition of cross sectional area

$$I = \frac{1}{8} \pi D_m^3 t \quad and \quad A = \pi D_m t. \tag{8}$$

Finally, substituting equations (2), (4), (6), (7) and (8) into equation (1), formulas for membrane and bending stresses are defined as

$$\sigma_m(\varphi) = \frac{\alpha E \Delta T_3}{\pi} \left(\varphi_1 + \frac{\varphi_2 - \varphi_1}{2} \right) - \alpha E \Delta T(\varphi) \, Ri = \frac{g'l}{U^2} \tag{9}$$

$$\sigma_b(\varphi) = \frac{2\alpha E \Delta T_3 \cos(\varphi)}{\pi} \left(\sin(\varphi) - \frac{\cos(\varphi_1) - \cos(\varphi_2) + \varphi_1 \sin(\varphi_2) - \varphi_2 \sin(\varphi_2)}{\varphi_1 - \varphi_2} \right). \tag{10}$$

Obtained formulas (9) and (10) for membrane and bending stresses are then validated with simple FEM model shown in Figure 36. Simple supports are applied by restricting translation of topmost nodes at each pipe end. Material, loading and geometrical properties used are listed in Table 8.

Table 8: Input data for validation model.

E (GPa)	α (1/K)	T_H (K)	T_C (K)	D_m (mm)	t (mm)	H (mm)	ς (°)
193	$16 \cdot 10^{-6}$	400	300	950	50	100/200	90/100
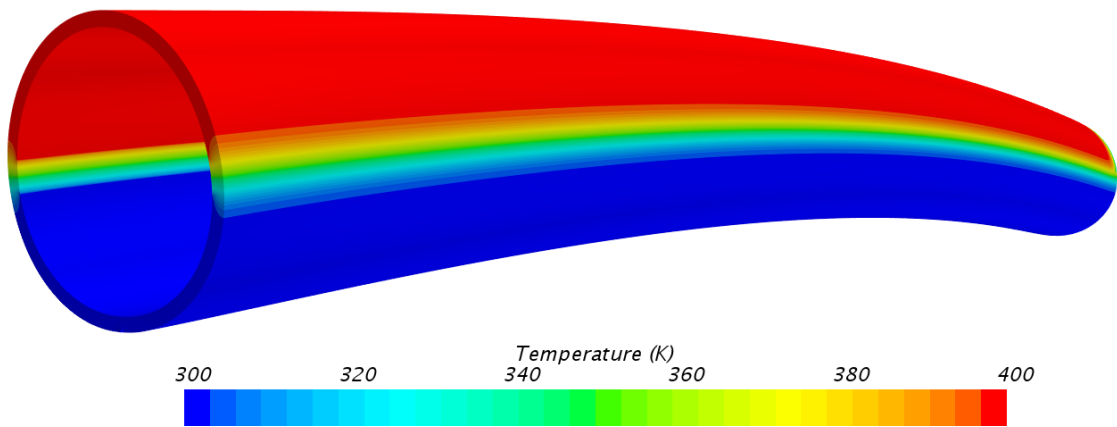
Figure 36: FEM model for validation of derived formulas.

In Figure 37 and Figure 38, stress values are plotted for both derived formulas and FEM model. Stress extremes obtained are in clear agreement with stresses at inner wall of the pipe, whereas slight over prediction is realized at outer surface. Overall, calculated values are inline with FEM solution and thus use of formulas derived here is validated.
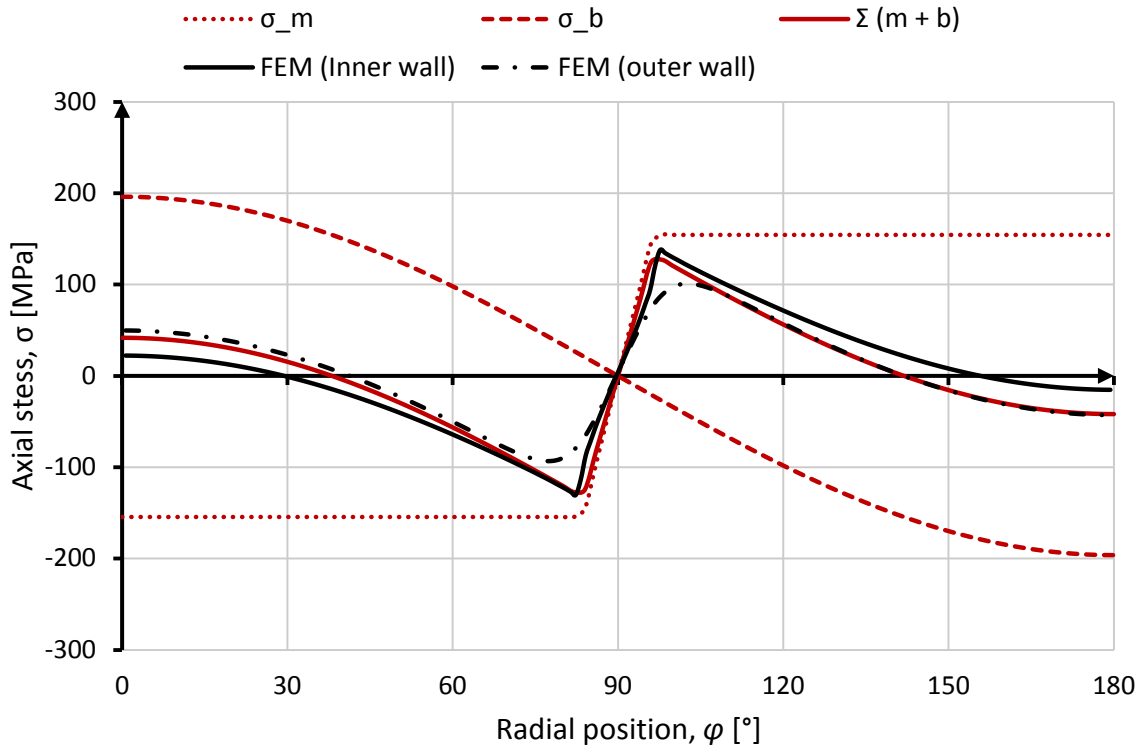
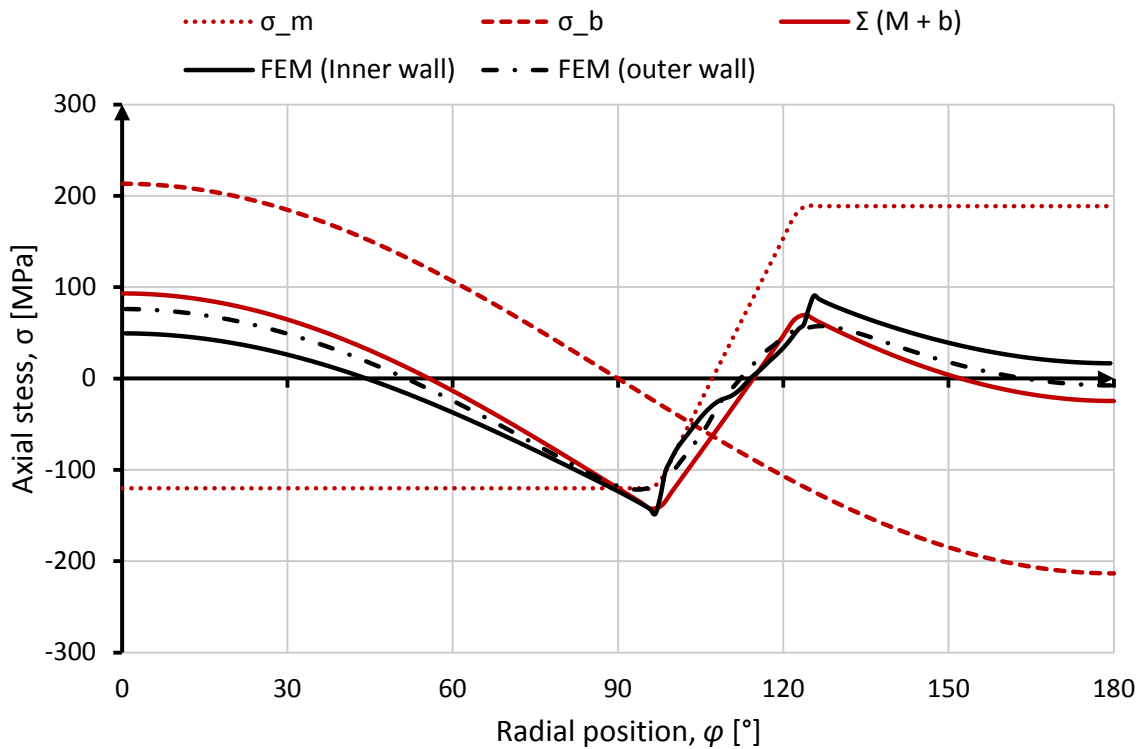*Figure 37: Stresses according to formulas and FEM model, H = 0.1 and ς = 90°.*

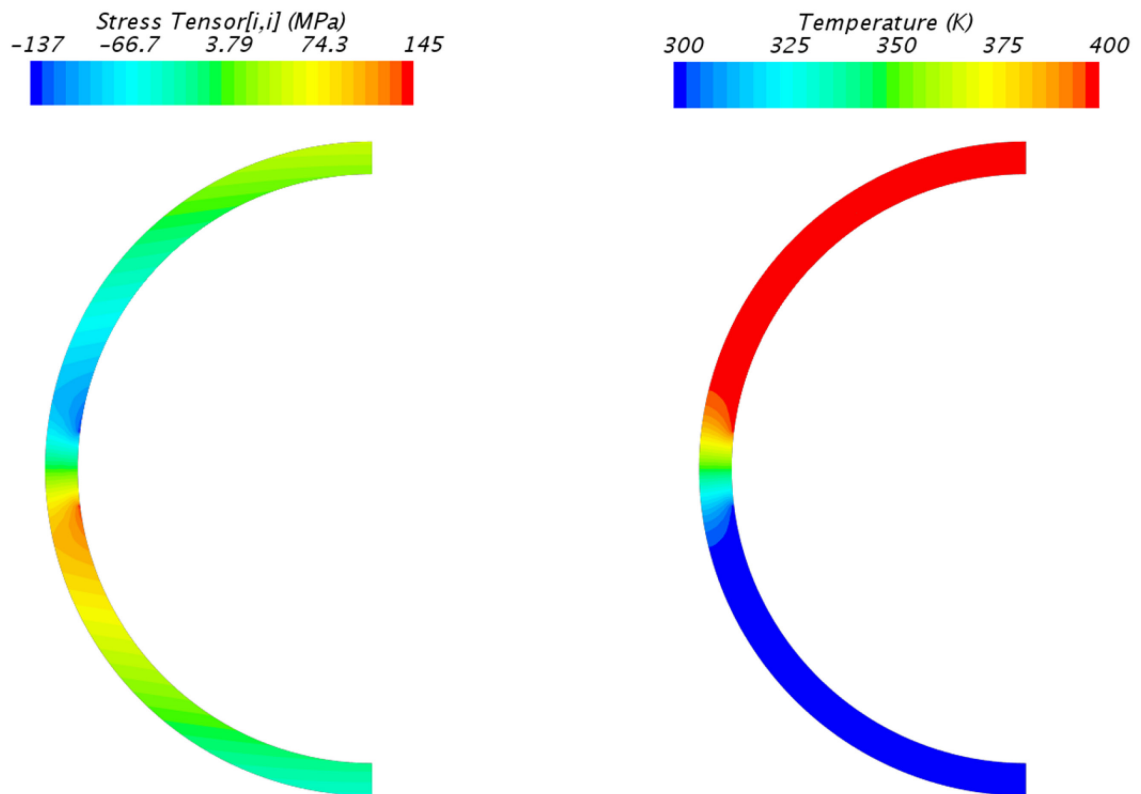*Figure 38: Stresses according to formulas and FEM model, H = 0.2 and ς = 110°.*

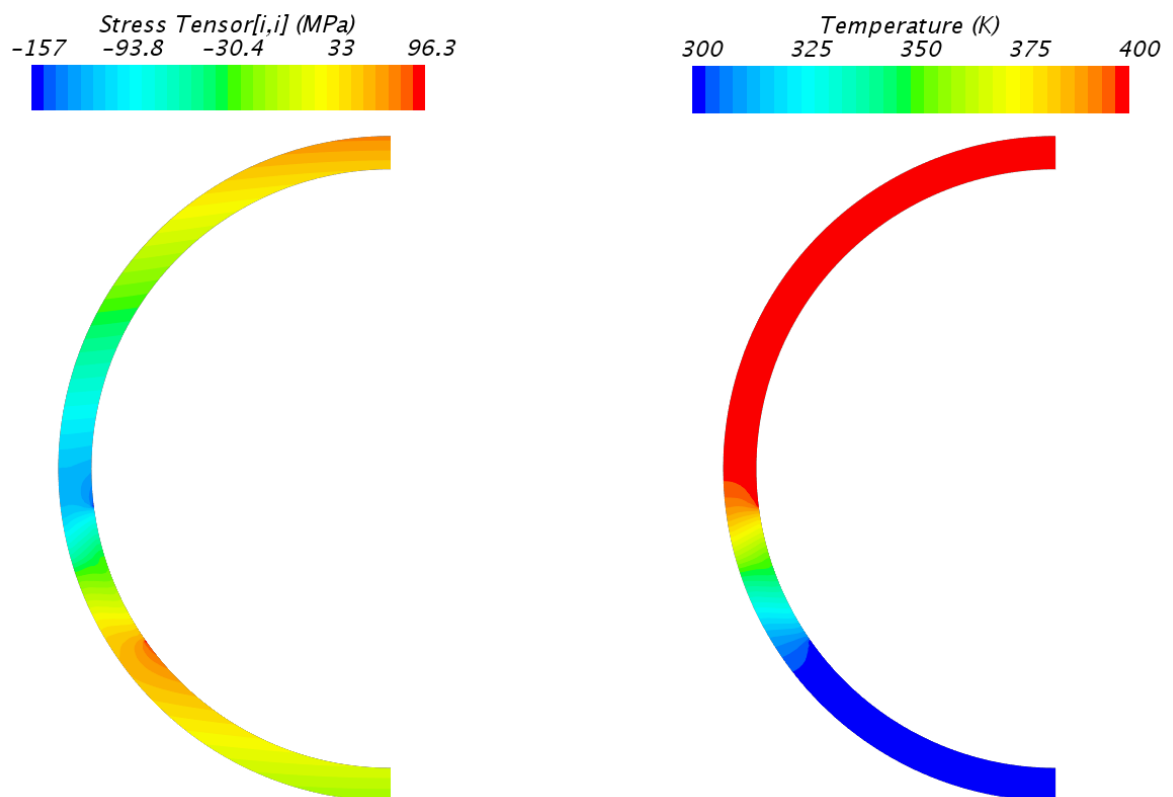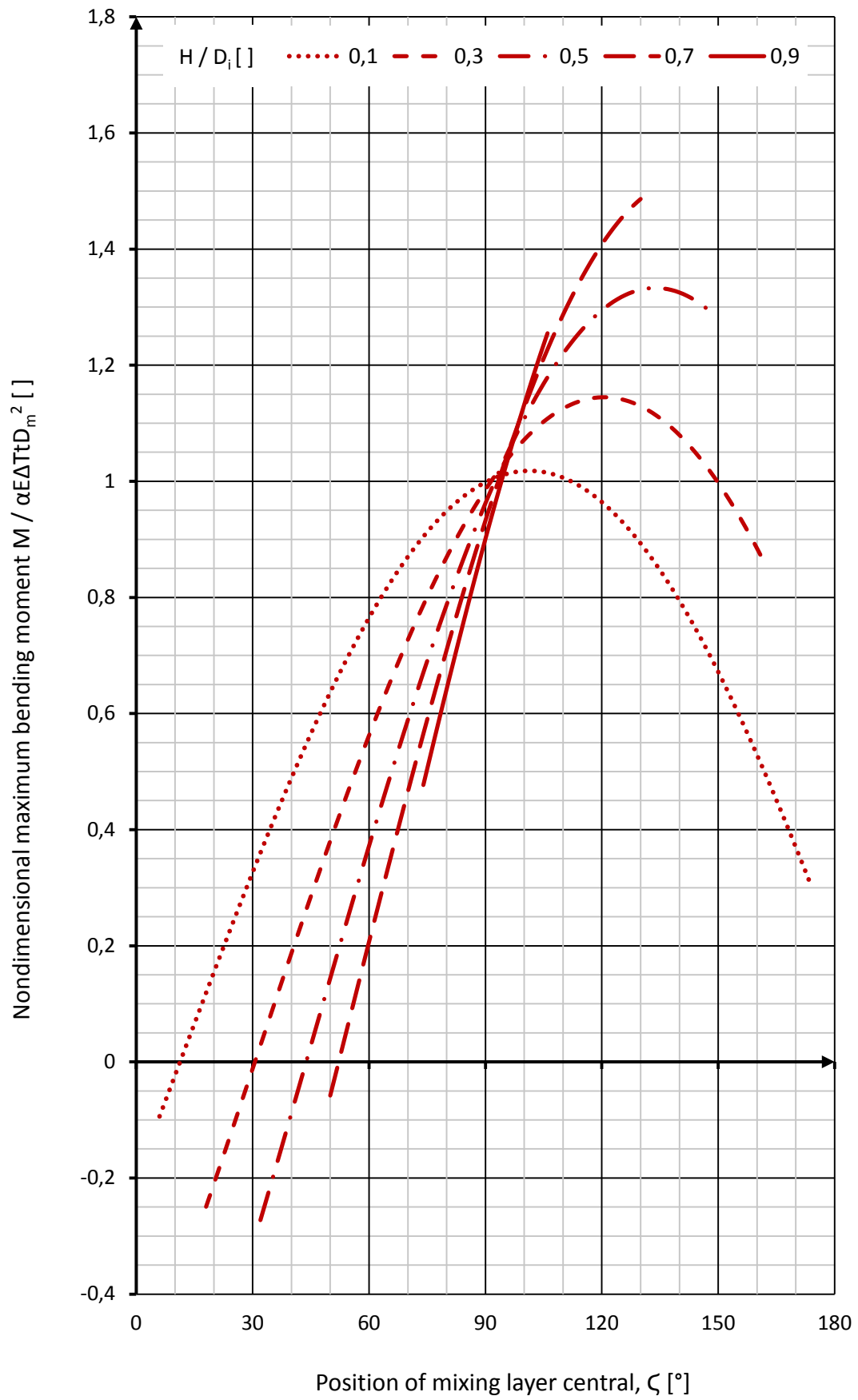*Figure 39: Stress and temperature fields at middle cross-section, H = 0.1 and ς = 90°.*

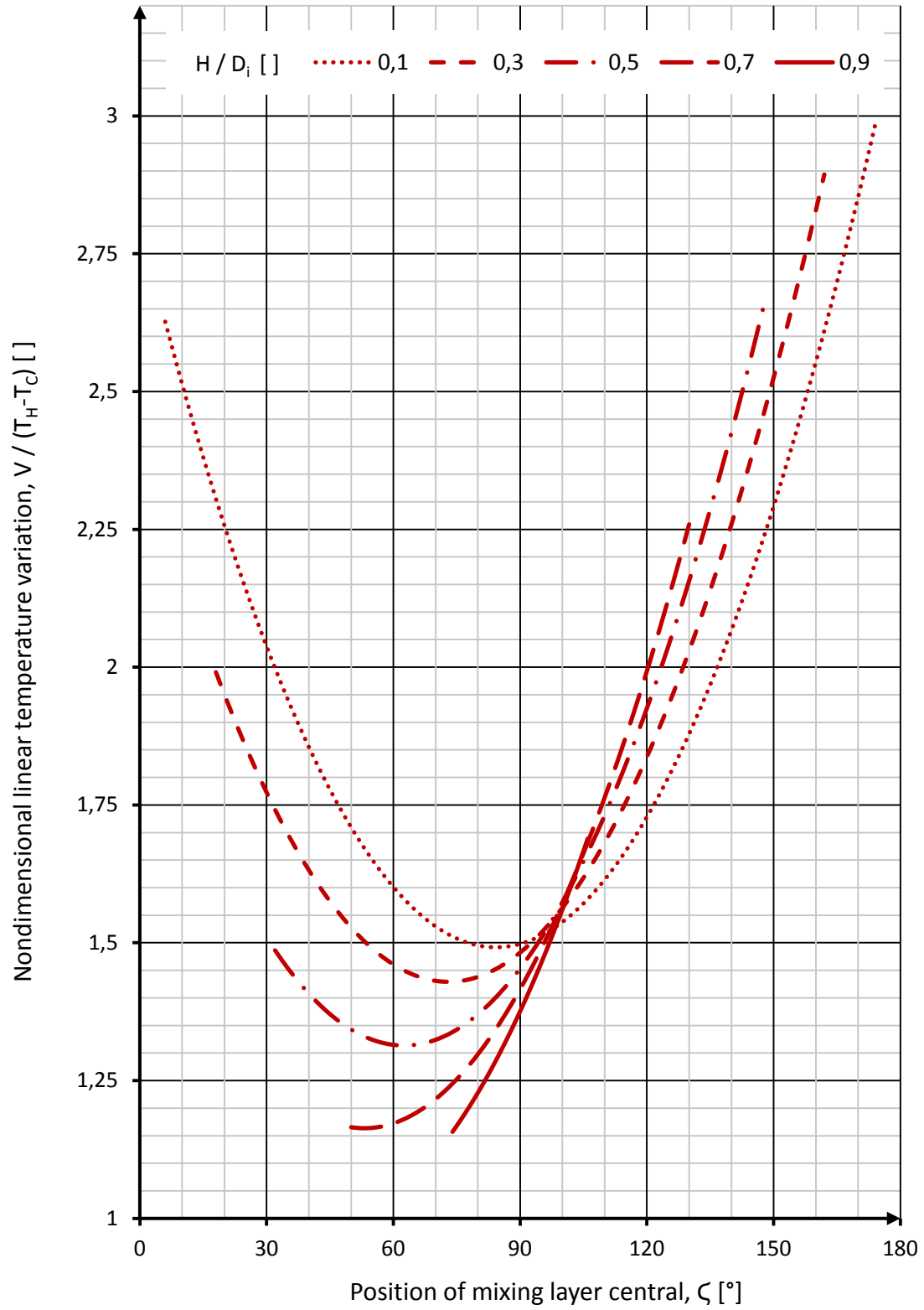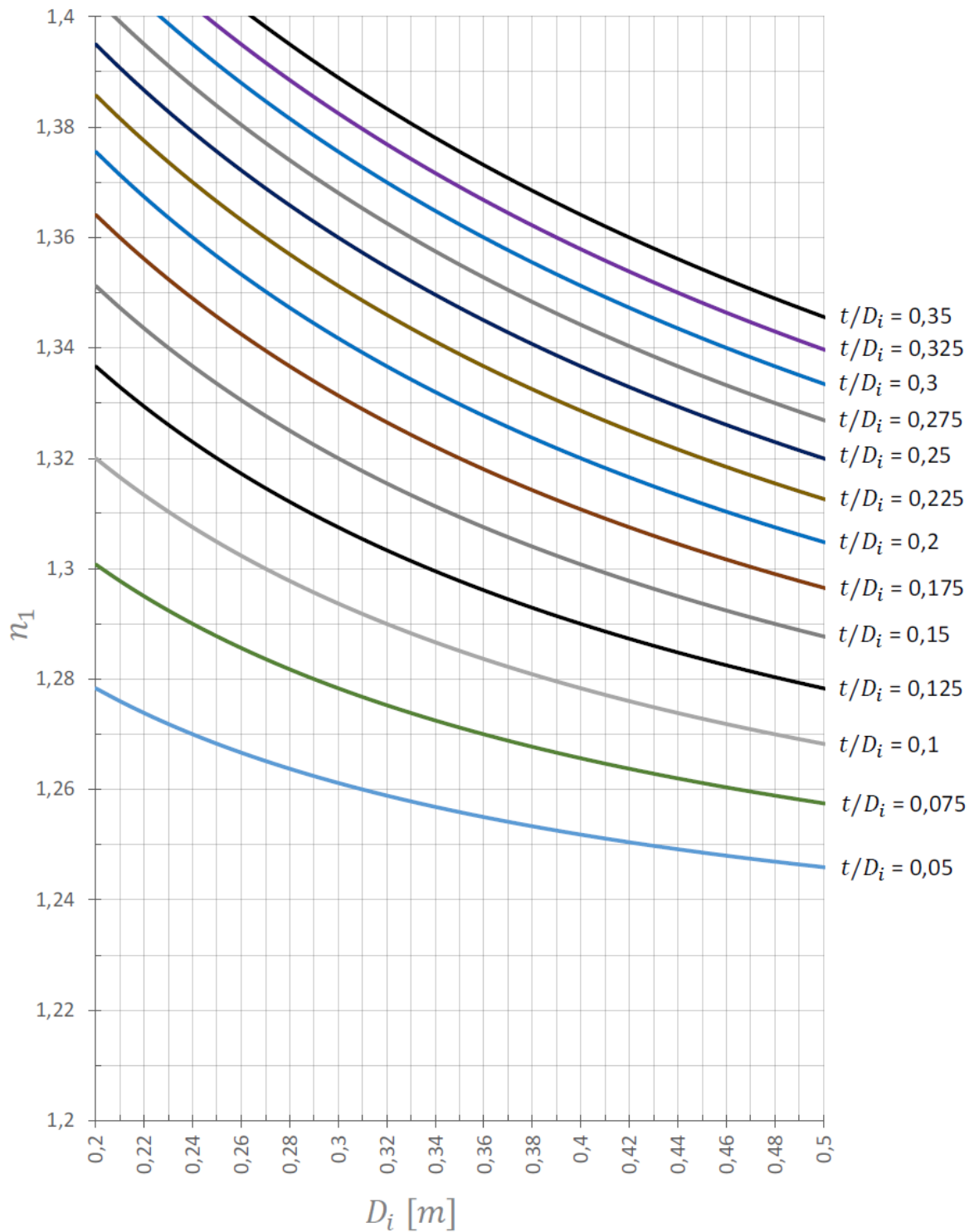*Figure 40: Stress and temperature fields at middle cross-section, H = 0.2 and ς = 110°.*
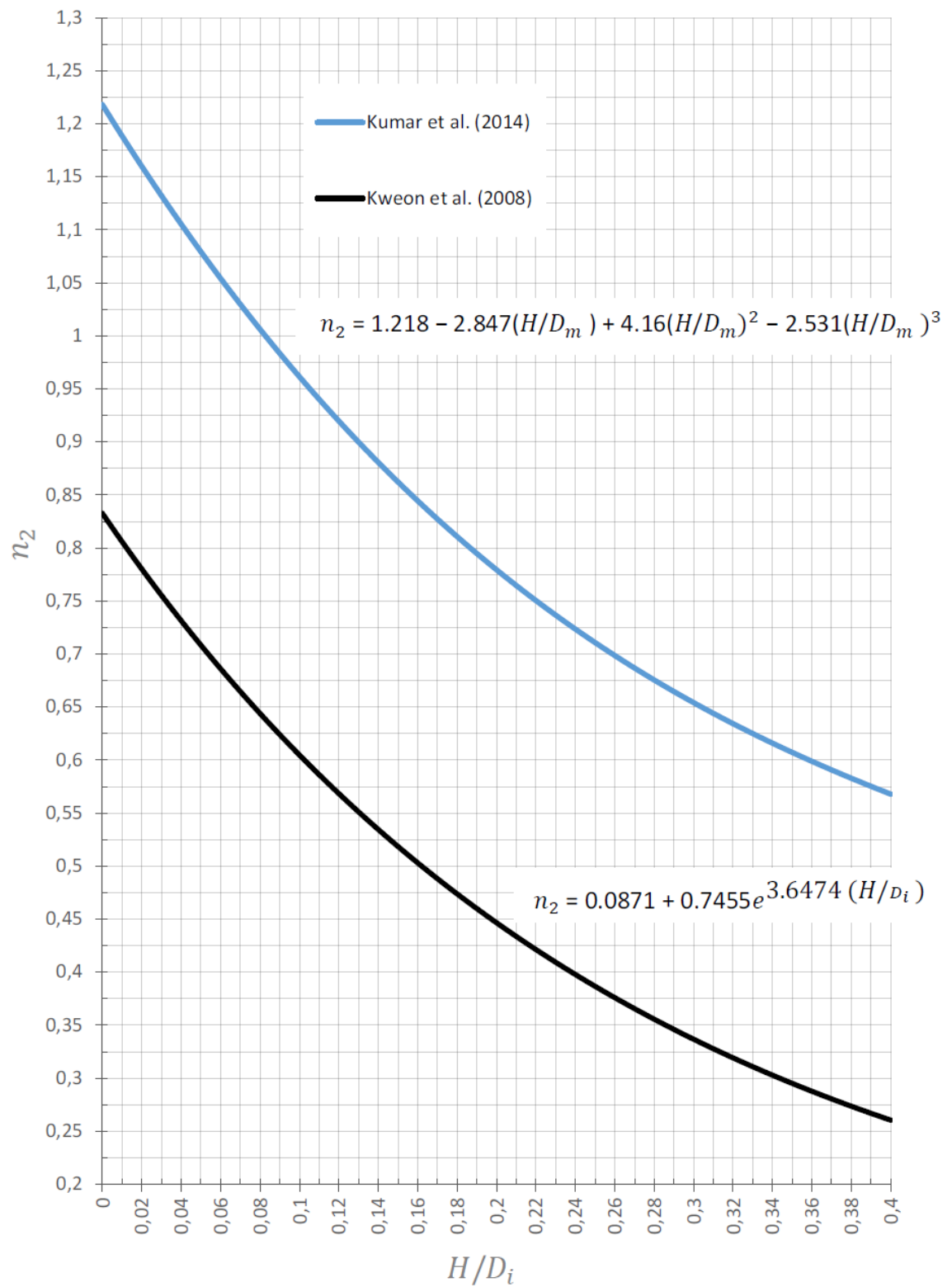
Appendix 3. Charts for Decomposition Method

$$n_1 = 1.22 + 0.35(2t/D_o)$$

$t/D_i = 0,35$
$t/D_i = 0,325$
$t/D_i = 0,3$
$t/D_i = 0,275$
$t/D_i = 0,25$
$t/D_i = 0,225$
$t/D_i = 0,2$
$t/D_i = 0,175$
$t/D_i = 0,15$
$t/D_i = 0,125$
$t/D_i = 0,1$
$t/D_i = 0,075$
$t/D_i = 0,05$

Effectiveness factor n_1 for Kweon et al. (2008)

Chart from Hautala (2017)

$$n_2 = 1.218 - 2.847(H/D_m) + 4.16(H/D_m)^2 - 2.531(H/D_m)^3$$

$$n_2 = 0.0871 + 0.7455e^{3.6474\,(H/D_i)}$$

Effectiveness factor n_2 for Kumar et al. (2014) and Kweon et al. (2008)

Chart from Hautala 2017